OPTIMAL GENERATION SCHEDULING FOR RENEWABLE MICROGRIDS USING HYDROGEN STORAGE SYSTEMS

MARIO PETROLLESE

Dottorato di Ricerca in Ingegneria Industriale
Università degli Studi di Cagliari
XXVII Ciclo

OPTIMAL GENERATION SCHEDULING FOR RENEWABLE MICROGRIDS USING HYDROGEN STORAGE SYSTEMS

MARIO PETROLLESE

Supervisor:
Professor Daniele COCCO
University of Cagliari, Italy

Co-supervisors:
Prof. Sören KNUDSEN KÆR
Aalborg University, DK

Dottorato di Ricerca in Ingegneria Industriale
Università degli Studi di Cagliari
XXVII Ciclo

This work was carried out as part of a collaboration agreement with the Sardegna Ricerche Consortium for the management, scientific coordination and development of research activities of the Concentrated Solar Technologies and Hydrogen from RES Laboratory.

MIUR is also acknowledged for the PhD fellowship.

Acknowledgements

First of all, I would like to thank my supervisor, Prof. Daniele Cocco, for the possibility of undertaking this PhD, and for his support and advice during these three years at the Department of Mechanical, Chemical Engineering and Materials (DIMCM), University of Cagliari, Italy.

I wish to thank prof. Giorgio Cau for his support and advices for my research.

I would also like to thank my Danish supervisor, prof. Sören Knudsen Kær, for his help during my stay at the Aalborg University – Department of Energy Technology (DK).

Another special thanks to Luis Valverde from HyLAB, University of Seville for his time and for giving me the opportunity to finish the last part of my research.

A sincere thanks to Fabio Serra and Marialaura Lucariello from the LABH_2FER Laboratory (Sardegna Ricerche) for their constant willingness and valuable collaboration.

Thanks to my colleagues at the Department of Mechanical, Chemical Engineering and Materials, for the wonderful time spent together and for being good friends.

Special thanks to Laura for the love and joy she give me during this experience we spent together in our life.

Last, I am grateful to my family, who has always believed in me, and this has permitted me to be what I am, and therefore to reach this important goal.

Abstract

The topic of this thesis is the development of a tool for an optimal energy management strategy (EMS) of the generators and energy storage systems constituent microgrids, both grid-connected or isolated (stand-alone power system) powered by Renewable Energy Sources (RES). In particular, a novel control system is designed based on the resolution of the unit commitment problem. For each time step, the proposed control system compares the expected power produced by the renewable generators with the expected load demand and determines the scheduling of the different energy storage devices and generators for the next few hours, which minimizes the operating cost of the overall microgrid. To take into account for forecasting uncertainties, the generation of the different scenarios is carried out through a discretization of the probability distribution function of the forecasting errors for wind speed, solar radiation and load requests by a set of finite states. A set of various scenarios are therefore analyzed and compared by the control system to find the minimum operating costs.

The proposed algorithm is firstly applied to a microgrid at $LABH_2FER$ (Sardegna Ricerche, Italy). Since the microgrid is under construction, the expected performance is evaluated through a simulation modeling, implemented in Matlab-Simulink. Furthermore, in order to highlight the benefits of including weather forecasts and operating costs in the EMS, a comparative analysis with a simpler EMS based on control states of storage devices is carried out. The results of the comparative study demonstrate that a reduction of almost 5-10% in the annual operating costs and energy losses is achieved thanks to the implementation of the proposed control system.

Moreover, the proposed control strategy is implemented and tested to a microgrid present at the University of Seville. Experimental results demonstrate the feasibility and the actual functionality of the control system. Additional benefits are also observed, such as the reduction in

power exchanged with the upstream grid thanks to a better management of the storage systems.

Contents

List of figures

List of Tables

Chapter 1

Introduction

1.1. Motivation and objective

Renewable energy sources (RES) have grown considerably in the last decade, and a further increase in RES is foreseen for the future to reduce greenhouse gas emissions and diversify energy supplies. However, there are still some serious concerns about RES technologies and their implementation into the exiting energy production and distribution systems. The main issue is the intermittent nature of many RES. In particular, wind and solar power plants cannot produce power steadily since wind speed and solar radiation change during the day and the year. In large electricity networks, these fluctuations can be balanced by conventional power plants and up to now, critical situations have occurred only in local power grids with a high penetration of renewable sources. In these systems, the introduction of energy storage systems, mainly based on batteries, is essential. In the future, the expected greater penetration of RES calls for a significant introduction of energy storage systems (ESSs) also in extended grids.

The involvement of different ESS technologies to achieve the optimal operation of the overall energy production system is required by the considerable variation of the energy produced by RES generators throughout the year. In particular, the optimal management of the energy flows in power generation systems with a high RES penetration requires the integration of short-term and long-term energy storage systems. Batteries are suitable for short-term storage but do not appear to be the best solution for long-term storage because they have a low energy storage density and

suffer from the self-discharge phenomenon. Among the different long-term ESS technologies, such as hydro-pumps, compressed air energy storage etc., the use of hydrogen storage systems appears today one of the most interesting options.

The integration of multiple energy generation and storage systems forming the so-called microgrids seems nowadays to be the new architecture that the grid will assume in the future. The higher energy conversion efficiencies, the avoidance of transmission and distribution losses, the enhanced flexibility of the local electricity networks and the increased levels of reliability/security of supply, together with the reduction of polluting emissions, are the main advantages of decentralized energy production. However, the control strategies and the dynamic behavior of a microgrid, particularly for stand-alone power systems based on RES technologies, can be noticeably different from those of a conventional grid. Furthermore, unlike the well-established energy management strategies of interconnected power systems, those envisioned for microgrids are more influenced by the load requirements, the expected operational scenarios and the adopted technologies for generators and energy storage systems.

Several operating strategies based on energy, economic or environmental criteria can be adopted to meet the required power demand, which varies over the day and over the year. However, among the others, it is preferable to use an optimum or suboptimum operating strategy based on economic criteria. In other words, an important goal of the energy management strategy is to meet the power demand at minimum operating costs. In order to supply high-quality electric power to customers in a secure and economic manner, an optimization process for the unit commitment (UC) of the different generating and storage units should be adopted. The optimal UC determines the schedule of all the equipment within a power system, under the different operating constraints and it will result in a great saving for electric utilities. In fact, the main objective of the UC problem is to minimize the total operating costs while satisfying all of the constraints required to meet the load with a given security level.

The application of UC methodology to microgrid systems is largely studied in literature as reassumed in this review [1]. However, these studies are mainly based on microgrids with a single energy storage system. If more than a single ESS is involved (typically short-term and long-term storage

systems) in the microgrid, the management of the power flows fluctuation will require another optimization process for the optimal choice between the short and long-term storage. For a more accurate techno-economic optimization of the overall system, the inclusion of investment costs, operating costs and lifetimes of the main plant components is required in the definition of the optimal control strategy.

The main objective of this study is the development of a tool for solving the generation scheduling problem in microgrids with high-penetration of RES generators and different energy storage systems. Starting from the expected difference between power produced by RES and user request, a proper control system is developed in order to determine the optimal scheduling of the different devices constituent the microgrid. One of the original contributions of this work refers to the involvement in the generating scheduling problem of different energy storage systems, other than conventional Diesel generators. In fact, a single energy storage system is usually considered in literature to face the variability and the high uncertainty related to load demand to power production by RES. Moreover, the optimal management of the excess power produced by RES generators and not used by the load is carried out by the proposed control system. Based on the weather and load forecast of the following days, the control system properly alternates the short-term and long-term storage in order to minimize the power curtailment of RES generators.
A novel approach to manage the uncertainties based on scenario tree is developed and a more robust solution is achieved with a less sensitivity on unexpected demand and on errors in the forecast conditions. Moreover, thanks to the use of the scenarios tree, the control strategy adopted for the following hours takes into account not only the contingent situation of the microgrid but also the expected conditions that the microgrid will meet during the following days. The ability to integrate the scenario tree approach with a rolling planning that each hour updates the energy management strategy led to different benefits in the performance of microgrids with high penetration of RES.
Finally, this study demonstrates of the feasibility of using hydrogen as long-term energy storage system. The benefits and disadvantages (both in technical and economic terms) brought by the introduction of the hydrogen storage system are examined together with the study of its optimal integration in microgrids.

1.2. Overview of the thesis

This Thesis is structured in six main chapters subdivided in paragraphs for each topic.

A brief description of each chapter is given in the following:

- **Chapter 2**: A general overview of the distributed generation and microgrid concepts is given. An introduction to the energy storage technologies is presented, focusing the attention to batteries and hydrogen storage systems. This chapter introduces the reader from the importance of an effective energy management strategy to ensure the optimal operation of the microgrid;
- **Chapter 3**: a novel algorithm for the optimal scheduling of the microgrid equipment is introduced. Since the achievement of the optimal control strategy is strongly influenced by the uncertainties of both renewable sources availability and load demand, a stochastic approach was adopted through a scenario tree method;
- **Chapter 4**: a first analysis of the benefits and the drawbacks led by the proposed algorithm is given related to a stand-alone microgrid present at the Concentrating Solar and Hydrogen from Renewable Energy Sources Laboratory, in Sardinia (Italy)
- **Chapter 5:** the experimental results obtained by the implementation of the proposed control system to the microgrid located at the University of Seville facilities (Spain) are reported and analyzed.
- **Chapter 6**: the main conclusions and the possible future development of this research are discussed.

1.3. Publication

Some of the topics discussed in this Thesis have been already published in international journal, and presented at national and international conferences.

International Journal Papers:

1. G.Cau, D. Cocco, M. Petrollese, *Modeling and simulation of an isolated hybrid microgrid with hydrogen production and storage*, Energy Procedia, Volume 45, 2014, Pages 12-21

2. G.Cau, D. Cocco, M. Petrollese, C. Milan, S.K. Kear, *Energy management strategy based on short-term generation scheduling for a renewable microgrid using a hydrogen storage system*. Energy Conversion and Management 87 (2014) 820–831

National and International Conferences:

1. G.Cau, D. Cocco, M. Petrollese, V. Tola, *Assessment of a hybrid stand-alone power system with hydrogen production and storage*, MICROGEN3, Naples, Italy
2. G.Cau, D. Cocco, M. Petrollese, *Modellazione e simulazione di una microrete ibrida isolata con produzione e stoccaggio di idrogeno,* 68th ATI Conference, Bologna, Italy
3. G.Cau, D. Cocco, M. Lucariello, M. Petrollese, *Optimal generation scheduling for a hybrid stand-alone power system using renewable energy sources and hydrogen storage*, ECOS2014, Turku, Finland
4. G.Cau, D. Cocco, M. Lucariello, M. Petrollese, *Hydrogen as a clean energy carrier: the microgrid at the "Concentrating Solar and Hydrogen from Renewable Energy Sources Laboratory*, 10ESEE2014, Chia, Sardinia, Italy

Chapter 2

Distributed generation and energy storage systems

With the increase of the use of renewable energy sources for energy production, a profound change in the energy management and in the same concept of electricity production is taking place nowadays.
Concepts such as self-generation or distributed generation have questioned the central role the large conventional energy plants had since the second industrial revolution. Increasingly it is catching on the microgrid concept linked to an intelligent use of energy. The on-site energy production and consumption assisted by an intelligent management and control system (the so-called smart grid) could replace the traditional electricity grid within a few years with several technical and economic advantages. In the development of this new energy policy, energy storage systems have a key role. In fact, they act as energy flywheel and are essential to cover the inevitable mismatch between demand and supply of energy in a high RES penetration power system.

An overview of the key concepts about distributed generation and the state of the art on the main energy storage systems is presented in this chapter.

2.1. Distributed generation and microgrid

The existing electricity grid is unidirectional in nature. It converts only about one-third of fuel energy into electricity, without recovering the waste heat. In the European electricity grid, almost 8% of electricity production is lost along its transmission lines, while 20% of its generation capacity is

used to meet peak demand only (i.e., it is in use only 5% of the time) [2]. In addition of that, different problems occur in the use of centralized power generation based on conventional power plants such as the gradual depletion of fossil fuels, transmission and distribution losses and high environmental pollution.

These problems have led to the new concept of generating power locally at distribution voltage level by using non-conventional/renewable energy sources like biogas, wind power, solar photovoltaic cells, fuel cells, combined heat and power (CHP) systems, microturbines, and Stirling engines and their integration into the utility distribution network. This type of power generation is termed as distributed generation (DG) and the energy sources are termed as distributed energy resources (DERs).
A consistent definition of DG was firstly given by Ackermann et al. [3]. The purpose of distributed generation is to provide a source of active electric power. The location of distributed generation is defined as the installation and operation of electric power generation units connected directly to the distribution network or connected to the network on the customer site of the meter.
DG implementation has many benefits from both the economical and technical point of view: the reduction of costs during the installation of new transmission lines, the flexibility in the location of the plant, the diversification of the energy sources, the reduction of the network power losses, the improvement in the system continuity and reliability, etc.

There are different types of DGs from the constructional and technological points of view. According to [4], it is possible to divide the DGs using traditional generators and non-traditional ones, as shown in Figure 2.1. About the use of traditional generators, an interesting and emerging technology involves the use of micro-turbines. They are small size gas turbines, which can operate using natural gas, propane, biogas and fuel oil. In a simple form, they consist of a compressor, combustor, recuperator, turbine, and generator. They can be installed on-site especially if there are space limitations. They are very efficient (more than 80% as combined heat and power efficiency) and have lower polluting emissions (less than 10 ppm NO_x) with respect to large scale gas turbines.
About non-traditional generators, solar and wind energy sources are often viewed as technologies that can be employed to both satisfy transient

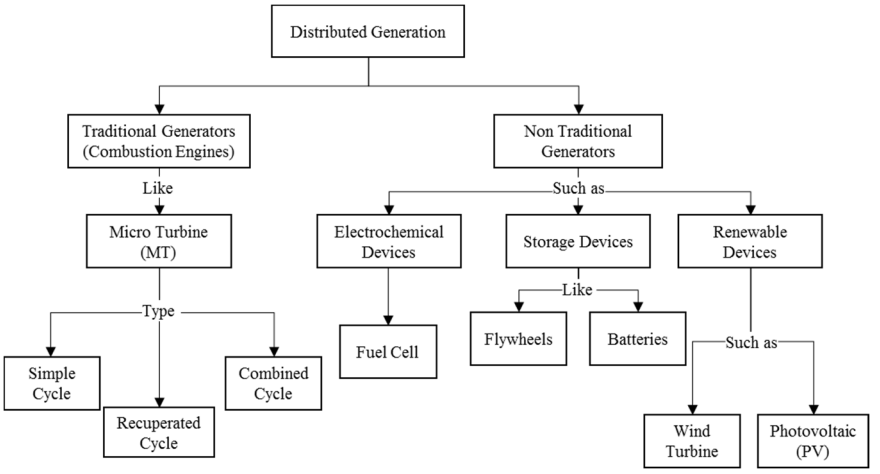

Figure 2.1 - Distributed generation types and technologies **[4]**

local needs and supply energy into the electricity distribution grid. However, their output generally only roughly matches the time dependent requirements of the grid. Thus, energy storage systems are required to assist their integration into large-scale power systems. Typical storage devices are batteries, flywheels and capacitors, which are charged during low load demand and used when required. One of the most interesting options, subject of many studies and research activities in recent years, is the use of hydrogen storage systems. In the latter, excess electricity can be converted to hydrogen through an electrolyzer (EL) and stored in pressurized tanks. The stored hydrogen can be later used to produce electricity by a fuel cell (FC).

As proposed by [5] , different phases of development toward a complete distribution generation system can be forecasted and identified. In the first phase of development, the first DER units are introduced and the system operator has to adopt suitable codes and guidelines. At this phase the main concern is making the interconnection as simple as possible without endangering the safe and secure operation of the grid. In the second phase the penetration degree increases, so that the DER must be taken into account in the system operation. This requires the creation of rules and practices for various management functions considering the power and energy management as well as for the voltage level control. In the third phase the DER units are considered as an integrated part of the system. A

large number of active elements is present in the system and the active customer participation has a key role as well. Recently, the name smart grid has become common to describe these future power networks that will make extensive use of modern information and communication technologies to support flexible, secure and cost-effective decarbonized electrical power systems.

The grid architecture will deeply change in the future with the increasing use of DER and the aggregation of localized grouping of DER units to supply the local loads. Microgrids are small-scale networks designed to supply electrical and heat loads for a small community, such as a suburban locality, or an academic or public community such as a university or school, a commercial area, an industrial site, a trading estate or a municipal region. A microgrid is essentially an active distribution network because it is the conglomerate of DG systems and different loads at distribution voltage level (typical 50 V). The generators or microsources employed in a microgrid are usually renewable/non-conventional DERs integrated together to generate power at distribution voltage. From an operational point of view, the microsources must be equipped with power electronic interfaces (PEIs) and control systems to provide the required flexibility to ensure operation as a single aggregated system and to maintain the specified power quality and energy output. This control flexibility would allow the microgrid to interface with the main utility power system as a single controlled unit that meets local energy needs for reliability and security. [6]

A microgrid can operate in grid-connected or islanded mode, and hence increases the reliability of energy supplies by disconnecting from the main distribution network in the case of network faults or reduced power quality [7]. It can also reduce transmission and distribution losses by supplying loads from local generation and from elements of the distribution system. Operating a microgrid in islanded mode has very considerable technical challenges, as normally the main power system provides to grid-connected microgenerators:

- a well-defined frequency and voltage reference;
- a reliable and predictable source of short-circuit current;
- a sink or source of real and reactive power if the local load does not instantaneously match the microgeneration

In all the microgrid experiments conducted to date, it has been found necessary to use electrical energy storage to ensure stable operation when the microgrid is disconnected from the distribution network and to accommodate load changes when the microgrid is operating in islanded mode.

2.1.1. Stand-alone microgrid

According to the IEA [8], today more than one billion people worldwide lack access to electricity. Various options for supplying this electricity need to be considered: these include on-grid and isolated off-grid configurations. Decentralized options are an important alternative in cases where grid extensions are too expensive and autonomous stand-alone microgrids have proven to be one of the most interesting and environmentally friendly technological solutions for the electrification of remote consumers.

An important characteristic that distinguishes the design of remote microgrids from interconnected networks is that the sources of power generation in remote systems have to be sized to completely cover the demands of the connected loads and to have sufficient reserve capacity to deal with any contingencies that might arise [9]. Stand-alone power systems using fossil fuels suffer from the high costs of these fuels, pollution and greenhouse gas emissions, while stand-alone microgrids completely powered by renewable energy sources (RES) can overcome these problems. One of the main drawbacks of using energy conversion systems based on RES, such as photovoltaic systems (PV) and wind turbines (WT), is their discontinuity in energy production, so that an effective energy storage section is required to ensure a continuous electrical energy supply.

In addition, as isolated systems do not have the voltage and frequency references that a distribution network provides in interconnected systems, they have a greater degree of complexity in terms of control engineering. Equilibrium has to be found between the output and load to ensure that the voltage and frequency of the microgrid are kept within acceptable limits. To guarantee such equilibrium at any given moment, the sole management of electrical generators and energy storage systems may be insufficient and it may be required to act on loads, some of which it might on occasions be convenient to disconnect, connect or adjust [10].

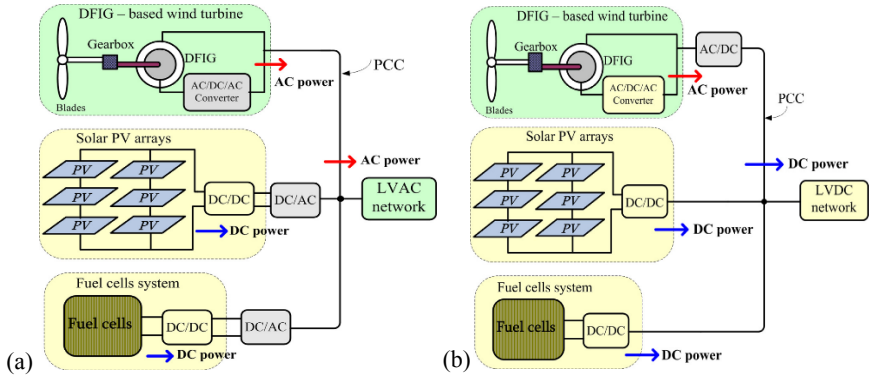

Figure 2.2 - Typical configuration of an AC-coupled microgrid (a) and DC-coupled microgrid (b)

2.1.2. Microgrid configuration

There are two basic ways to connect system equipment, generators and end user in a microgrid: AC coupled and DC coupled.

In the first topology, all electricity generating units with AC power output are directly connected to an AC bus line and then to the main system via power converters for their stable coupling. Examples of the DG units that produce an AC output power include wind turbines, low-head hydro turbines, biogas engines, tidal and wave turbines [11]. On the other hand, DC equipment (i.e. PV systems, batteries, fuel cells etc.) may need the presence of a DC/AC inverter. A typical configuration of this system is shown in Figure 2.2(a).

In the second topology, all generators are coupled on a DC bus. In that way, the DC generators and energy storage devices produce the DC power and only a DC/DC converter is required for the adjustment of output voltage to the DC bus voltage. The storage systems can also be charged/discharged with the DC network and DC loads can be directly connected [6,7]. In this case, the AC power generating units and AC load need an AC/DC power converter for their connection to the DC network as indicated in the Figure 2.2(b).

Nowadays, with the concept of smart grid coming up, the interest for low-voltage DC networks such as those used for industrial power supplies and commercial buildings is increasing [12]. In the future, DC distribution systems will probably become an alternative way to supply all the electrical equipment connected by a bus system and optimally controlled by an

energy management system (EMS). Different advantages are presented in the use of a DC distribution line, such as a more efficient power transmission thanks to the absence of reactance in the line and a low line resistance. Moreover, no frequency monitoring is needed and there are no problem with transient stability and electromagnetic interference [13].

2.2. Energy storage systems

Electricity has become the most common means of energy transport in electricity grids and one of the most common means of transport for the information in telecommunications. However, it cannot be accumulated in its state, and to be stored a conversion into another form of energy (chemical, mechanical, electrostatic, electromagnetic) is required.

The important role of ESS in integrated power systems with renewable power sources was already highlighted in the previous paragraph. The benefits stemming from the adoption of energy storage systems may be summarized as the possibility to reduce energy losses, to increase the reliability of energy supply (since an extra power source is available) and to improve the operation of the power system (e.g. operation of conventional units at optimum point). Maximum exploitation of RES is possible via the utilization of ESSs across the entire range of applications, i.e. from the remote consumer level (stand-alone microgrids) to large-scale RES systems.
However, some drawbacks are present, such as the high initial cost of the system and the inherent transformation and conversion energy losses.

Depending on the system configuration (AC or DC network), the EESs may need the presence of a inverter/rectifier: since most of EESs components produce DC power, a DC/AC transformation done by an inverter is needed during the deficit period to satisfy the AC loads. On the other hand, if RES generators are present in the microgrid, such as wind turbines, and an excess of power occurs, the latter will be converted to DC power by a rectifier to be stored.

As known, an ESS is used to store energy during periods of low energy demand (provided that an energy surplus is available), and to deliver the stored energy during periods of high energy consumption, i.e. when energy production is not sufficient. However, both the production and the request of energy varies with the day, the week and the season. For example, the

peak energy production for PV systems is typically observed around noon while it is almost zero during the evening. On the other hand, a peak of load demand typically occurs during the evening for residential use of heating or cooking appliances whereas the request during the night is usually low. The load curve may be not constant during the week: many activities are different on weekends than they are during weekdays.
The magnitude of the electrical power demand also varies during the year. There is more power used in the winter for heating, and in the summer for air conditioning. At the same time, the energy production by RES generators is greatly affected by the season (i.e. for a location situated in the south of Italy, the average daily global irradiation per square meter varies about ±30% between winter and summer in comparison with the yearly average irradiation).
The ability to balance this variations is strongly linked to the storage capacity. Therefore, the ESSs can be classified depending on the storage duration:

- ***Long-term storage***: it generally involves very large installations in order to carry large amount of energy throughout the seasons. Usually, these storage systems have very large storage capacities, not suffer of self-discharging and have a great autonomy. An example of these EESs are the large hydropower system with reservoirs and dams that accumulate water primarily during the rainy (or snowy) season of the year. Electric power is produced in hydroelectric facilities by passing water through large turbines.
- ***Medium-term storage***: it is introduced to deal with the daily cycle of different RES generators, or to smooth the daily or weekly peaks of load. The storage capacity is less than the previous case. Typically, these systems are subject to frequent charging/discharging cycles. For this reason, an important parameter is the durability intended as number of times the storage unit can release the energy level it was designed for after each recharge, expressed as the maximum number of cycles. A wide selection of EESs are candidates to supply of this demand i.e. hydrogen storage systems, compressed air energy storage (CAES) etc.
- ***Short-term storage***: this kind of storage system is needed to face the short time transients. These transients can lead to rotor angle

instability, which means oscillations and unstable operating conditions. Voltage instability can also occur when the load and the associated transmission system require a large amount of reactive, rather than real, power. This can result in a sudden and drastic voltage drop. Short-term power outages can also occur. The rapid response characteristics of flywheel systems make it possible to use them to reduce the problem of short-term transients. Other options that are being used include battery system and supercapacitors [14].

An overview of several storage technologies and application in relationship with the storage duration is shown in Table 2.1.

2.2.1. Energy storage technologies

The electricity can be converted into different forms of energy. Electrochemical batteries (lead-acid batteries, lithium, etc.) and hydrogen storage systems convert electrical energy into chemical energy. Mechanical storage includes compressed air energy storage systems (CAES), high and low speed flywheels or water pumping systems.

Table 2.1 - Storage technologies and application **[15]**

Full power duration of storage	**Application of storage and possible replacement of conventional electricity system controls**	**H_2 storage system**	**Large hydro**	**CAES**	**Pumped hydro**	**Batteries**	**Flywheel**	**Supercapacitots**
4 Months	Annual smoothing of loads, PV, wind and small hydro	✓	✓					
3 days	Weekly smoothing of loads and most weather variations	✓	✓	✓	✓			
8 h	Daily load cycle, PV, wind, transmission line repair	✓	✓	✓	✓	✓		
2 h	Peak load looping, wind power smoothing etc	✓	✓	✓	✓	✓		
20 min	Spinning reserve, wind power smoothing, clouds on PV	✓	✓	✓	✓	✓	✓	
3 min	Spinning reserve, wind power smoothing of gusts	✓			✓	✓	✓	
20 s	Line or local faults, Voltage and frequency control					✓	✓	✓

The electric storage is represented by capacitors and supercapacitors. The storage technologies that answer to specific technical and economic criteria, which vary considerably as a function of the applications and needs, can obviously be of different types.
This work is focused on the use of chemical conversion in particular batteries and hydrogen storage system. However, they are only a possible alternative. In the future, together with the increase of distributed generation, a distributed storage with the probable involvement of different energy storage technologies is expected. In this framework, the actual challenge is the development of smart energy management systems for an efficient and reliable integration of these different generators and ESS technologies.

Batteries

The electrochemical energy accumulators, also known as batteries, are the most conventional technology for the storage of electrical energy. They store the electrical energy in an electrochemical form, and they are characterized by totally reversible reactions.
A battery is generally constituted by several electrolytic cells connected in series and/or parallel. Each electrolytic cell consists of two half cells connected in series by a conductive electrolyte containing anions and cations. The half-cell including the electrolyte and the positive electrode is the cathode. Negatively charged ions called anions migrate to the cathode. The other half-cell including electrolyte and the negative electrode is the anode. The positively charged ions called cations migrate to the anode. In the redox reaction that powers the battery, cations are reduced (electrons are added) at the cathode, while anions are oxidized (electrons are removed) at the anode. The electrodes are electrically connected only by the electrolyte.
The material used to realize the electrodes and the electrolyte type identify the electrochemical couple with which is classified an accumulator. A wide range of technologies are used in the fabrication of accumulators with differences in energy densities and technological maturity. The main types are lead-acid, nickel based and lithium-ion batteries.
The lead-acid batteries are the most common solution for the electrochemical storage both in industrial applications and in the distributed generation thanks to their energy characteristics (an energy density around

30 Wh/kg and a roundtrip efficiency usually of 80-85%) and their low initial costs. Their success is primarily due to the low cost and wide availability of lead, in addition to a good reliability, a relatively simple technology and a well-established manufacturing. However, they have several negative aspects, such as a rather low lifetime, the need of large space, the need to install adequate ventilation systems since a hydrogen production can occur in the charge phase. Moreover, the not simple determination of the actual state of charge could be a critical aspect in the energy management of the system.
The electromotive force (EMF) of the lead acid electrolytic cell is nominally 2 V. Actually, its value depends on various external factors, such as the electrolyte density, ambient temperature, state of charge and circulating current. Another phenomenon to be considered is the self-discharge. In lead-acid batteries self-discharge is due to various side reactions that lead in time to the discharge of the battery. In normal conditions, the self-discharge leads to a reduction of the charge of the battery of about 2-3% per month.

The most widely nickel-based batteries are the nickel/cadmium (Ni/Cd) and the nickel/metal hydride (Ni/MH). Until a few years ago, the Ni/Cd batteries were largely used thanks to some advantages in comparison with lead-acid, including the higher lifetime, robustness, reliability, and better performance at low temperatures. However, they are in decline today, both for economic reasons and environmental problems linked to the presence of cadmium and therefore to its disposal.
The Ni/MH batteries are derived from the Ni/Cd batteries with the substitution of cadmium electrode with a mixture of metal hydrides. The technology of metal hydrides involves the use of expensive materials, therefore, these accumulators are widely used for small portable applications, where the benefits of the low volume partially offset the higher costs. The specific energy of these batteries is in the range of 40-85 Wh/kg, slightly higher than that of the Ni/Cd ones. The roundtrip efficiency is around 65% while a performance deterioration, still lower than that of lead-acid ones, is observed at low temperature. Their self-discharge value is about 20% per month at ambient temperature with a rapidly increase with temperature.

Lithium batteries are one of the most promising electrochemical storage technologies, with a very rapid development in recent years, partially driven by the possibility to supply the electric vehicles but also in the field of distributed generation. Lithium batteries can be divided into three categories. The most widespread and technically mature are the lithium-ion batteries with a liquid electrolyte (commonly called lithium-ion). Another possibility is the use of lithium-ion polymer batteries, which have a solid polymeric electrolyte with fewer risks in terms of safety. The third type is the lithium metal/polymer battery, in which lithium is in metallic form and liquid state. Currently, it has a limited development and is not commercially available because of the presence of safety problems.
The lithium-ion batteries have a specific energy capacity between 130-180 Wh/kg (the highest among all the electrochemical storage systems). The specific power can reach peak values of 1800 W/kg (but a reduction of the specific energy capacity), for batteries specifically designed to work with high power. The lithium-ion-polymers batteries have very similar specific energy values (140-150 Wh/kg), while the specific power can get to 2800 W/kg. Roundtrip efficiency is very high for both technologies, with values up to 95% depending on the operating conditions. The battery lifetime is 500 cycles with a 100% depth-of-discharge.
One of the drawback of this technology is the progressive degradation, which results in a progressive reduction of its capacity regardless of the number of cycles of charge/discharge.

Hydrogen storage system

Like electricity, hydrogen is an energy carrier, and not a primary energy source. Therefore, hydrogen requires energy to extract it from substances like water, natural gas, coal, or any other fossil fuel. The interest for its use, both for stationary applications and for the traction, mainly arise from environmental benefits: the pollution produced during its combustion with air is almost zero. The exhaust gas are only composed by water vapor when used with electrochemical systems (fuel cells). Traces of nitrogen oxides can be found in case of combustion process, which can be easily reduced by well-known technologies.
The hydrogen has excellent energy characteristics with reference to the unit of mass, with the highest value of low heating value (LHV) in comparison with all other fuels.

Table 2.2 - Comparing hydrogen properties with other fuels in standard condition (p=1atm, T=25°C)

	Hydrogen	**Methane**	**Gasoline**	**Diesel**
LHV [MJ/kg]	120	50	44.5	42.5
Energy density [MJ/m^3]	10.8	32.6	31240	36340
Density [kg/m^3]	0.0898	0.71	702	855

However, it is also the lightest element in nature for which, referring to the unit of volume, the energy characteristics are lower than conventional fuels (Table 2.2).

Currently, hydrogen is produced from natural gas and oil, but it generates carbon dioxide (typical greenhouse gas), and it is used mainly in the petrochemical and chemical industries. Nevertheless, the use of hydrogen from conventional sources to feed a fuel cell vehicle, taking into account the emissions produced for its production, lead to a 43% reduction of greenhouse gases compared to a gasoline-powered vehicle [16].
The steam reforming of methane is the most common process to produce hydrogen, covering about 50% of its production. It is based on the chemical reaction of methane (CH_4) with water vapor. The first step in this process is the elimination of impurities, such as sulfur, from the methane-rich natural gas. The methane is then reacted with steam at a relatively high temperature:

$$CH_4 + H_2O \rightarrow CO + 3H_2 \tag{2.1}$$

This is then followed by the water–gas shift reaction to decrease the content of CO and increase the hydrogen production:

$$CO + H_2O \rightarrow CO_2 + H_2 \tag{2.2}$$

after the carbon dioxide can be captured to limit emissions of greenhouse gases.
An alternative way for limiting or avoiding emissions of greenhouse gases, is represented by the gasification of coal, with simultaneous production of concentrated CO_2 and its subsequent capture and geological sequestration.
The only solution that allows the hydrogen production without producing greenhouse gas emissions is the water electrolysis, by imposing a proper voltage between two electrodes. The result is the evolution of hydrogen gas at the negative electrode, and oxygen gas at the positive electrode. Today, this technology covers only 5% of world production, being economically

prohibitive compared to other solutions. Moreover, this technology requires a considerable expenditure of electrical energy with conversion efficiency below 70%. However, it looks very interesting if it is coupled with renewable energy generators. The electrolysis is a simple and always activated process, which allows to produce hydrogen during periods of excess energy. Furthermore, it does not require large central facilities but a distributed generation is possible using smaller units. They can be located at places where the hydrogen will be used in order to reduce transportation costs.

Two electrolyzer technologies, alkaline and PEM, are commercially available with solid oxide electrolysis in the research phase. The alkaline electrolyzer is a well-established technology that employs an aqueous solution of water and typically 25-30%$_{wt}$ of potassium hydroxide (KOH). The liquid electrolyte enables the conduction of ions between the electrodes therefore it is not consumed in the reaction although it needs to be replenished occasionally. The reactions for the alkaline anode and cathode are:

$$4OH^-_{(aq)} \rightarrow O_{2(g)} + 2H_2O_{(l)} \tag{2.3}$$

$$2H_2O_{(l)} + 2e \rightarrow H_{2(g)} + 2OH^-_{(aq)} \tag{2.4}$$

The Proton Exchange Membrane (PEM) electrolysis is a system that incorporates a solid proton-conducting membrane, which is not electrically conductive. The membrane serves as gas separation device and ion (proton) conductor. The protons (H^+) are pulled through the membrane under the influence of an electric field and rejoin with electrons being supplied by the power source at the cathode to form hydrogen gas. PEM electrolyzers are typically operated at roughly an order of magnitude higher current density than the alkaline ones but they suffer from lower efficiency at the higher production rates. PEM also holds other advantages over alkaline including the ability to maintain a differential pressure across the anode (oxygen) and cathode (hydrogen) sides of the membrane to reduce the compression stages for high-pressure storage. Finally, without any additional purification, PEM electrolyzers generate purer hydrogen gas than alkaline. The PEM anode and cathode reactions are, respectively:

$$2H_2O \rightarrow 4H^+ + 4e + O_2 \tag{2.5}$$

$$2H^+ + 2e \rightarrow H_2 \quad (2.6)$$

In order to develop hydrogen storage systems, together with the use of electrolyzers, it is necessary both a storage section and another device to reconvert the hydrogen into electricity. About the storage section, the hydrogen can be stored in different phases, such as compressed, liquefied, metal hydride, etc. One of the traditional methods for storing hydrogen involves the use of high pressure tanks. Because of electrolyzers usually produce hydrogen with a relatively low pressure, a proper gas compression is usually carried out to increase the hydrogen pressure to 200-300 bar. In this way, the need of very large space for the storage is avoided. At the same time, that means the introduction of energy losses and safety issues in addition to the increase of the initial costs.

The hydrogen storage in the liquid state may be used to obtain a higher energy ratio per unit of volume. However, it is stable at a temperature of -253 °C. Therefore, the hydrogen should be contained in special cryogenic tanks with double walls, inside which a vacuum is created. Moreover, the energy needed to liquefy the gas corresponds to about 30% of the overall energy contained in the tank unlike of 8% in the case of compressed gas.

One of the most interesting options for the hydrogen storage is the metal hydrides storage based on the characteristic of the hydrogen to bond with various metals and metal alloys. The metal hydrides are binary compounds hosting the hydrogen in atomic form in the interatomic space inside their crystal structures. The formation of a metal hydride, in general, involves the breaking of the diatomic molecule of hydrogen on the metal surface and its subsequent diffusion in atomic form in the crystal lattice. Metals candidates for the use for hydrogen storage are palladium, some transition metals such as titanium, vanadium, niobium, tantalum and nickel. Typical examples of metal alloy are the $LaNi_5$. It can absorb up to six hydrogen atoms per molecule, to form $LaNi_5H_6$. Another example is the alloy FeTi, which can absorb two hydrogen atoms per molecule, forming $FeTiH_2$. This type of storage has several advantages compared to previous ones: the possibility to achieve high storage capacity at low pressure and temperature (close to ambient values), low energy costs, reduced overall dimensions, lower initial costs. Their major disadvantage, however, is the relatively small amount of hydrogen that they can store per unit weight. Furthermore, there are some difficulties in the management of these system as the storage capacity of these materials is strongly influenced by the reaction

temperature. As hydrogenation process is an exothermic process, it is necessary to dissipate the heat generated during the charge phase and vice versa to provide heat to the system during the discharge phase.

The hydrogen produced and stored can be used as fuel both for electricity generation and for transportation. The use of hydrogen in centralized power plants (gas turbines) and internal combustion engines is feasible based on existing technologies, with significantly reduced emissions. However, its most interesting use is for feeding proper electrochemical systems, known as fuel cells. Their development will heavily affect the future of hydrogen as an energy carrier. A fuel cell converts the chemical energy contained in the fuel directly into electricity and heat, without polluting emissions. Therefore, its performance are generally better than traditional combustion engines because of its efficiency has not the limitation of thermodynamic cycles.

As the electrolyzer technology, a single cell consists of two electrodes of porous material, separated by an electrolyte. The reactions occurring at the electrodes mainly consume hydrogen and oxygen and produce water, activating an electric current in the external circuit. The electrolyte, which has the function of conducting the ions produced by the reaction, closes the electrical circuit within the cell. Constructively the cells are arranged in series and assembled into modules, called stack, to achieve the required power. Depending on the electrolyte, it is possible to define different fuel cell technologies, as shown in Table 2.3.

Table 2.3 - Types of Fuel Cells

Type	**Electrolyte**	**Operative temperature**	**Hydrogen Purity**
Alkaline Fuel Cell (AFC)	potassium hydroxide (KOH)	60-250°C	High
Proton Exchange Membrane Fuel Cell (PEMFC)	Polymer membrane	60-80°C	Really high
Phosphoric Acid Fuel Cell (PAFC)	Concentrated phosphoric acid	150-220°C	High
Molten Carbonate Fuel Cell (MCFC)	Combination of alkali carbonates	600-700°C	Low
Solid Oxide Fuel Cell (SOFC)	Solid, nonporous metal oxide (usually YSZ)	800-1000°C	Low

The choice of the electrolyte mainly influences the operating temperature, but also the hydrogen purity the fuel cell can accept.
Sometimes, a direct methanol fuel cell (DMFC) is categorized as another type of fuel cell. However, according to the categorization based on electrolyte, it is essentially a PEMFC that uses methanol instead of hydrogen as a fuel. The main electrochemical reactions in various fuel cell are summarized in Figure 2.3.

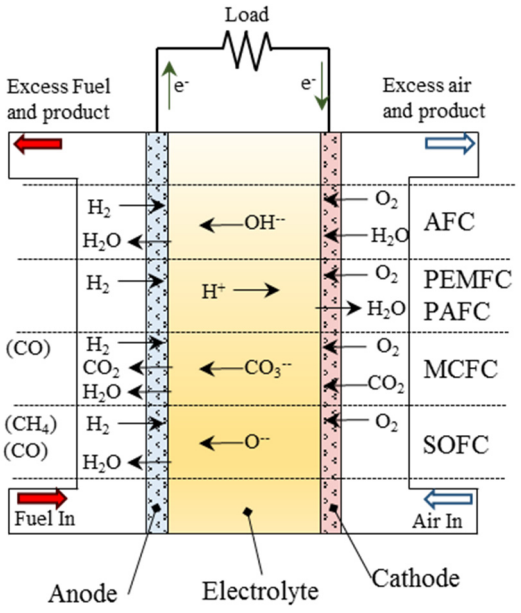

Figure 2.3 - Reactions inside the fuel cells

Chapter 3

Optimal generation scheduling for microgrids

The control and operational strategies of a microgrid can be significantly different from those of the conventional power systems because of the different characteristics of its supply and demand. In particular, in large electricity networks, variations of different loads inside the grid may neutralize or attenuate the effects on the total demand, resulting in less variation and especially less outliers in system load [17]. On the other hand, smaller electrical grids, such as microgrids, causes weaker smoothing effects of load aggregation, leading to higher volatility and sharper variations in the microgrid load [18]. Another important difference is due to the intermittent nature in power production of renewable generators. Because of wind speed and solar radiation change with time of day and seasons, variable power productions are introduced in the grid. Nowadays, these fluctuations can be balanced by conventional power systems while problems with intermittent electricity from RES could especially occur in microgrids with a high penetration of renewable sources. The uncertainty on power production and load request becomes extremely high in stand-alone power systems, where the absence of an upstream grid prevents compensation and regulation actions and local generators are the only source of power supply.

Optimizing the operation of a microgrid is essential to reduce fuel costs, energy not served, power losses, and polluting emissions. To achieve this objective, it is important to provide the control system of advanced tools

and techniques for the optimal operation of the facility. Among them, the introduction of a generation scheduling of the different devices in the energy management strategy (EMS) is a fundamental task. Generation scheduling can be divided into two different problems: Unit Commitment (UC) and Economic Dispatch (ED) [19]. The Unit Commitment strategy defines the on/off status of devices over a daily or weekly time horizon while respecting system constraints. The Economic Dispatch strategy defines the operating power of the units committed by the UC problem for a shorter time horizon (hourly or in real-time). In other words, the UC problem determines the startup and shut down units scheduling of to meet the required demand. For this reason, the UC problem is typically a mixed integer optimization problem. The output usually involves binary variables where the state "1" indicates the commitment of the unit. Instead, the objective of the Economic Dispatch is to allocate the power demand among the generators committed by the UC strategy in the most economical manner while all physical constraints are satisfied. The use of the committed generators is imposed as a constraint in the formulation of this problem while the output entails the use of real variables for the definition of the power levels.

Both ED and UC problems involve the use of forecasts of load demand and RES availability. For its statistical nature, these data are affected by errors, and the uncertainty increases with decreasing the number of different loads as well as increasing the penetration of renewable energy sources in the microgrid. Especially for the unit commitment problem, the inclusion of appropriate tools for managing uncertainties is essential. For this reason, two approaches are usually adopted in literature: reserve requirements and stochastic approach programming [20]. The first one uses a deterministic approach and introduces an explicit excess load capacity (called operating reserve) to be satisfy in the formulation. Reserve requirements are widely used in the industry and there is extensive research published on the least-cost operation of power systems subject to operating reserve constraints. However, the uncertainty is not modeled explicitly with this approach, and the resulting policy may not be economically efficient. Instead, the stochastic approach programming for uncertainty management is stochastic programming, which uses an explicit model of uncertainty in the decision process. Despite the higher computational costs of stochastic approach with respect to a deterministic formulation, a more robust schedule is produced:

a less sensitivity on unexpected demand is achieved and a variation in the foreseen conditions marginally affects the results of the scheduling. Moreover, a reduction in the expected costs should be attained due to the lower necessity of the operating reserve requirement.

Unlike the unit commitment problem with the involvement of sole power generators, a proper EMS should be implemented if energy storage systems are also introduced in the microgrid. In this circumstance, the EMS should be able to find not only the best way to satisfy the load demand but also the management of the excess energy. For microgrid with a single energy storage system, for instance batteries, the excess energy can be stored or sold to the upstream grid, depending on the requests and demand of energy and the prize of electricity. If several energy storage systems are present, a greater involvement of generation scheduling is required in the management of excess energy. For instance in stand-alone power systems or in microgrids with a high RES penetration, batteries are suitable for short-term storage but do not appear to be appropriate for medium-term or long-term storage because they have a low energy storage density and suffer from the self-discharge phenomenon. In this case, the EMS must be able to schedule in an appropriate way the use of the various energy storage systems in order to guarantee the electrical energy required by the users, efficiently manage all the equipment and minimize the operating costs. For example, when a high excess of energy was produced by RES generators and a proper energy reserve was still present, the use of the long-term storage system should be preferred. Vice versa, if high volatility in the demand and energy production was detected, short-term storage should be favorite.

In this chapter, a novel algorithm for the optimal generation scheduling of the microgrid equipment is introduced. In particular, a mathematical model to minimize the utilization cost and maximize the overall efficiency of the microgrid is presented while different constraints due to equipment limits must be satisfied. A stochastic approach instead of a deterministic one is chosen to take into account the uncertainties. Starting from the weather forecast data and the expected load demand, different scenarios are generated and collected in a scenario tree. Rolling planning is used to update data and permit a continuous revision of the results.

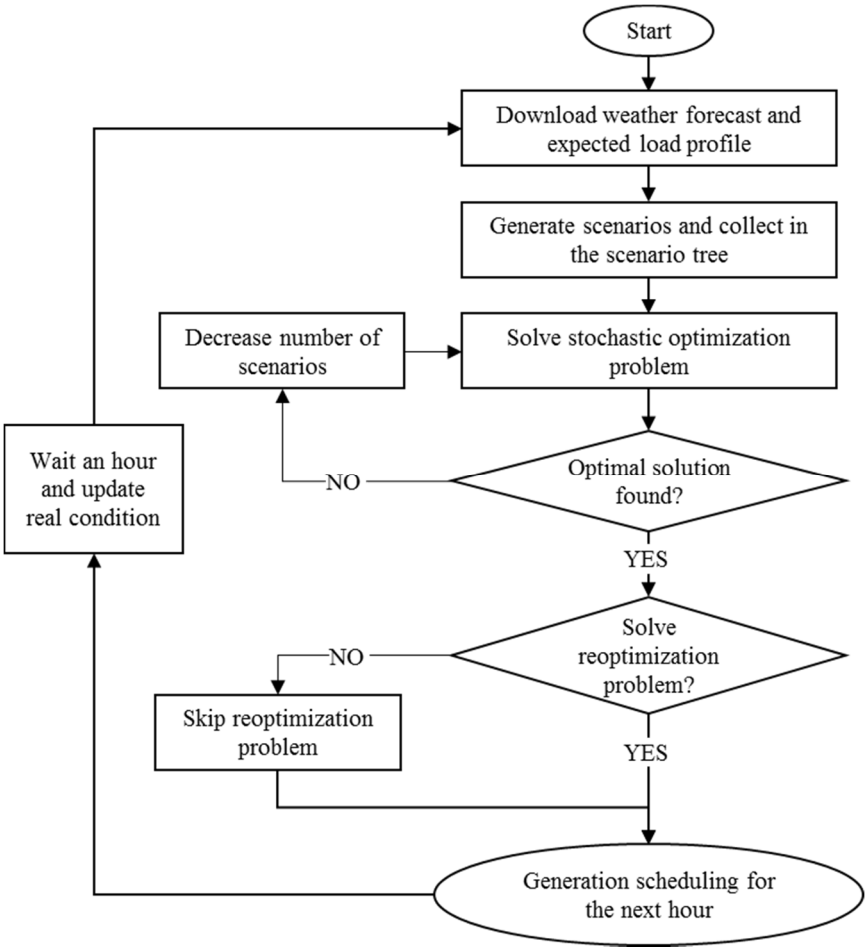

Figure 3.1 - Optimal generation scheduling algorithm

3.1. Overview of the proposed approach

The optimization processes in operation phase are often complicated due to the calculation time constraint to which they are subject. Models not too complex, possibly linear or linearizable, are often preferred and proper precautions should be taken if the optimum was not found in the required time. The developed algorithm to solve the generation scheduling problem is shown in Figure 3.1. The first step of the algorithm is the input phase where current conditions of the system are measured, meteorological data are downloaded via a weather forecast service and the most probable load curve is generated.

According to the provided conditions, the generation of the various scenarios and the formulation of the stochastic optimization problem are carried out followed by the resolution step. If the solver does not find the optimum, a simplification phase may occur with the decrease of the number of scenarios. Eventually, the statistical problem will be reduced to a deterministic problem with the most probabilistic scenario if problems in the finding the optimum persist. The results obtained by the stochastic problem resolution represent the unit commitment of the microgrid for the next hours. If the resolution of the economic dispatch problem is also needed or rather indications about the power flow are required, a re-optimization phase is planned and the results are sent to the control system. Schedules are constantly updated to take into account changes in wind, load and available units from one planning period to the next.

In this thesis, the proposed approach will be applied to small micro-grids based on the use of renewable sources, with particular reference to solar and wind power plants, integrated with energy storage systems using batteries and hydrogen storage systems. For this reason, a proper mathematical problem will be formulated for this specific microgrid configuration. However the proposed approach is generally applicable to all microgrid configurations, with the involvement of other energy storage systems, loads and RES generators.

3.2. Scenario tree approach:

The scenario tree approach was adopted to introduce uncertainties into the methodology, since weather data can be forecast only within a very limited time frame and are always subject to deviations. Similarly, another system variable that cannot be directly controlled is the actual energy demand of the microgrid, which depends on many factors (weather conditions, occupants' behavior, etc.). To deal with these uncertainties in energy consumption and electricity production from PV and WT, a scenrario approach is usually chosen. As described in [21], the usual approach for a scenario analysis is to model a set of S independent scenarios to find the best one. However, this approach is very calculation intensive, since in many cases a large number of scenarios have to be considered.

Moreover, the calculations must be continuously replicated when the new forecasts are available. To reduce the number of decision variables

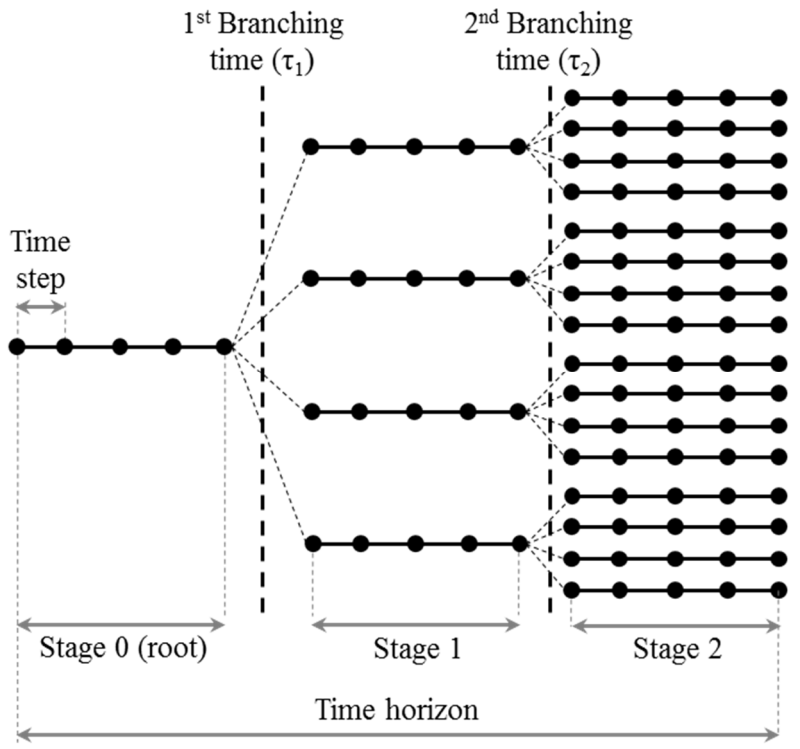

Figure 3.2 - Scenario tree structure

Pallottino et al. [21] used a so-called scenario tree approach applied to the water resource management. This approach aggregates into a single bundle the set of scenarios sharing a common portion of data. In this way, the common portions of the S independent scenarios are aggregated into bundles by producing a tree structure, as shown in Figure 3.2. The main concepts behind the aggregation process of the scenario tree are the branching time and the stage. The branching time τ is the time in which the scenarios begin to differ, while the stage is the period between two branching times. Each dot of Figure 3.2 represents the generation scheduling during a time step Δt. Up to the first branching time, that is during stage 0, all decisions for the different scenarios are the same despite different evolutions in load demand and RES availability are already considered in this period: this represents the root of the scenario tree.
After the first branching time, a number n_1 (4 in the Figure) of different possible decisions can occur, in stage 2 a number $n_1 \times n_2$ (16 in the Figure)

can befall, and if a further branching time is present, a new multiplication of the number of scenarios will occur until the time horizon will be reached. In the problem under consideration, different evolutions of the variables affected by uncertainties are generated with a corresponding probability and possible generation scheduling are aggregated in a scenario tree. The root of the scenario tree corresponds to the time at which decisions have been taken (common to all scenarios). In other words, up to the first branching time the generation scheduling is the same for each scenarios. In this way, the decision could be non-optimal for an individual expected load and RES availability scenario but the optimum taking into account the weighted average of all of the possible load and weather evolution (where the weights are the probabilities of the event occurrence). The decision will still be feasible even if the worst scenario occurs (i.e. those with the smallest probability). In other words, this approach allows to obtain more robust decisions than the simple deterministic case. The leaves of the scenario tree represent possible evolutions of the generation scheduling in the last stage. Each back path from a leaf to the root identifies a possible scenario of the generation scheduling.
The implementation of this stochastic approach to the mathematical model is expressed through a set of congruity constraints representing the requirement that the subsets of decision variables, corresponding to the indistinguishable part of different scenarios, must be equal among themselves.

The main parameters greatly affecting the generation scheduling are the first branching time, the time step and the time horizon. The first branching time defines the duration of the stage 0 that is the period in which the decision is taken. An excessive duration of the stage 0 could introduce a too strict constraint and the problem could become infeasible, especially if the difference between the best and worst scenario is remarkable. On the other hand, a first branching time too close in time could lead to a less robust solution.
The time step is the minimum amount of time in which each decision remains unchanged, represented in the scenario tree in Figure 3.2 by dots. A small value of this parameter introduces flexibility in decisions and a more rapid response to prospective events. On the other hand, with a small time step an increase of the computational load could occur and the model may not be suitable for a real-time control. In addition, a more strict

constraint in the minimum up and down time of the generators should be introduced.

The time horizon (or forecast horizon) is a fixed point of time in the future at which the generation scheduling will be evaluated. A high value of this parameter enables the control system to predict and to figure out what will be the future events and then to take a more consistent decision in the present time. However, the uncertainties and errors in the predictions increase with time (especially for the weather forecast) and the additional data would therefore be useless if not harmful for the control system. Furthermore a significant increase in the computational load will occur due to the increase of the number of variables with possible problems in the determination of the optimum.

3.2.1. Rolling planning

A rolling planning strategy is used to update data and permit a continuous revision of the results. The update time of the generation scheduling (called rolling time) depends on the specific system configuration. Microgrids with a high penetration of RES generators greater benefit from a more frequent rolling time: the error are significantly limited and the decisions taken by the control system are closer to the optimum reached by a perfect forecast of the actual weather conditions. Moreover, a more frequent rolling time might be helpful when the load commonly diverged than expected and the real-time control is forced to change the generation scheduling. In this case, the status conditions of the storage systems are frequently updated and the demands of user are fulfilled optimally. The EMS benefits from the update status of storage systems and real user requirements. In contrast, a too frequent rolling time would be useless and would only lead to a raise in the computational time especially for systems where the role of RES is marginal or generators with high start-up times are present.

An example of application of the rolling planning with the scenario tree approach is shown in Figure 3.3. The example shows how a scenario tree with a stage 0 duration of 3 hours, a time step of 1 h and a total number of 4 scenarios is updated in time with a frequency of rolling equal to 1 h. From the starting point, a first scenario tree is generated, with a first branching time expected after 3 hours.

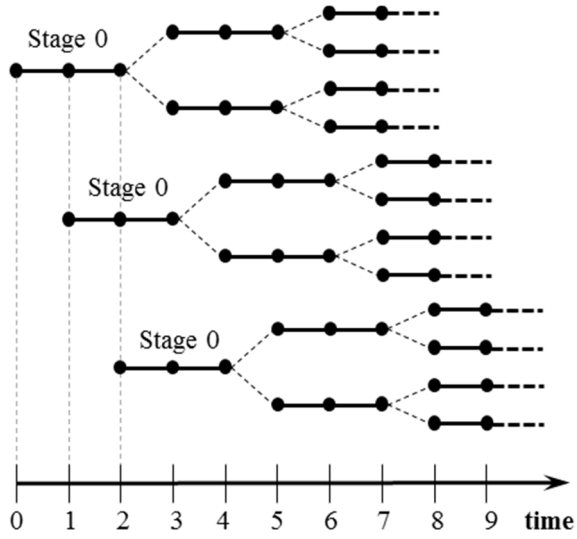

Figure 3.3 - Rolling planning with scenario tree

However, only the decision taken in the first hours is actually applied because an update of the scenario tree occurs after one hour and a new scenario tree is generated with possible changes respect to the previous generation scheduling. This update will be carried out again the next hour and so on. It is worth noting that despite a decision for the next three hours was taken, it is changed over time. In other word there is a partial independence of the frequency of rolling with the first branching time as it may be less than or at least equal to the duration of the stage 0.

3.2.2. Scenario definition

Several methods were introduced in the literature to generate the load and renewable power scenarios ([22], [23], [24]). One common method is to discretize the probability distribution function (PDF) of the forecasting error by a set of finite states such that a probability is assigned to each state. In this way, by coupling the error value of the i^{th} state (e^i) with its corresponding probability (ρ^i), it is possible to define discrete probability distribution sets for load demand (δ_D), wind speed (δ_W) and solar radiation (δ_G) in accordance with [24]:

$$\delta_D = \{(e_D^1, \rho_D^1), (e_D^2, \rho_D^2), \dots, (e_D^n, \rho_D^n),\} \quad (3.1)$$

$$\delta_W = \{(e_W^1, \rho_W^1), (e_W^2, \rho_W^2), \dots, (e_W^m, \rho_W^m),\} \quad (3.2)$$

$$\delta_G = \{(e_G^1, \rho_G^1), (e_G^2, \rho_G^2), \dots, (e_G^q, \rho_G^q),\} \quad (3.3)$$

where n, m and q are the number of states in the discrete set of load, wind speed and solar radiation forecasting errors. A set of scenarios can be created from the discrete sets δ_D, δ_W and δ_G to take into account possible deviations from the load, wind speed and solar radiation forecasting values. The product of the number of states n, m and q is equal to the total number of scenarios (S), whereas the probability for each scenario (ρ) is equal to the product of the probabilities of the states corresponding to that scenario. A possible discretization of the PDF curves is shown in Figure 3.4 with a discretization in 3 states for solar radiation and 5 states for load and wind speed.

The solar radiation PDF shows a low value of standard deviation with a high probability in the 100% forecast scenario whereas a more uniform distribution occurs for the wind speed and load due to a higher probability of errors in the forecast.

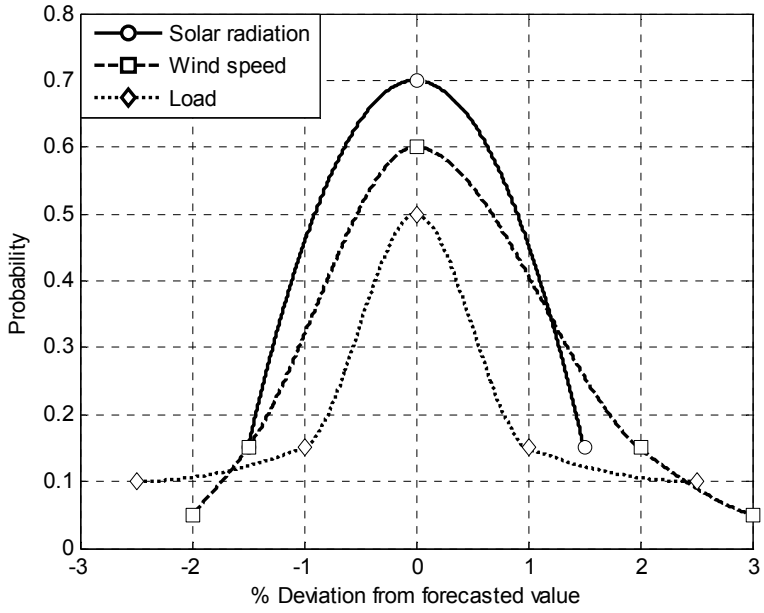

Figure 3.4 - Discretized probability distribution functions of the load, wind speed, and solar radiation forecasting errors.

Despite a constant shape of the PDFs can be used in the generation scheduling, a more accurate and efficient scenario generation is achieved when changes in the PDF shapes are introduced as function of the current and foreseen conditions. Hereinafter, the methodology used to create various scenarios is described.

Solar radiation

Solar energy have an intrinsic uncertainty due to the temporary weather conditions. In addition, it is characterized by having interruptions for the alternating day-night and it is affected by the seasonal cycle that varies the daily production throughout the year. Situations may arise in which the occasional passage of clouds covers all or part of the solar panels, or the solar power system does not receive for a long time direct solar energy due to bad weather conditions.

The solar cycles and their daily and seasonal variations are widely known. The uncertainty of the solar source is mainly due to the cloud cover to which the site under consideration is subject. In clear sky conditions, the direct solar radiation is predominant on the diffuse one and close to the extraterrestrial solar radiation. In these conditions, the error of the weather forecast is minimal and a higher solar radiation is impossible. The creation of a scenario with a solar radiation higher than that expected is impossible for the nature of the source and the discretization of the solar radiation PDF has to take into account of it.

The methodology used to deal with the uncertainty of the solar radiation starts from the calculation of the clearness index Kt. The latter is defined as the ratio of the horizontal global irradiance to the corresponding irradiance available out of the atmosphere (the extraterrestrial irradiance is the Solar constant -1367 W/m²- corrected by a yearly sinus function of amplitude 3.3% accounting for earth orbit ellipticity).

Therefore, an indirect definition of the cloudiness of the site under consideration is possible and a subdivision by solar radiation for classes is carried out:

1. Class 1 – Clear sky conditions, clearness index higher than 70%
2. Class 2 – Partly cloudy, clearness index of between 30% and 70%
3. Class 3 – Cloudy day, clearness index lower than 30%

Depending on the assigned class, the algorithm generates three different scenarios of which probability are functions of the clearness index and the distance in time.

Table 3.1 shows the probability assigned to each scenario. The values reported in the table are the results of a preliminary comparative analysis between forecasts and actual conditions. The subdivision into 3 sun classes was carried out to prevent a substantial increase in the number of scenarios. However, a larger number of classes could be considered with an increase of the generated scenarios. As explained in Table 3.1, if a clear day is expected (Class 1) for the current day, the probability that this scenario occurs is very high. However, two other scenarios are generated: a partly cloudy and an overcast scenario. The first one presents a small probability but fleeting clouds formation is possible. Instead, the probability of overcast weather is very low and only due to an algorithm error. For instance, solar radiation daily profiles generated for a summer sunny day is shown in Figure 3.5.
A similar generation scenarios is carried out during bad weather conditions where the cloudy day scenario has a high probability while the occurrence of the clear sky scenario is almost impossible. Unlike the other 2 cases, the case of partial cloudiness is rather uncertain: a sudden worsening of weather conditions could cause a significant reduction of the power produced by solar power systems (especially for concentrating solar power plants) or a sudden improvement may increase production. This increased sensitivity is properly taken into account by the discretization of the PDF.

Table 3.1 - Scenario probability for solar radiation

		Clear sky scenario	Partly cloudy scenario	Cloudy day scenario
TODAY	**Class 1**	0.84	0.25	0.01
	Class 2	0.22	0.56	0.22
	Class 3	0.01	0.20	0.79
TOMORROW	**Class 1**	0.75	0.24	0.01
	Class 2	0.24	0.52	0.24
	Class 3	0.01	0.28	0.71
DAYS AFTER TOMORROW	**Class 1**	0.68	0.30	0.02
	Class 2	0.26	0.48	0.26
	Class 3	0.02	0.34	0.64

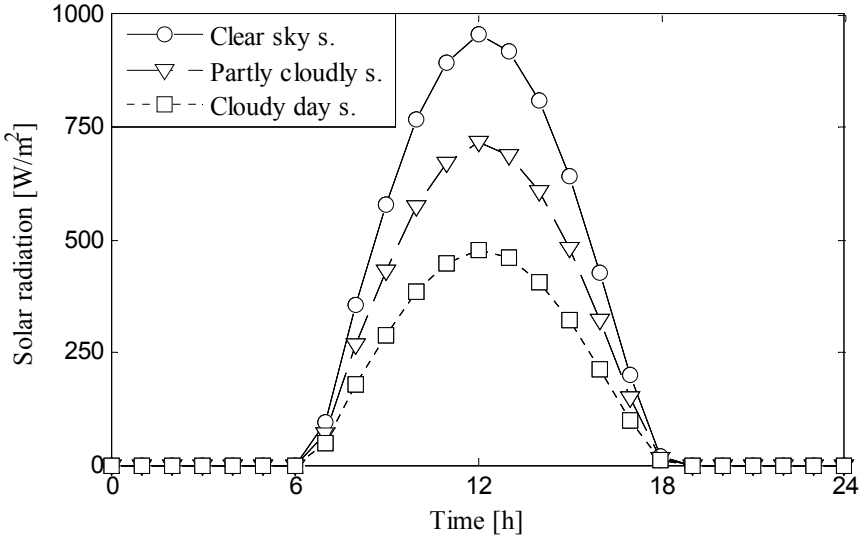

Figure 3.5 - Different solar radiation scenarios for a sunny day

Although a partly cloudy scenario preserves the highest probability of occurrence, both the clear sky and overcast scenarios have a significant probability.

Wind speed

The accuracy of the wind speed forecast is usually lower than that of solar radiation forecast. The wind velocity could remarkably change during the time step and a much more volatile and uncertain WT power production may occur. Moreover, even if a mean wind speed value was perfectly forecasted, errors in the wind turbine power production could be introduced by the effect of gust of wind. Various different factors contribute to the overall WT power forecast error such as the accuracy of the forecasts for individual wind farms, the forecast horizon, the size of the individual wind farms and the atmosphere stability.

In this work, only three effects are taken into account in the definition of the wind power forecast error: the error in the foreseen mean wind speed, the effect of gusts and the effect of forecast horizon. The error due to imprecision in the average wind velocity can be expressed as a normal distribution as shown in Figure 3.4.

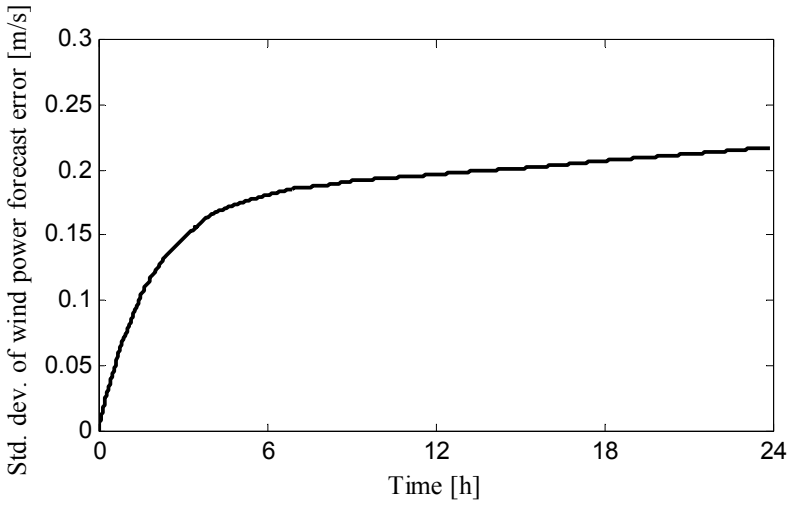

Figure 3.6 - Standard deviation of wind power forecast errors versus the forecast horizon

The wind gust value is usually included in the weather service. The gap between this value and the average speed can be a qualitative measure of the turbulence of the atmosphere and an increase of the standard deviation of the PDF with this difference should be introduced. For instance, a wind turbine present a cut-in speed, that is the speed at which the turbine first starts to rotate and generate power (usually between 3 and 4 m/s).
If a mean wind speed lower than the cut-in speed is forecast, the most probable scenarios will be a no power production from wind turbine. However, a small amount of power could be produced anyway by gust of wind and the probability of the more optimistic scenario should be increased. Finally, wind power forecast errors generally increase as the forecast horizon increases. According to [25], an increase in the standard deviation is introduced as shown in Figure 3.6.

Load forecast

Like any forecast, load forecasts have an error associated with them. Due to the highly repetitive nature of the daily load profile, load forecast errors are not especially sensitive to the forecast horizon and are usually proportional to the size of the load at any given hour. The hourly load forecast error is modeled as a Gaussian stochastic variable with a mean of zero as shown in Figure 3.4

3.3. Problem formulation

Starting from the different generated scenarios of solar radiation and wind speed conditions, the expected power produced by the solar power system and wind turbine can be calculated for each time step Δt until the forecast horizon θ. Since these systems are powered by renewable sources, it is assumed that they always operate at their maximum power point.

For given values of the possible load demand and renewable generator production, the purpose of the generation scheduling is to determine the optimal operation of storage devices (batteries, electrolyzer, fuel cell) and other generators (i.e. Diesel generators) that assure the minimum operating cost of for the microgrid.

3.3.1. Model definition

To enable the EMS to predict the performance of the system, a simple simulation model of each device is introduced. In the following subchapters, the simulation models for each component are described in detail. Despite the lower accuracy, the adoption of simple simulation models is essential to reduce the computational time and to allow a fast running of the EMS during the operating phase of the microgrid. In this work, only photovoltaic system and wind turbine are considered. Nevertheless, it is possible the introduction of other renewable generators such as concentrated solar system, micro hydro, biogas engines etc.

Photovoltaic system

It is assumed that the PV system always operates at its maximum power point and therefore its operation is independent from the EMS. At a given irradiation condition and module temperature, the working voltage of the PV is adjusted by the MPPT (Maximum Power Point Tracking) control system to maximize the power output of the array. The following relation is used to describe the power output P_{PV} of the PV system:

$$P_{PV} = G \cdot A_{PV} \cdot N_{PV} \cdot \eta_{PV} \tag{3.4}$$

where G is global sun irradiance (W/m^2), A_{PV} the panel area (m^2) and N_{PV} the total number of panels. The efficiency of the solar panel η_{PV} is expressed as a function of irradiance G and ambient temperature T_{AMB} as follows:

$$\eta_{PV} = \eta_{PV,REF}\left[1 - \alpha\left(T_{AMB} + G\frac{NOCT - 20}{800} - T_{REF}\right)\right] \quad (3.5)$$

where $\eta_{PV,REF}$ is the efficiency of the panel under reference conditions (1000 W/m^2 of solar irradiation and 25 °C of cell temperature), α is the temperature coefficient (1/K), NOCT is the nominal operating cell temperature and T_{REF} is the reference module temperature (25 °C). All of these parameters are provided by the panel manufacturer.

Wind turbine

Similarly to the PV system, the power produced by the wind turbine is independent from the EMS. Based on wind speed at hub height, the power output of the wind turbine is calculated from the manufacturer's power curve.

Batteries

The use of batteries to compensate for the differences between energy production and energy demand is the most common solution in microgrid projects involving RES. The addition of a hydrogen storage system leads to a different managing of batteries to maximize their efficiency and lifetime. The available energy content of an electric battery is commonly measured through the so-called "state of charge" (SOC). The latter is the ratio between the stored energy and its nominal storage capacity and is calculated by monitoring the charging (P_{BC}) and discharging power (P_{BD}) over time:

$$SOC_t = SOC_{t-1} + \frac{(P_{BC} \cdot \eta_{BC} - P_{BD}/\eta_{BD})\,\Delta t}{N_B U_B\, Q_B} \quad (3.6)$$

where η_{BC} and η_{BD} are the battery efficiencies during charge and discharge processes respectively, Δt is the applied time step (h), N_B is the number of batteries, Q_B is the battery nominal capacity (Ah) and U_B is the battery nominal voltage (V). The assessment of the actual batteries efficiency is often difficult. It depends on various parameters such as current, SOC, power demand, charging or discharging phase, lifetime etc. In order to simplify the model, a constant value equal to the square root of the roundtrip efficiency provided by the manufacturer could be used. However, a mismatch between forecast and actual data should be expected in this case.

Hydrogen storage system

The use of hydrogen storage systems, alone or in addition to batteries, has been the subject of several studies and research activities in recent years. In hydrogen storage systems, an electrolyzer produces hydrogen when the power delivered by RES is higher than demand. Applying Faraday's law, the hydrogen molar flow of the electrolyzer ($n_{H_2,EL}$) can be expressed as a function of the supplied electric power (P_{EL}):

$$n_{H_2,EL} = \frac{\eta_{EL}\, P_{EL}}{LHV_{H_2}} \tag{3.7}$$

where LHV_{H_2} is the lower heating value of hydrogen (240 MJ/kmol) and η_{EL} is electrolyzer efficiency.

The hydrogen can be used to produce electrical energy by means of a fuel cell during peaking periods. Hydrogen consumption of the fuel cell ($n_{H_2,FC}$) is directly related to its power output (P_{FC}) through the following relationship:

$$n_{H_2,FC} = \frac{P_{FC}}{\eta_{FC}\, LHV_{H_2}} \tag{3.8}$$

where η_{FC} is fuel cell efficiency. Both electrolyzer and fuel cell efficiencies take into account electrochemical, ohmic and ancillary losses and are function of the power. Consequently, Eq. (3.7) and (3.8) are nonlinear equations. However, the nonlinearity can be well approximated with a piecewise linear interpolation, especially when ohmic losses are prevalent. An important control variable of a hydrogen storage system is the hydrogen tank level HL defined as the ratio of the hydrogen content at certain time t to the hydrogen content where the tanks are fully charge. Therefore, hydrogen tank level measures the hydrogen content inside the vessels and can be expressed in function of the produced ($n_{H_2,EL}$) and consumed hydrogen molar flows ($n_{H_2,FC}$) as well as the level at the previous time step HL_{t-1} as follows:

$$HL_t = HL_{t-1} + \frac{V_M}{V_{H_2}}(n_{H_2,EL} - n_{H_2,FC})\Delta t \tag{3.9}$$

where V_M is the molar volume and V_{H_2} is the overall tank volume.

It is worth noting that the value of the hydrogen tank level is directly proportional to the tank pressure for a gas-pressurize storage, while this dependence becomes a function of the pressure– composition–temperature (P–C–T) curve if a metal hydride storage system is used. If a compressor is not included in the hydrogen storage section, the maximum pressure of the hydrogen tanks corresponds to the hydrogen delivery pressure of the electrolyzer.

3.3.2. Utilization costs during charging process

When excess power produced by PV and WT generators needs to be stored, the proposed algorithm allows to assess the most convenient storage system. In particular, the control system calculates and compares the utilization costs of the batteries and the hydrogen storage systems for cycling the energy corresponding to the available power P during a time step Δt in alternative to sell this excess energy to the grid. Because of the absence of fuel costs, the utilization cost C takes into account only depreciation and replacement costs C_{IN} and operating and maintenance cost $C_{O\&M,}$ for each device used:

$$C = \frac{1}{\eta}\sum_{i}\left(\frac{C_{IN,i}}{L_i} + C_{O\&M,i}\right) \tag{3.10}$$

where L_i is the lifetime of the i^{th} device and η is the roundtrip efficiency. The latter has been included in Eq. (3.10) to take into account the different energy losses inside the storage systems referring to a same value of output energy. Starting from Eq. (3.10) and according to [26], the battery utilization costs C_B during charging are calculated as:

$$C_B = \frac{C_{B,IN}/L_{BC} + C_{O\&M,B}}{\eta_{BC}\eta_{BD}} \tag{3.11}$$

where $C_{B,IN}$ is the capital cost of the battery bank (€) and L_{BC} (h) is the battery lifetime evaluated during charging while the product of the battery efficiencies during charging and discharging processes gives the battery roundtrip efficiency. The O&M costs of the batteries $C_{O\&M,B}$ are of minor importance and therefore they are neglected in this study.

The battery lifetime L_{BC} in terms of hours is difficult to know, while it is more significant referring to the equivalent number of full charge/discharge cycles N_{CYCLES}:

$$L_{BC} = \frac{N_B U_B Q_B}{P_{BC}} N_{CYCLES} \tag{3.12}$$

In Eq. (3.12), the ratio of the cycled energy and its nominal capacity gives the battery operation time in terms of equivalent full cycles.

Similar to battery utilization costs, the hydrogen storage utilization costs refer to the costs of producing hydrogen through the electrolyzer and using it for fuelling the fuel cell:

$$C_{H2} = \frac{\left(\frac{C_{EL,IN}}{L_{EL}} + C_{O\&M,EL}\right) + \left(\frac{C_{FC,IN}}{L_{FC}} + C_{O\&M,FC}\right) \cdot \frac{\Delta t_{FC}}{\Delta t}}{\eta_{EL} \cdot \eta_{FC}} \tag{3.13}$$

where $C_{EL,IN}$ and $C_{FC,IN}$ are the electrolyzer and fuel cell acquisition costs, L_{EL} and L_{FC} the electrolyzer and the fuel cell lifetimes, $C_{O\&M,EL}$ and $C_{O\&M,FC}$ the O&M costs of the electrolyzer and the fuel cell, $\eta_{EL}$and η_{FC} are the electrolyzer and fuel cell efficiencies and $\frac{\Delta t_{FC}}{\Delta t}$ is the operation time of the fuel cell. Unlike the assumption of [26], the fuel cell operation time is different from the electrolyzer operation time. The operation time $\frac{\Delta t_{FC}}{\Delta t}$ is calculated assuming that the fuel cell operates at its nominal power $P_{NOM,FC}$ and uses all the hydrogen produced by the electrolyzer during the time step Δt:

$$\Delta t_{FC}/\Delta t = \eta_{EL} \cdot \eta_{FC} \cdot \frac{P_{H2,CH}}{P_{NOM,FC}} \tag{3.14}$$

The cost of excess power depends on the configuration of the microgrid (in grid-connected or stand-alone).

In case of connection with an upstream grid, the cost of excess energy C_{EX} should consider not only the income for selling energy ($C_{E,S}$) but also the future cost to buy back the same amount of energy from the grid ($C_{E,P}$) and a penalization cost due to the reduction in the spinning reserve(C_{SR}):

$$C_{EX} = C_{E,P} + C_{SR} - C_{E,S} \tag{3.15}$$

In stand-alone power systems, if the renewable generators can supply the entire demand and the storage systems are fully charged, any excess of renewable energy cannot be stored and a reduction of the power produced

by the generators is necessary. In order to avoid this power curtailment, a high virtual cost is associated with excess power.

3.3.3. Utilization costs during discharging process

If the user energy demand has to be provided by the storage system, the control system calculates the cost of supplying the energy with the batteries, fuel cells or other generators.

If the energy demand has to be provided by the storage system, the battery utilization costs during the discharge phase are equal to the average cost of supplying a certain power $P_{B,DIS}$ with the batteries for a time step Δt and is calculated as:

$$C_{BD} = C_{B,IN}/L_{BD} + C_{O\&M,B} \tag{3.16}$$

where L_{BD} (h) is the battery lifetime evaluated in a discharging step and defined as:

$$L_{BD} = \frac{N_B U_B Q_B}{P_{BD}/\eta_{BD}} N_{CYCLES} \tag{3.17}$$

If the energy demand has to be provided by the hydrogen storage system, the utilization cost of supplying the energy with the fuel cell C_{FC} is the average cost of supplying the power P_{FC} for a time step Δt:

$$C_{FC} = C_{FC,IN}/L_{FC} + C_{O\&M,FC} \tag{3.18}$$

The average cost of supplying a certain power with the Diesel generator for time step Δt is similar to the fuel cell cost but a variable cost due to fuel consumption has to be considered:

$$C_G = C_{G,IN}/L_G + C_{O\&M,G} + (\alpha + \beta P_G)C_{fuel} \tag{3.19}$$

where $C_{G,IN}$ is the generator acquisition cost, L_G the diesel generator lifetime, $C_{O\&M,G}$ the O&M costs of the generator and C_{fuel} is the fuel price (€/kg). The fuel consumption is a function of the power of the generator and can be approximated by a linear consumption curve where α and β and are the coefficients of the consumption curve.

Finally, the purchase of energy from the upstream grid could be required if the demand exceeded the production capacity of the microgrid. The cost of this power is directly connected with the price of electricity in the main grid

increased by some penalties imposed by the main distributor. For this reason, a higher cost is usually imposed for this option in comparison with the other utilization costs.
In case of no grid connection, if demand exceeds the capacity of the renewable generators and storage system is unable to cover this deficit, load shedding is needed to preserve the power balance. In order to minimize this undelivered power as much as possible, an high virtual costs is associated with this choice.

3.3.4. Start-up and shutdown costs

For each generation unit the transition phases between the offline and online states are known as the start-up and shutdown phases. During the start-up and shutdown phases, the unit is subjected to thermal stresses, which can lead to fatigue and possible permanent damages of the unit components requiring future maintenance or repairs. The sum of the average additional maintenance costs resulting from each start-up together with the total cost of the fuel used to bring the unit within its operating limits is known as the start-up cost.
Fuel cells and electrolyzer may incur in relatively large start-up cost and may take additional time to heat up various components in a controlled manner and to begin operation. Furthermore fuel cells and electrolyzers have a high thermal mass implying greater energy consumption during warm up. Start-up and shutdown costs are incurred also by diesel generators due to the use of fuel and electricity during the start/stop process. For example, compressors or other balance-of-plant equipment may operate when the prime mover starts, requiring a draw of electricity from storage or the electricity grid.

The start-up cost can be expressed as an exponential function of the amount of time the generator has been off (corresponding to large start-up costs if the generator is completely cold, reducing to small values when the generator is still warm) [27]:

$$ST_{t,i} = a_{ST_i} + b_{ST_i}\left(1 - e^{T_{t,i}^{off}/\tau_{ST_i}}\right) \tag{3.20}$$

where a_{ST_i} and b_{ST_i} are hot and cold start up cost of i^{th} generator respectively, $T_{t,i}^{off}$ the time the i^{th} generator has been off (h), and τ_{ST_i} its cooling time constant.

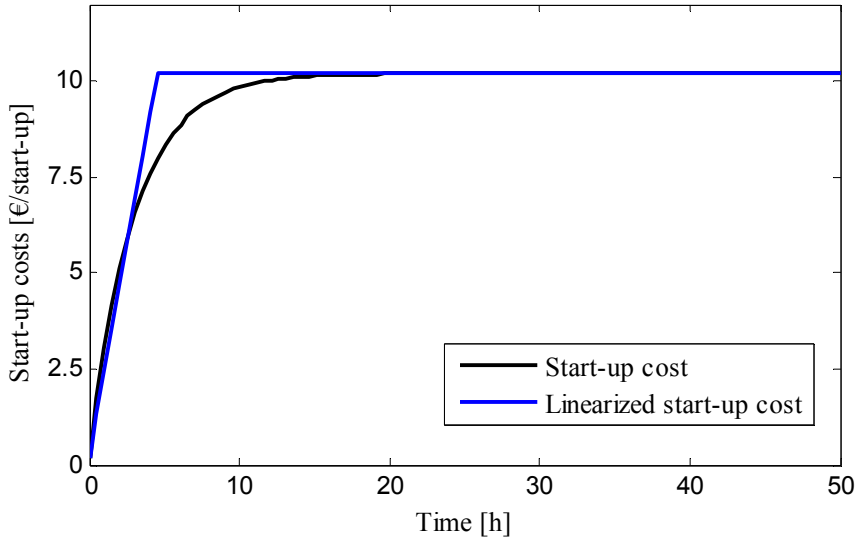

Figure 3.7 - Comparison between start-up cost curve and its linearization

In order to avoid non-linear behavior, a linearization in the start-up cost equation was introduced. In particular, starting from the hot start-up cost, the cold start-up cost is reached after an off time twice the cooling time constant with a linear trend. After that, a constant value equal to the cold start-up cost is kept. The comparison between the start-up cost curves defined with Eq. (3.20) and it linearization is shown in Figure 3.7.

3.3.5. Mathematical model

The purpose of the EMS based on the proposed generation scheduling is to determine for each time step the status of the overall microgrid giving the minimum operating costs. For this reason, the objective function (f) is formulated with the aim to minimize the sum of the utilization costs of all devices (batteries, electrolyzer and fuel cell, generators) included in the microgrid and the costs related to excess and undelivered power. According to the scheduling determined by the control system, the power values of each device (P_i) are linked with binary variables (Y_i) that determine the status of the device.

$$f = \min \sum_{s=1}^{S} \rho_s \left[\sum_{t=1}^{\theta} \left(C_{B_{s,t}} + \sum_{i=1}^{EL_n} \left(C_{H2} Y_{E_{s,t,i}} + ST_{E_{s,t,i}} \right) + C_{EX_t} P_{EX_{s,t}} \right) + \sum_{t=1}^{\theta} \left(C_{BD_{s,t}} + \sum_{i=1}^{FC_n} \left(C_{FC} Y_{FC_{s,t,i}} + ST_{FC_{s,t,i}} \right) + \sum_{i=1}^{G} \left(C_G (P_{G_{s,t,i}}) + ST_{G_{s,t,i}} \right) + C_{UN_t} P_{UN_{s,t}} \right) \right] \quad (3.21)$$

The minimization problem is subject to the following constraints:

1. Energy balance equation

The overall input power in the microgrid has to be equal to the overall output power, whatever the time step and scenario:

$$P_{PV_{s,t}} + P_{WT_{s,t}} + P_{BD_{s,t}} + \sum_{i=1}^{FC_N} P_{FC_{s,t,i}} + \sum_{i=1}^{G} P_{G_{s,t,i}} + P_{UN_{s,t}} = P_{LD_{s,t}} + P_{BC_{s,t}} + \sum_{i=1}^{EL_N} P_{EL_{s,t,i}} + P_{EX_{s,t}} \quad (3.22)$$

2. Unit generation limits

For batteries, maximum charging and discharging power ($P_{B,MAX}$) is introduced since efficiency decreases considerably for high power flows. For the same reason, a limit on the maximum power is introduced for electrolyzers (P_{EL,MAX_i}), fuel cells (P_{FC,MAX_i}) and other generators (P_{G,MAX_i}). Although the electrolytic cells can efficiently operate even at low power levels, a significant increase in ancillary losses occurs at low values of power with a decrease in the overall efficiency. Therefore, a limit on the minimum power of electrolyzers and fuel cells (P_{EL,MIN_i} and P_{FC,MIN_i}) is imposed. A minimum power limit (P_{G,MIN_i}) is also recommended for diesel generators:

$$P_{BC_{s,t}}, P_{BD_{s,t}} \leq P_{B,MAX} \quad (3.23)$$

$$P_{EL,MIN_i} \leq P_{EL_{s,t,i}} \leq P_{EL,MAX_i} \quad (3.24)$$

$$P_{FC,MIN_i} \leq P_{FC_{s,t,i}} \leq P_{FC,MAX_i} \quad (3.25)$$

$$P_{G,MIN_i} \leq P_{G_{s,t,i}} \leq P_{G,MAX_i} \quad (3.26)$$

Depending on the contract with the upstream grid, the introduction of a maximum purchasing and selling power limit could be required in the grid-connected mode:

$$P_{UN_{s,t}}, P_{EX_{s,t}} \leq P_{grid,MAX} \quad (3.27)$$

3. Storage limits

The batteries usually have a minimum SOC (SOC_{MIN}) recommended by the manufacturer below which they should not operate. The minimum SOC value greatly affects battery lifetime because a deep discharge of the batteries causes a significant decrease in the number of cycles before replacement. The maximum SOC (SOC_{MAX}) is usually reached when batteries are fully charged (100% of the SOC). However, due to the wear of batteries, this value decrease over time.

Similarly to the batteries, a minimum value of the hydrogen level (HL_{MIN}) is suggested due to a constraint on minimum fuel cell supply pressure. The maximum hydrogen level usually correspond to the maximum pressure achievable in the tanks:

$$SOC_{MIN} \leq SOC_{s,t} \leq SOC_{MAX} \quad (3.28)$$

$$HL_{MIN} \leq HL_{s,t} \leq HL_{MAX} \quad (3.29)$$

4. Ramp constraint

For several units, rapid changes in operating temperature or electrical output may lead to increased maintenance costs. Consequently, safe ramp up and ramp down rates are provided by the manufacturer. However, these may be so high, that they are not considered in the model (i.e. the ramp rate might allow for an increase from zero to full output in less than a time step). In this case, the ramp constraint can be neglected.

$$\left|P_{EL_{s,t,i}} - P_{EL_{s,t-1,i}}\right| \leq \Delta P_{EL_i} \quad (3.30)$$

$$\left|P_{FC_{s,t,i}} - P_{FC_{s,t-1,i}}\right| \leq \Delta P_{FC_i} \quad (3.31)$$

$$\left|P_{G_{s,t,i}} - P_{G_{s,t-1,i}}\right| \leq \Delta P_{G_i} \tag{3.32}$$

5. Minimum up and down times

These constraints refer to the minimum time the unit has to be on once it starts up (MUT) and the minimum time it has to be off, once a shutdown occurs (MDT). MDT constraints arise due to necessary maintenance after a unit has been shut down whereas MUT constraints typically reflect the need to minimize thermal stresses in the equipment, which could otherwise arise. Like the ramp constraint, these constraints will not be binding if the MUT and MDT are lower than the time step.

$$\left(T^{on}_{s,t-1,i} - MUT_i\right)\left(Y_{s,t-1,i} - Y_{s,t,i}\right) \geq 0 \tag{3.33}$$

$$\left(T^{off}_{s,t-1,i} - MDT_i\right)\left(Y_{s,t,i} - Y_{s,t-1,i}\right) \geq 0 \tag{3.34}$$

where T^{on} and T^{off} represent the cumulative time in which the device is switch on and off respectively.

6. Congruity constraint

This constraint requires that the binary variables determining the status of electrolyzers, fuel cells and other generators in each scenario of the same bundle are identical up to the first branching time.

$$Y_{EL_{s_1,t<\tau,i}} = Y_{EL_{s_2,t<\tau,i}} \tag{3.35}$$

$$Y_{FC_{s_1,t<\tau,i}} = Y_{FC_{s_2,t<\tau,i}} \qquad \forall s_1, s_2 \in S \tag{3.36}$$

$$Y_{G_{s_1,t<\tau,i}} = Y_{G_{s_2,t<\tau,i}} \tag{3.37}$$

3.3.6. Resolution and reoptimization process:

The formulated problem involves continuous and binary variables and it should be dealt with a mixed-integer nonlinear programming (MINLP) problem. However, several issues can occur during the solving process (time-consuming, local optimum and optimality of the solution not guarantee etc.) that force to use an alternative linear formulation of the problem.

As previously described, non-linear constraints are introduced in the minimum up and down times. However, they can be replaced with an

equivalent linear formulation as described in [28]. Starting from the definition of a new variable L_i:

$$L_i = \min\{\theta, (MUT_i - \mathrm{T}_{0,\mathrm{i}}^{\mathrm{on}})\mathrm{Y}_{0,\mathrm{i}}\} \tag{3.38}$$

It can be shown that the nonlinear constraints (3.33) for i[th] unit and $t \in [1, \theta]$ is equivalent to the following constraints:

$$\sum_{t=1}^{L_i} \mathrm{Y}_{\mathrm{t,i}} = L_i \tag{3.39}$$

$$\sum_{t=k}^{k+MUT_i-1} \mathrm{Y}_{\mathrm{t,i}} \geq \mathrm{MUT}_{\mathrm{i}}\left(Y_{k,i} - Y_{k-1,i}\right) \quad k \in (L_i, \theta - MUT_i - 1] \tag{3.40}$$

$$\sum_{t=k}^{\theta} \mathrm{Y}_{\mathrm{t,i}} \geq \sum_{t=k}^{\theta} \left(\mathrm{Y}_{\mathrm{k,i}} - \mathrm{Y}_{\mathrm{k-1,i}}\right) \quad k \in (\theta - MUT_i - 1, \theta] \tag{3.41}$$

Suppose that the i[th] unit is initially in operation and $\mathrm{T}_{0,\mathrm{i}}^{\mathrm{on}} \leq MUT_i$, Eq. (3.39) will guaranty the minimum up time constraint. Clearly, if the unit is initially de-committed or committed and $\mathrm{T}_{0,\mathrm{i}}^{\mathrm{on}} > MUT_i$, constraint (3.39) is trivial. Constraint (3.40) guaranties i[th] unit remains committed at least for MUT_i hours if it is started at $\mathrm{t} \geq 0$. Finally, the minimum up time constraints will be satisfied by Eq. (3.41) in the last $MUT_i - 1$ of the scheduling horizon. Similarly, it is possible to replace the nonlinear constraints (3.34) with the following constraints:

$$\sum_{t=1}^{F_i} \left(1 - \mathrm{Y}_{\mathrm{t,i}}\right) = F_i \tag{3.42}$$

$$\sum_{t=k}^{k+MDT_i-1} \left(1 - \mathrm{Y}_{\mathrm{t,i}}\right) \geq \mathrm{MDT}_{\mathrm{i}}\left(Y_{k-1,i} - Y_{k,i}\right) \quad k \in (\theta - MDT_i - 1, \theta] \tag{3.43}$$

$$\sum_{t=k}^{\theta} \left(1 - \mathrm{Y}_{\mathrm{t,i}}\right) \geq \sum_{t=k}^{\theta} \left(\mathrm{Y}_{\mathrm{k-1,i}} - \mathrm{Y}_{\mathrm{k,i}}\right) \quad k \in (\theta - MDT_i - 1, \theta] \tag{3.44}$$

Where F_i is defined as following:

$$F_i = \min\{\theta, (MDT_i - \mathrm{T}_{0,\mathrm{i}}^{\mathrm{off}})\left(1 - \mathrm{Y}_{\mathrm{t,i}}\right)\} \tag{3.45}$$

If nonlinear efficiency curves of batteries, electrolyzer and fuel cells were introduced, a nonlinear behavior of utilization costs (Eq. (3.11), (3.13), (3.16)) as well as of battery SOC (Eq. (3.6)) and hydrogen level (Eq. (3.9)) would occur. However, through a piecewise linear approximation [29] it is possible to solve the problem as a mixed-integer linear programming (MIP) problem.

The output signal is a binary vector that defines the commitment (value equal to 1) or not (value equal to 0) of the i^{th} unit for the next hours (depending on the scenario root duration). However, depending on the real-time control, it may be required (for example, in a coupling with a model predictive control) an indication of the optimal power of the i^{th}-committed unit. Because of the congruity constraint is applied only on the status (on/off), different values of supplied/required power are achieved depending on the considered scenario. An involvement of continuous variables, such as power values and storage levels, in the congruity constraints would make the problem infeasible. A reoptimization planning may be carried out in order to overcome this problem. From another point of view, the resolution of the economic dispatch problem could be needed depending on the real-time control system. The generation scheduling obtained with the resolution of the stochastic problem is utilized as input data together with the most probable scenario data. A new optimal solution will be found, with the same scheduling of the upstream problem and with unique values of the continuous variables.

Chapter 4

Optimal generation scheduling for the microgrid at the H_2FER Laboratory

The developed algorithm has found its first application in the management and control of a microgrid present at the H_2FER Laboratory. The microgrid was designed for studying the issues related to the use of hydrogen storage systems coupled with renewable energy systems such as photovoltaic panels and wind turbines with the objective to cover all the energy requirement of the laboratory by the microgrid as a stand-alone power plant. The use of non-programmable source generators involves the availability of proper energy storage sections and the development of suitable energy management strategies that take into account the uncertainties of both the primary energy source and the energy demand.

The microgrid is today still under construction and its completion is scheduled for the first half of 2015. This circumstance has led to the impossibility of carrying out a complete experimental tests. The modeling and simulation followed by validation tests of the models whereas it was possible allowed to overcome partially this drawback.

Together with the microgrid under consideration, the number of facilities that produce hydrogen from RES is increasing all over the world and most of them use the hydrogen for energy storage in stand-alone power generation systems [29]. In these facilities, the hydrogen storage system is often coupled with a battery bank for short-term energy storage. The

integration of batteries and hydrogen storage technologies leads to better management of transient loads and intermittent power peaks and increases bus stability [30]. Moreover, batteries usually play an important role in the control strategy of these systems, since the battery State-of-Charge (SOC) is used as the main control variable.
This kind of control system, following called SOC-based EMS**,** considers only battery SOC and hydrogen storage level to determine the power flows between the different devices as shown in Figure 4.1. In particular, when generated power exceeds the power demand and SOC is below its maximum value (SOC_{MAX}), the batteries are charged. When the batteries are fully charged and the excess power is above the electrolyzer minimum operating power, it is activated until the maximum pressure inside the hydrogen tanks is achieved. Vice versa, when generated power is less than the power required by the user, the batteries start to discharge until a minimum value of SOC (SOC_{MIN}) is reached. If the batteries reach their minimum SOC and there is enough hydrogen in the tanks, the fuel cell is turned on. The SOC-based EMS is very simple and suitable for real-time control since it requires very low computational times. However, this EMS is unable to ensure the optimal management of the system because it does not take into account the costs associated with the on/off status of the devices. Furthermore, the efficiency of the different storage devices is neglected.

The SOC-based control system is largely studied and adopted in literature and for this reason it was taken as the reference control strategy in the comparative analysis performed during the development of this thesis.
Ulleberg [31] introduced a control strategy based on the battery SOC for a PV-hydrogen storage system and showed how the performance of these systems is highly dependent on the management and control of the storage devices. Ipsakis and al. [32] presented the performance of a stand-alone power system that comprised PV, WT batteries and hydrogen storage system for three different EMS over a typical four-month periods. Several operation modes for the electrolyzer and the fuel cell were investigated introducing different hysteresis bands. A similar strategy was applied in [33], where a SOC-based EMS was used to study the performance of a microgrid based on PV, WT, batteries and unitized regenerative fuel cell system

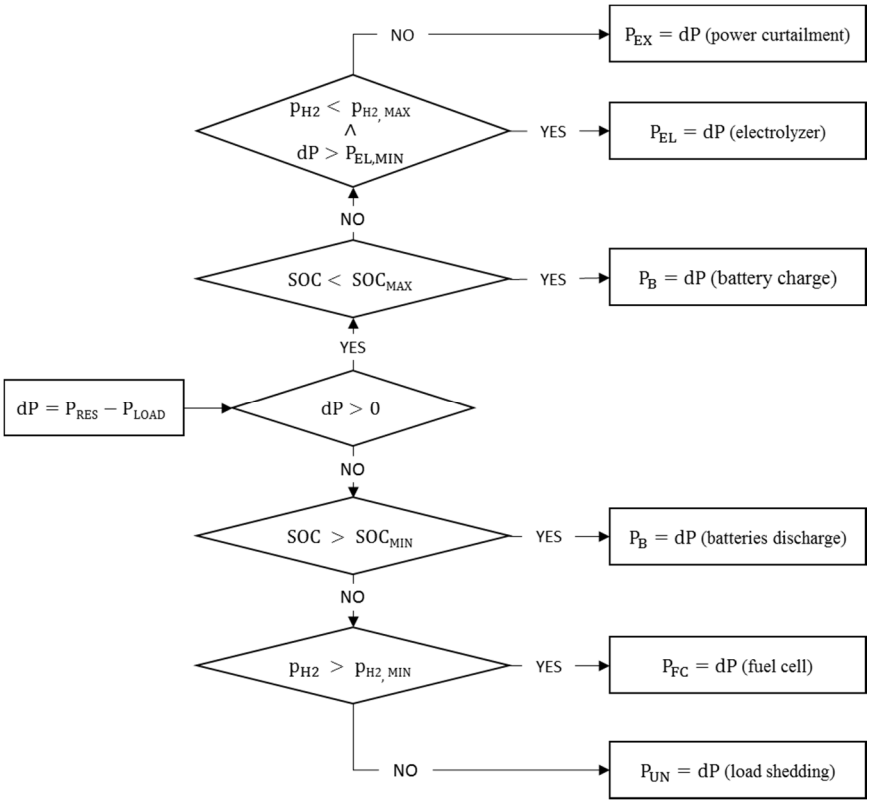

Figure 4.1 - Flowchart of the SOC-based EMS

However, none of these strategies considers the utilization costs and lifetimes of the different devices. A different EMS, based on a stand-alone power system that takes into account the utilization cost of the energy storage system, was introduced by Torreglosa et al. [34]. The comparative study carried out by Castañeda et al. [35] highlighted that the EMS based on the minimization of utilization costs leads to a higher utilization of the hydrogen system compared to EMS based on the use of the battery SOC.

All of these strategies are based on very small time horizons, of the order of seconds, therefore they are unable to predict the benefits of using the long-term ESS instead of the short-term EMS. Often the hydrogen storage system is committed when batteries are almost completely discharged in these control strategies due to its higher utilization costs in comparison with the battery. Instead, the proposed control system is based on an optimization problem that minimize the utilization costs of the microgrid

with a longer time horizon. Therefore, a greater awareness of the possible evolution of weather and load conditions are introduced in the decisions taken by the EMS and a better alternation between short-term and long-term energy storage could be achieved.

In this chapter, after an initial introduction to the mission and the activities of LabH_2FER, the simulation models of the different devices are presented in details. The capabilities of the proposed control system are subsequently discussed and compared with the results obtained with a perfect forecasted case and an EMS based on control states. Finally, the expected benefits in terms of reduction of operating costs and energy losses are assessed in an annual based comparative analysis.

4.1. Hybrid stand-alone power plant

The Concentrating Solar and Hydrogen From Renewable Energy Sources (H_2FER) Laboratory is one of the laboratories of the Renewable Energy Cluster of Sardegna Ricerche, the Sardinian Agency for R&TD. The other laboratories refer to biomass and biofuel and PV systems.
The laboratories of the Renewable Energy Cluster are closely connected to each other, and carry out their scientific and technology activities in partnership with enterprises, universities and other research centres.

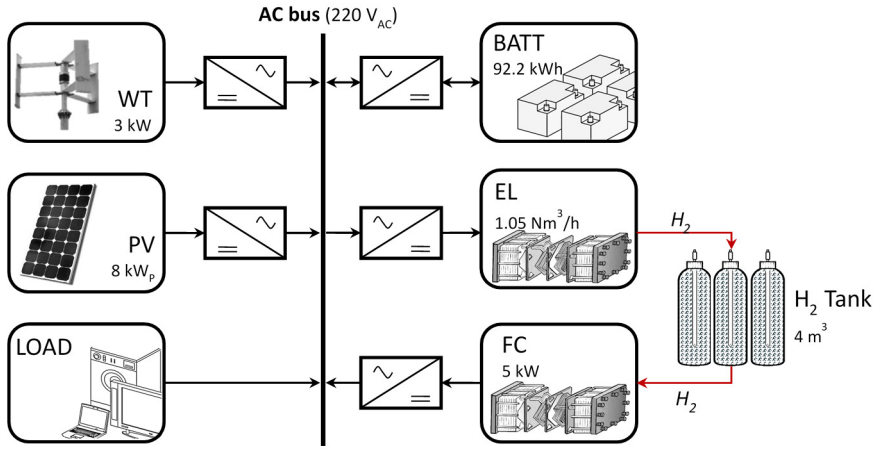

Figure 4.2 - Configuration of the microgrid at H_2FER Laboratory.

Table 4.1 - Main components and characteristics of the microgrid.

Photovoltaic system		**Electrolyzer**	
Panel peak power	0.225 kW	H_2 Net Production Rate:	1.05 Nm^3/h
Efficiency	18.1%	Delivery Pressure	13.8 barg
Solar cells	72	Nominal power	6 kW
Panel number	36	Number of cell	20
Wind turbine		**Fuel Cell**	
Rated power @ 14 m/s	3 kW	Nominal power	5 kW
Configuration	3 blades, vertical axis	H_2 rated consumption	65 Nl/min
Rotor diameter	3 m	Nominal voltage	48 V_{DC}
Hub height	5.8 m	Nominal current	115 A
Batteries		**Hydrogen Tank**	
Nominal voltage	12 V	Number	4
Rated Capacity (C100)	270 Ah	Volume/Tank	1 m^3
Batteries per string	4	Max operating pressure	22 bar
Max. Charge Current	48 A		

These laboratories are open arenas to promote cooperation of universities, research centres and industries in the field of renewable energy sources.
In particular, the activities of the Concentrating Solar and Hydrogen From Renewable Energy Sources Laboratory are oriented toward the implementation, testing and demonstration of the technologies related to the production, storage and use of hydrogen as energy carrier. The Laboratory carries out research activities on the diagnostics and electrochemical characterisation of small fuel cells and their materials, with the aim of increasing performance in terms of durability and efficiency, taking into consideration the issues related to stationary and mobile applications of fuel cells. Moreover, one of the main activities of the Laboratory is represented by the study of stand-alone hybrid systems based on renewable energy sources and hydrogen storage technologies. For this reason, the Laboratory includes a small microgrid equipped with two renewable power plants and two different energy storage systems. Figure 4.2 shows the configuration of the microgrid and Table 4.1 reports the main characteristics of its different devices.

4.2. Modeling of the microgrid devices

In order to simulate the behavior of the main components of the microgrid under different weather conditions and user demand, a specific modeling for each device was developed. The models allow to evaluate the power produced or required by the different devices on the basis of the main parameters, such us voltage, current, operating temperature, operating pressure etc. All components of the microgrid are modeled starting from their current-voltage characteristic curve and from their energy balance. However, some simplifying assumptions have been considered. The simulation models have been implemented in Matlab-Simulink.

4.2.1. Photovoltaic panel

The modeling of the electrical behavior of a single photovoltaic cell, and thus of the entire system, is performed using the equivalent circuit shown in Figure 4.3 (a) [36]. The current generator (I_{SC}) simulates the electric current created by the photovoltaic effect which is directly proportional to the solar radiation. The diode in parallel represents the physical behavior of a PN junction, the series resistor (R_S) represents the material resistance and the parallel resistor (R_P) represents the percentage of current that does not reach the external circuit. The equation of cell current (I_{PV}) as a function of voltage (V_{PV}) is:

$$I_{PV} = N_{CELL}\left[I_{SC} - I_0\left(e^{\frac{V_{PV}-R_S I_{PV}}{V_T}} - 1\right) - \frac{V_{PV} - R_S I_{PV}}{R_P}\right] \tag{4.1}$$

where I_0 is the reverse saturation current of the diode and V_T the thermal voltage, which depends on the temperature. Using the values provided by the manufacturer, it is possible to evaluate all the parameters in Eq. (4.1). The current produced by the photovoltaic effect is a function of the incident radiation (Φ) and the cell temperature (T_{cell}):

$$I_{SC} = \frac{\Phi}{\Phi_{rif}}\left[I_{SC,rif} + \alpha_{SC}(T_{cell} - T_{cell,rif})\right] \tag{4.2}$$

where $I_{SC,rif}$ is the short-circuit current at reference conditions (Φ_{rif}= 1000 W/m^2 and $T_{cell,rif}$= 25°C) and α_{SC} is the temperature coefficient provided by the manufacturer.

The evaluation of the cell temperature is carried out through the energy balance of the PV module [37]: the absorbed solar energy ($\dot{Q}_{PV,in}$) is converted into electrical energy output ($I_{PV}V_{PV}$), thermal radiative ($\dot{Q}_{rad}$) and convective energy losses ($\dot{Q}_{conv}$), and thermal energy stored in the PV module, causing the change in T_{cell}. The rate of change of T_{cell} is:

$$(mc_P)_{PV}\frac{dT_{cell}}{dt} = \dot{Q}_{PV,in} - \dot{Q}_{rad} - \dot{Q}_{conv} - I_{PV}V_{PV} \quad (4.3)$$

where $(mc_P)_{PV}$ is the effective thermal capacity of the PV module at temperature T_{cell}. The absorbed solar energy is a function of the solar radiation and it can be expressed as:

$$\dot{Q}_{PV,in} = \alpha_{abs}A_{PV}\Phi \quad (4.4)$$

where α_{abs} is the overall absorption coefficient and A_{PV} is the total area of the PV module. Because of the cell temperature is generally different from the ground and sky temperature, radiative heat transfer take place between the panel and the sky and between the panel and the ground. However, the latter can be neglected in this study, as the PV panels are placed on the roof of the Laboratory and the temperature difference between panel and ground is very little. Therefore, the radiation heat loss is given by:

$$\dot{Q}_{rad} = \sigma A_{PV}F_{ps}(\varepsilon_{PV}T_{cell}^4 - \varepsilon_{sky}T_{sky}^4) \quad (4.5)$$

Where σ is the Stephan-Boltzmann constant ($5.67 \cdot 10^{-8}$ W/m^2K^4), F_{ps} is the panel-to-sky view factor, assumed equal to 1, ε_{PV} and ε_{sky} are the average emissivity of the panel and the sky respectively and T_{sky} is the sky temperature. As suggested by [38], the values of ε_{PV} and ε_{sky} of 0.88 and 1, respectively, are used in this study while the sky temperature is calculated as a simple function of the ambient temperature (T_{amb}):

$T_{sky} = 0.914T_{amb}$.

Finally, the convective energy losses are calculated as:

$$\dot{Q}_{conv} = hA_{PV}(T_{cell} - T_{amb}) \quad (4.6)$$

Where h is the convective heat transfer coefficient. For panel tilt angles (β) below 25° and from low to moderate wind speed (v_{wind}), h can be expressed as suggested by [37]:

$$h = 1.2475[\cos\beta\,(T_{cell} - T_{amb})] + 2.685v_{wind} \quad (4.7)$$

To date, the PV system is not yet in operation, so it was impossible to carry out experimental tests in loco. Therefore, experimental data provided by the manufacturer are used for the validation of the simulation model. The comparison between simulation and experimental results are shown in Figure 4.3 (b) in terms of current/voltage characteristics.

In particular, the continuous line represents simulation data whereas circular markers indicate experimental results. A good match is achieved for both different irradiance and temperature conditions. The photovoltaic system is appropriately configured in strings of modules, connected in parallel to satisfy the inverter request. PV voltage is adjusted by appropriate switching of the DC/DC converter to maximize the average power output of the array.

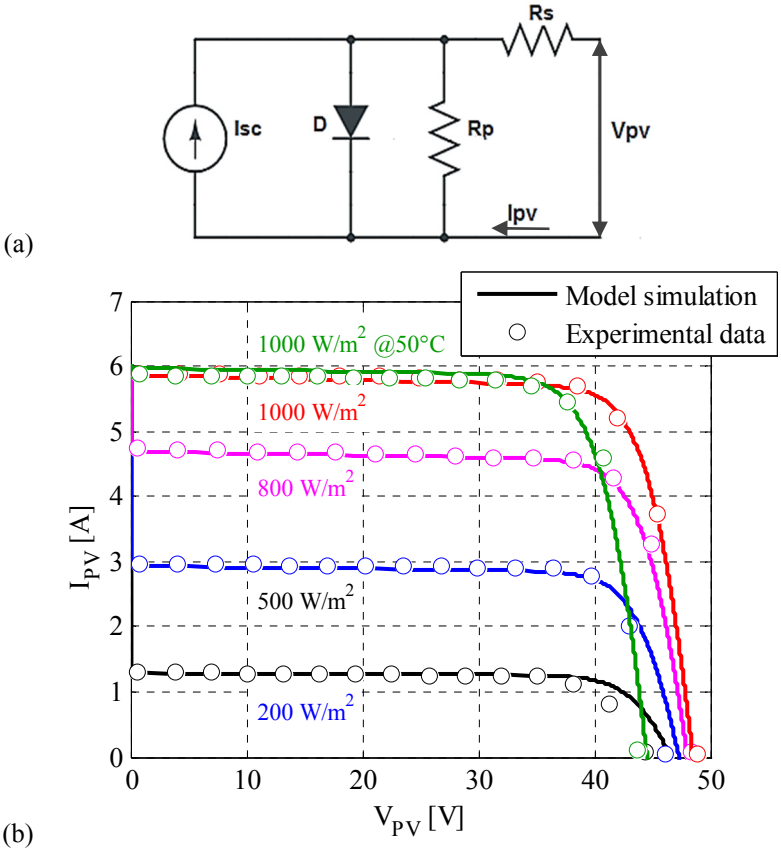

Figure 4.3 - (a) Equivalent circuit of photovoltaic cell; (b) experimental and simulated characteristic curve of photovoltaic panel.

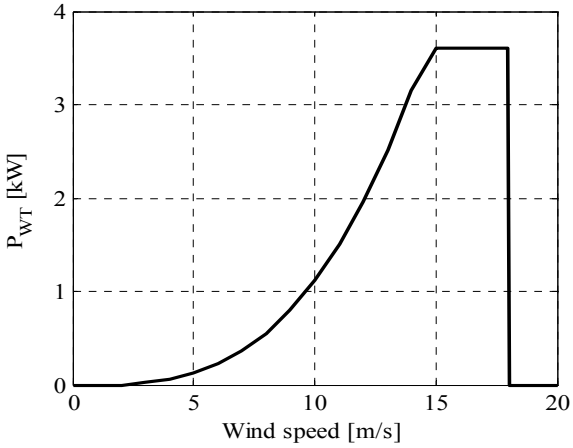

Figure 4.4 - Wind turbine power curve**.**

For given values of irradiation and temperature, the working voltage of the PV system is suitably varied by the MPPT control. The latter is carried out by a function implemented in Matlab. In addition, to take into account the energy losses of the inverter, an efficiency curve provided by the manufacturer is also introduced.

4.2.2. Wind turbine

The power produced by the wind turbine is obtained by the power curve provided by the manufacturer. Figure 4.4 shows the wind turbine power curve as a function of wind speed at hub height. A wind shear is modeled to take into account the difference in height between the hub and the anemometer.

The wind shear is a function of both altitude and roughness of the ground. The relation used to calculate the wind speed at hub height (v_{WT}) as a function of wind speed recorded by the anemometer (v_{AN}) is:

$$v_{WT} = v_{AN} \cdot \ln\left(\frac{z_{WT}}{z_0}\right) \Big/ \ln\left(\frac{z_{AN}}{z_0}\right) \tag{4.8}$$

where z_{WT} and z_{AN} are the heights from the ground of the hub and anemometer respectively while z_0 is surface roughness (assumed equal to 0.0025 m for the location of the microgrid).

The electrical behavior of the wind turbine is determined by the control of two state variables: the rotor speed (ω_r) and the generated current (I_{WT}).

Starting from wind speed at hub height, the driving torque generated by the blades on the hub (T_a) can be calculated through an appropriate control system in function of the resistant torque of the permanent magnet generator ($T_l = k\phi I_{WT}$):

$$T_a = k\phi I_{WT} - J\frac{d\omega_r}{dt} + B\omega_r \tag{4.9}$$

where k is the generator constant, ϕ the magnetic flux linkage, J the moment of inertia and B a damping constant.

A set of classical DC machine equations is considered to represent the rectifier-coupled permanent magnet alternator, typically used to direct drive small turbines. The electric system is modeled by means of a voltage generator E_{WT} (indicating the electromotive force generated by the variation of the magnetic field on the coils and directly proportional to the speed of rotation of the machine, $E_{WT} = k\phi\omega_r$), a characteristic resistance R (to take into account the resistance of the material) and a characteristic inductance L (for the presence of coils). Therefore, the output voltage of the DC generator (V_{WT}) is:

$$V_{WT} = E_{WT} - L\frac{dI_{WT}}{dt} - RI_{WT} \tag{4.10}$$

Unlike solar panels, it was impossible to validate the simulation model with results obtained by experimental data. Therefore, literature values were used in the modeling of the permanent magnetic generator [39].

4.2.3. Batteries

The modeling of the battery is based on an equivalent circuit composed by a voltage source E_B and an internal resistance R_B. The controlled voltage source as well as the internal resistance are functions of the output current (I_B) and the actual battery state of charge (SOC) [40]:

$$E_B = E_{B,0} - \frac{K}{SOC} + A \cdot e^{(-B \cdot I_{B,t})} \tag{4.11}$$

$$V_B = E_B - R_B I_B \tag{4.12}$$

where $E_{B,0}$ is the voltage under standard conditions, K is the polarization voltage, A and B are constants linked to the exponential term and $I_{B,t}$ is the

time integral of the current ($I_{B,t} = \int I_B dt$). The values of the equation coefficients are estimated from data provided by the manufacturer and with reference to [40].

The proposed model is based on the assumption that the temperature does not affect the performance, the self-discharge of the battery is not considered and the battery has no memory effect.
The previous equations highlight the importance of the SOC in determining the performance of the battery. Moreover, this parameter has a significant importance in the control and management of batteries and it is widely used as a control parameter. Unfortunately, the SOC is not easy to calculate because its determination depends on several factors. The current integration method, also known as "coulomb counting", is used in this work to calculate the SOC by measuring the battery current and integrating it in time:

$$SOC = \left(\frac{Q_B - I_{B,t}}{Q_B}\right) \cdot 100 \tag{4.13}$$

where Q_B is the battery capacity. This method suffers from long-term drift and lack of a reference point: therefore, the SOC must be re-calibrated on a regular basis, such as by resetting the SOC to 100% when a proper measuring instrument determines that the battery is fully charged.

The variation of the battery voltage with the discharge time for different values of current is shown in Figure 4.5(a): starting from a maximum value for a fully charged battery, the voltage slightly decreases with the discharge time until a voltage drop occurs when the battery is fully discharged. As for the photovoltaic panels, it was not possible to carry out experimental tests to determine the real behavior of the batteries.
However, the manufacturer has provided several experimental data and a validation test of the simulation model was possible. Experimental results for the validation of the model are indicated by markers in Figure 4.5(a).
Figure 4.5(b) shows the battery voltage as a function of the state of charge. Despite the shape is very similar, the decrease of the voltage increasing the discharge current is noticeable. The latter is due to the rise of the voltage drop due to the equivalent internal resistance introduced in Eq. (4.12).

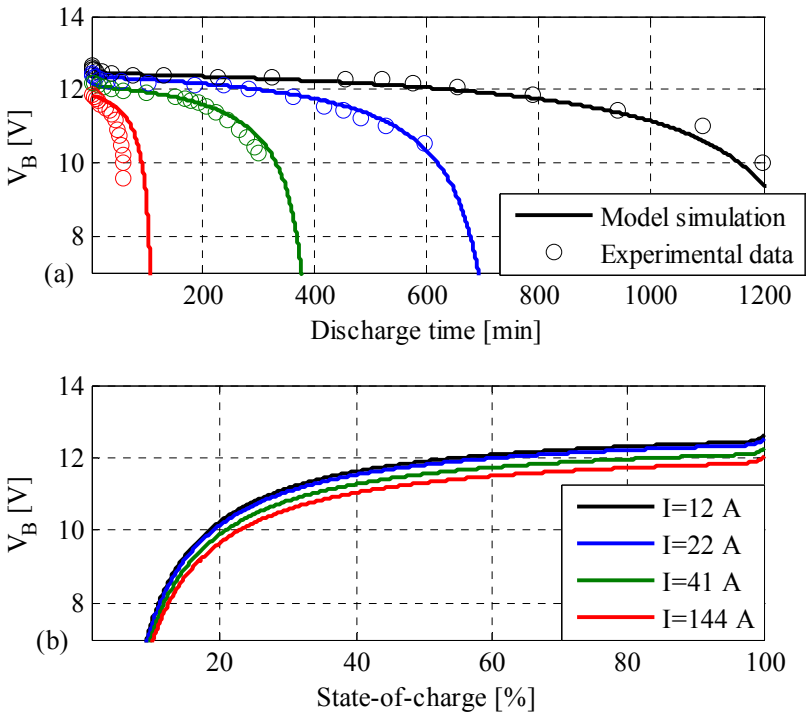

Figure 4.5 - Battery characteristics**.**

An important parameter for the batteries is the roundtrip efficiency. It indicates the electricity that can be recovered during the discharge phase as a percentage of the electricity used to charge the device. In other words, the roundtrip efficiency can be defined as the ratio of the discharged energy ($E_{B,DIS}$) to the energy needed to charge the batteries ($E_{B,CH}$):

$$\eta_B = \frac{E_{B,DIS}}{E_{B,CH}} = \frac{V_{B,DIS}}{V_{B,CH}} \cdot \frac{\int I_{B,DIS} dt}{\int I_{B,CH} dt} = \eta_{B,V} \cdot \eta_{B,C} \tag{4.14}$$

Eq. (4.14) highlights two different phenomena that affect the battery efficiency: the voltage efficiency $\eta_{B,V}$ and the coulomb efficiency $\eta_{B,C}$. The first is due to the decrease in voltage with respect to the ideal one (open circuit voltage $E_{B,0}$ in Eq. (4.11)) during the charging and discharging phases. Several factors affect its value: discharge and charge current, state-of-charge and internal resistance. Instead, the coulomb efficiency takes into

account the variation in the battery capacity and it is influenced mainly by current and state-of-charge.
The inverter/rectifier has the task of controlling and managing the battery bank. As for the PV inverter, the manufacturer provided the inverter efficiency curve as a function of power. A further loss of 10% in addition to inverter losses is assumed in the operation as the rectifier [41].
The battery efficiency including inverter losses is shown in Figure 4.6 as a function of power and SOC (shaded area).

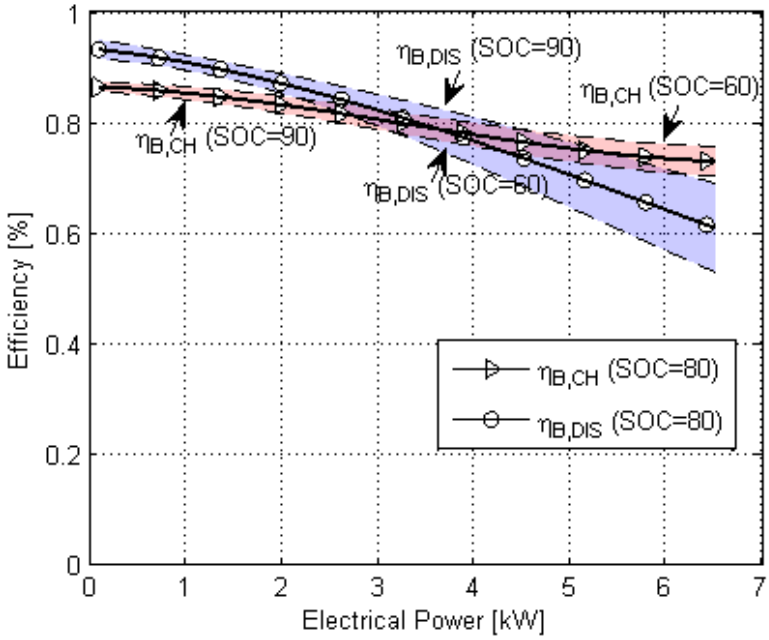

Figure 4.6 - Batteries efficiency as a function of power and SOC

4.2.4. Electrolyzer

The electrolyzer produces, through an electrochemical process, the splitting of the water molecule into oxygen and hydrogen with high purity. By the Faraday's law, the produced hydrogen flow (n_{H2}) is a function of the current (I_{EL}):

$$n_{H2} = \eta_F \frac{N_{C,EL} I_{EL}}{2F} \tag{4.15}$$

where $N_{C,EL}$ is the number of cells in parallel, F the Faraday constant (equal to 96485 C/mol) and η_F the Faraday efficiency equal to the ratio between the actual and the theoretical maximum amount of hydrogen produced by the electrolyzer. With reference to literature data ([42] [43] [44]) it is possible to evaluate the characteristic curve of the electrolyzer in function of the current and the operating temperature. The equation that define the reference voltage (V_{EL}) as a function of the current (I_{EL}) and the electrolyzer operating temperature (T_{EL}) is the following:

$$V_{EL} = E_{Nernst}(T_{EL}) + E_{act}(I_{EL}, T_{EL}) + E_{ohm}(I_{EL}, T_{EL}) \tag{4.16}$$

The ideal potential E_{Nernst} is a function of the operating temperature and the partial pressures of reactants and products:

$$E_{Nernst} = E_0 + \frac{RT_{EL}}{2F} \cdot \ln\left(\frac{p_{H2}\, p_{O2}^{0.5}}{p_{H2O}}\right) \tag{4.17}$$

where E_0 is the reversible electric potential in standard conditions (equal to 1.229 V), p_{H2}, p_{O2} and p_{H2O} the hydrogen, oxygen and water vapor partial pressure respectively (p_{H2} is kept constant and equal to 13.8 bar).

The real voltage differs from the ideal one due to irreversible phenomena that increase the voltage value. The phenomena that occur are mainly two. The first, felt especially at low current values, is related to activation losses produced when an overvoltage is required to ensure the detaching of formed ions from the electrode (E_{act}). This phenomenon can be described in a fairly accurate way by the Butler-Volmen equation:

$$E_{act} = \frac{RT_{EL}}{2\alpha_A F}\sinh^{-1}\left(\frac{I_{EL}}{2I_{A,0}}\right) + \frac{RT_{EL}}{2\alpha_C F}\sinh^{-1}\left(\frac{I_{EL}}{2I_{C,0}}\right) \tag{4.18}$$

where $I_{A,0}$ and $I_{C,0}$ are the exchange current at the anode and cathode, respectively and α_A and α_C are the charge transfer coefficients (CTC) at the anode and cathode, respectively. The CTC at the cathode is set at 0.5, but the CTC at the anode is a function of the temperature and therefore an average value at the respective temperatures is used [44].
The second phenomenon is related to the ohmic resistance of the membrane opposition to the flow of hydrogen ions (E_{ohm}):

$$E_{ohm} = R_{mem} I_{EL} = \frac{s_{mem}}{\sigma} I_{EL} \tag{4.19}$$

where s_{mem} is the dry thickness of the electrolyte–membrane (178 μm for Nafion^{TM}117), and σ is the conductivity of the membrane.
The electrolyzer characteristic curve $I_{EL} - V_{EL}$ as a function of the operating temperature is shown in Figure 4.7(a).

The assessment of the electrolyzer operating temperature is carried out through the implementation of the energy balance of the stack:

$$C_T \frac{dT_{EL}}{dt} = \dot{Q}_{gen} - \dot{Q}_{cool} - \dot{Q}_{loss} \quad (4.20)$$

where the time variation of the electrolyzer temperature is directly proportional to the heat fraction stored in the stack given by the difference between the heat generated by the passage of current and not used for the reaction ($\dot{Q}_{gen}$), the heat flow rate of the cooling system ($\dot{Q}_{cool}$) and the heat dispersed in the environment by radiation ($\dot{Q}_{loss}$).

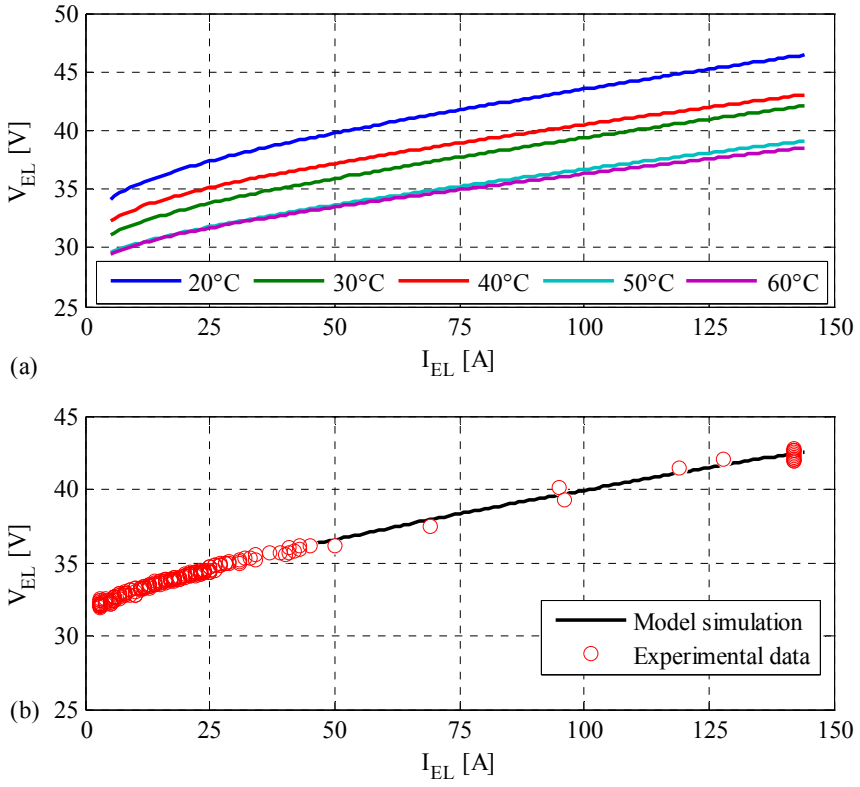

Figure 4.7 - Electrolyzer characteristics

In particular, $\dot{Q}_{gen}$ is directly proportional to the activation and ohmic losses and can be expressed as the difference between the electrical energy supplied to the electrolyzer and the energy content of the hydrogen produced:

$$\dot{Q}_{gen} = I_{EL}V_{EL} - n_{H2}LHV_{H2} \tag{4.21}$$

where LHV_{H2} is the hydrogen lower heating value (249 MJ/kmol). In order to keep the electrolyzer temperature in the range of 30-40°C, the hydrogen generator is equipped with an integrated cooling system. The unit onboard ventilation fan forces the ambient air across the radiator to dissipate some of the stack losses. The mixed-bed filter in the stack limits the operation of the system to roughly 60°C, at which point the resins used for deionization begin to break down. This operation mode is introduced in the simulation model with a PID controller that, starting from the difference between the set-point temperature (35°C) and the real electrolyzer temperature, acts on the fan speed to maintain the desired temperature. Finally, because of the low difference between the electrolyzer operating temperature and the ambient temperature, the heat losses by radiation is neglected.

Experimental tests were performed in the electrolyzer of the H_2FER laboratory in order to carry out the validation of the proposed simulation model. The comparison between simulation and experimental results is shown in Figure 4.7(b), for an average electrolyzer temperature of 35°C.

Both the ohmic and activation losses affect the electrolyzer efficiency, defined as the ratio between the energy of the hydrogen produced and the electrical energy used to produce it. However, ancillary losses, due to circulating pump, fan and inverter losses, also affect the overall system efficiency. Therefore, the electrolyzer efficiency can be defined as follows:

$$\eta_E = \frac{n_{H2}LHV_{H2}}{P_E} = \frac{n_{H2}LHV_{H2}}{V_E I_E} \cdot \frac{V_E I_E}{P_E} = \eta_{E,STACK}\eta_{E,BoP} \tag{4.22}$$

As shown in Figure 4.8, the increase of activation and ohmic losses with the electrolyzer current causes a reduction of stack efficiency. A great influence of ancillary equipment consumption occurs for low values of hydrogen production while the ancillary losses become less influent when the electrolyzer works close to the nominal condition.

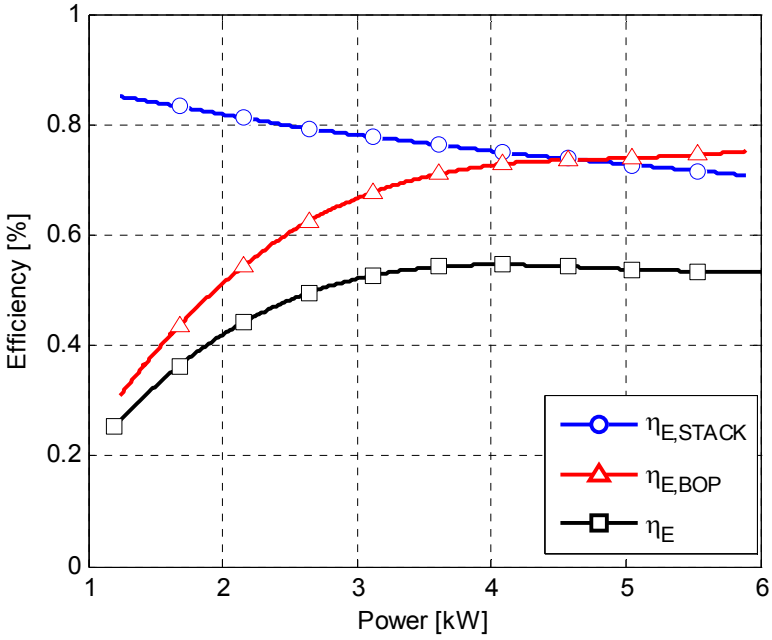

Figure 4.8 - Electrolyzer efficiency

The hydrogen produced is stored in four steel tanks which can store an amount of hydrogen equal to about 55 Nm^3 at 13.8 bar. To model these devices, the equation of ideal gases with a proper compressibility factor z is used:

$$p_S - p_{atm} = z \cdot \frac{n_{H2} R T_S}{MM_{H2} V_S} \tag{4.23}$$

where the tank temperature T_S is assumed constant and equal to 35°C. The compressibility factor z is a function of tank pressure approximated with a fourth order polynomial [45].

4.2.5. Fuel Cell

The fuel cell is a device that transform, through an electrochemical process, the chemical energy of a fuel gas (hydrogen in this case) into electrical energy. The fuel cell model has been developed based on the reconstruction of its characteristic curve and thus the operating point of the generator. In analogy with the operation of the electrolyzer, the main relation used to

characterize the electrical behaviour of the fuel cell is the Nernst equation (Eq. (4.17)). Overvoltage related to activation and ohmic losses in the case of fuel cells take on a negative sign. The real electric potential V_{FC} is given by:

$$V_{FC} = E_{Nernst}(T_{FC}) - E_{act}(T_{FC}, I_{FC}) - E_{ohm}(T_{FC}, I_{FC}) - E_{conc}(T_{FC}, I_{FC}) \quad (4.24)$$

The estimation of activation, ohmic and concentration losses is carried out with reference to [46] and [47]. Unlike of Eq. (4.16), in Eq. (4.24) there is an additional term, E_{conc}, which represents the overvoltage due to the concentration losses. These losses are felt for high values of current and they are due to the reagents inability to diffuse into the electrolyte and/or the products inability to leave space for new reagents. It is possible to define a limiting current (I_L) of the fuel cell, which is the current produced when the reactant concentration falls to zero:

$$E_{conc} = \frac{RT}{nF} \ln\left(\frac{I_L}{I - I_L}\right) \quad (4.25)$$

The operating temperature of the fuel cell is estimated by the implementation of the energy balance:

$$C_T \frac{dT_{FC}}{dt} = \dot{Q}_{gen} - P_{FC} - \dot{Q}_{cool} - \dot{Q}_{loss}$$

In this case the electric power (P_{FC}) is lower than the power generated by the system ($\dot{Q}_{gen}$) while a significant percentage of the chemical energy input is transformed into heat disposed by means of a water cooling circuit ($\dot{Q}_{cool}$) or dispersed in the environment by radiation ($\dot{Q}_{loss}$). The power generated by the system, $\dot{Q}_{gen}$, is directly related to the amount of hydrogen consumed. Since hydrogen consumption is dependent on the stack current and the number of the cells, the following expression can be used to determine the total power generated:

$$\dot{Q}_{gen} = \frac{N_{C,FC} I_{FC}}{2F} LHV_{H2} \quad (4.27)$$

The rate of heat removed by the cooling water could be related to the heat transfer coefficient (U), the surface area of the heat exchanger (A_{HX}) and the logarithmic mean temperature difference (LMTD) between the stack and the inlet/output cooling water:

$$\dot{Q}_{cool} = UA_{HX} \frac{(T_{FC} - T_{cw,in}) - (T_{FC} - T_{cw,out})}{\ln[(T_{FC} - T_{cw,in})/(T_{FC} - T_{cw,out})]} \quad (4.28)$$

Where $T_{cw,in}$ and $T_{cw,out}$ are the inlet and outlet water temperatures respectively. According to [48], an empirical formula is applied to determine the value of UA_{HX}:

$$UA_{HX} = h_{cond} + h_{conv} I_{FC} \quad (4.29)$$

where h_{cond} and h_{conv} are the conductive and convective heat transfer coefficients respectively. Finally, $\dot{Q}_{loss}$ is proportional to the difference between the fuel cell temperature and the ambient temperature:

$$\dot{Q}_{loss} = \frac{T_{FC} - T_{amb}}{R_t} \quad (4.30)$$

where R_t is the thermal resistance of the stack.

Figure 4.9(a) shows the polarization curve of the fuel cell as a function of the operating temperature. It is possible to define three characteristic regions. The activation polarization dominated region occurs at low current values and it is followed by the ohmic polarization dominated region where the activation losses become not relevant in comparison with the ohmic losses. Typically, it is the largest region and a linear decrease in the voltage occurs increasing the current.

Finally, the concentration polarization dominated region occurs for really high values of the current and a collapse of the system will happen if the limit current is reached (around 200 A for the fuel cell under consideration). Usually, the manufacturers discouraged to work in these extreme conditions mainly because of a significant performance drop and an increase in the operating temperature due to the inability to dispose of the heat produced. Despite the high efficiency, in the low current region the generated power can be lower than the power required by the auxiliary components such as blowers, pumps etc.
Experimental tests were carried out for this device for different power outputs. A comparison between simulation and experimental results is shown in Figure 4.9(b), which demonstrates the good accuracy of the simulation model.
The fuel cell efficiency is the ratio between the electricity produced and the energy of the hydrogen consumed.

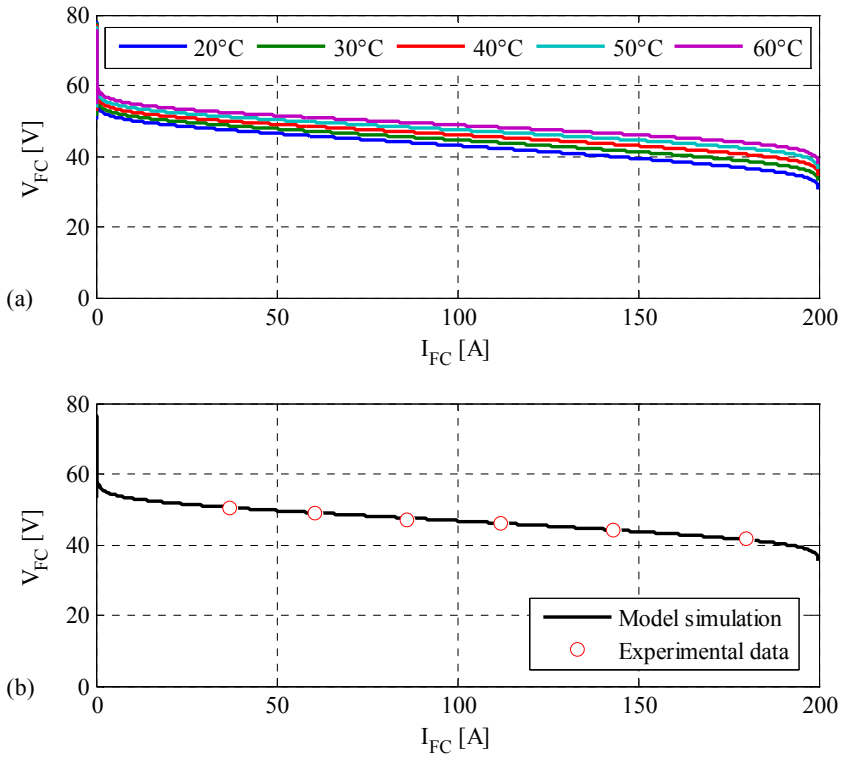

Figure 4.9 - Fuel Cell characteristics

The electricity produced is simply the product between voltage and current while the hydrogen consumed is directly proportional to the current, according to Faraday's law (Eq. (4.15)).

However, part of the electricity produced is used for the auxiliaries or lost as thermal energy in the inverter. These contributions define the overall performance of the fuel cell as shown below:

$$\eta_{FC} = \frac{P_{FC}}{n_{H2} LHV_{H2}} = \frac{V_{FC} I_{FC}}{n_{H2} LHV_{H2}} \frac{P_{FC}}{V_{FC} I_{FC}} = \eta_{FC,STACK} \eta_{FC,BoP} \qquad (4.31)$$

The fuel cell efficiency as a function of the output power is shown in Figure 4.10.

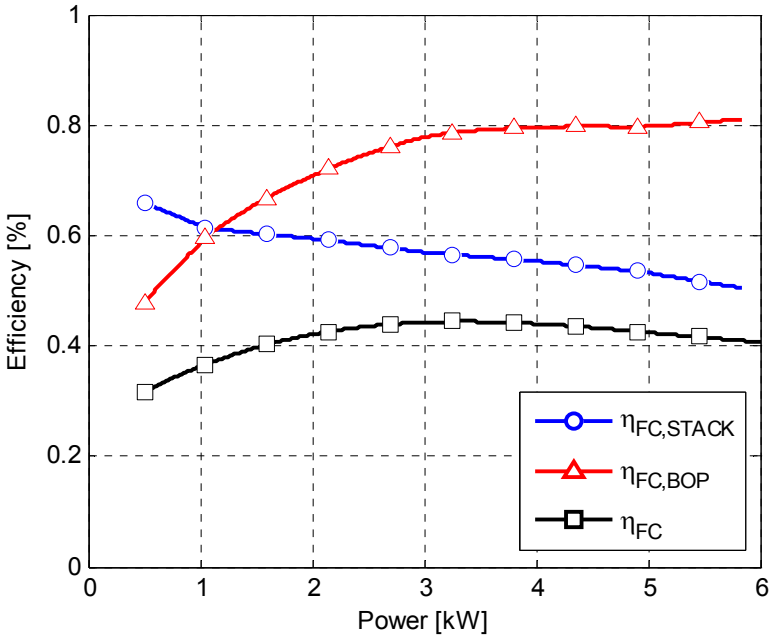

Figure 4.10 - Fuel Cell efficiency

4.3. Weekly analysis

The capabilities of the optimization approach presented in the previous chapter has been evaluated with reference to the microgrid configuration of the aforementioned Hydrogen from Renewable Energy Sources Laboratory. The analysis was carried out with reference of three different case studies: a week in August (summer case), a week in October (in-between season case) and a week in December (winter case).

Table 4.2 - Costs and estimated lifetime for storage devices

	Batteries:	**Electrolyzer:**	**Fuel Cell:**
Investment cost	400 €/battery	75000 €	28000 €
Estimated lifetime	1300 cycles (DOD = 30%)	30000 h	30000 h
O&M cost	-	0.2 €/h	0.2 €/h

The time step Δt and the branching time τ are set 0.25 hour and 6 hours respectively and a time horizon of 4 days is set to take into account the possible evolution of load and weather conditions. All these parameters were subjected to a sensitivity analysis and were optimized for the physical problem under consideration. Forecast data of solar radiation, wind speed and direction as well as ambient temperature with a sampling time of 1 hour are provided by accredited institutions ([49], [50]). A rolling time of 1 hour is imposed and weather forecast data are updated every 24 h. Starting from the forecast of solar radiation and wind speed, the expected power produced by the photovoltaic system and the wind turbine are calculated.This expected power represents the main scenario, but other scenarios are introduced with a corresponding probability to take forecasting errors into account.

Concerning the load profile, since measured data were not available, according to the foreseen demand of the laboratory activities, a variable load with an 8 h peak period centered at noon is expected. In particular, as discussed in [51], a peak load of 3200 W and a base load of 800 W for the remaining hours are assumed with an overall daily energy demand of 38.4 kWh. In fact, the latter load values maximize the energy supplied to the microgrid and ensure that the demand is covered throughout the year.

For the evaluation of utilization costs, data provided by the manufacturers are used (Table 4.2). Data for the PDF of forecasting errors in load profiles and wind speed are extrapolated from [22] whereas solar radiation scenarios are generated as discussed in the previous chapter. The PDFs for the load profile and wind speed were discretized into 5 states whereas only 3 states were used for solar radiation. Consequently, a total of 75 scenarios (5 x 5 x 3) was obtained. To reduce computational complexity and running time, the total number of scenarios was reduced to 15 by applying a reduction algorithm. The difference between the most extreme scenarios in terms of production and demand of energy was about 30%.

According to technical data of the H_2FER Lab equipment, Table 4.3 shows the values imposed for the initial conditions and maximum and minimum storage limits. The current case study involves 18367 variables of which 12360 binary variables for each scenario tree built at a certain rolling time.

Table 4.3 - EESs limits and initial values

Battery	
Minimum State-of-charge (SOC_{MIN})	60%
Maximum State-of-charge (SOC_{MAX})	90%
Initial State-of-charge (SOC_{IN})	80%
Maximum charging/discharging power ($P_{B,MAX}$)	18 kW
H2-Storage	
Minimum H_2 tank pressure ($p_{H2,MIN}$)	2 bar
Maximum H_2 tank pressure ($p_{H2,MAX}$)	13.8 bar
Initial H_2 tank pressure ($p_{H2,IN}$)	10 bar
Minimum electrolyzer power ($P_{E,MIN}$)	1.2 kW
Maximum electrolyzer power ($P_{E,MAX}$)	6.2 kW
Minimum fuel cell power ($P_{FC,MIN}$)	0.5 kW
Maximum fuel cell power ($P_{FC,MAX}$)	6 kW

4.3.1. Results

Starting from the initial conditions and the forecasted data, the solver gives the solution of the optimal scheduling problem that minimizes the utilization costs and maximizes the overall efficiency of the system, while different constraints due to equipment limits are satisfied. The main output of the program is therefore the on/off status of the various devices. In order to test the performance of the control system under real conditions, the simulation models introduced in the previous paragraph are used. Obviously, actual data values for weather condition and load demand differ from the corresponding forecasted values. Therefore, the actual energy flows are calculated by using actual values for solar radiation and wind speed instead of the forecasted values.

Summer case

The power produced by the two RES systems evaluated by using actual meteorological is shown in Figure 4.11(a). The overall electrical energy produced during the summer week is 340.0 kWh whereas the overall energy required is 268.8 kWh. Therefore, a surplus of energy production occurs especially during the central hours of the day due to the high PV energy production.

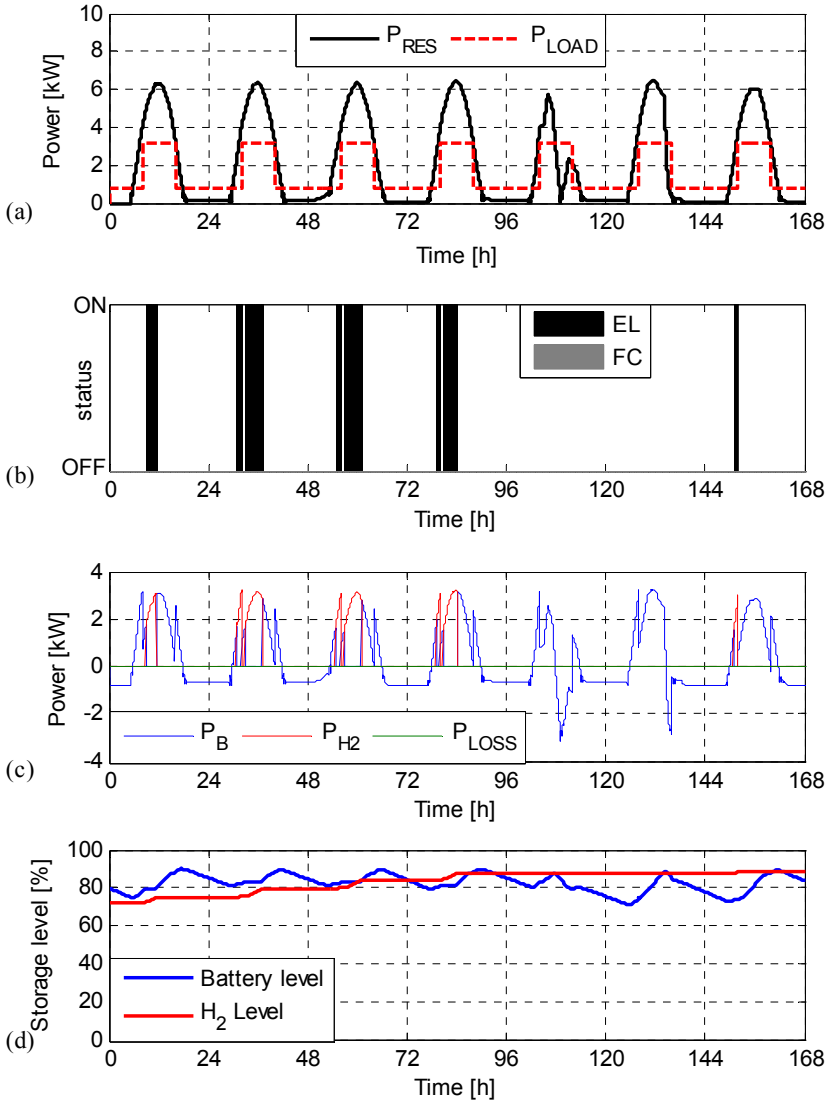

Figure 4.11 - (a)Power generation and load demand, (b)Generation scheduling of the hydrogen storage system, (c) Power flow and (d)time evolution of battery SOC and H_2 tank pressure for the summer case

Since the nominal power output of the PV generator is significantly higher than that of the WT generator, the energy production of the power generation section is greatly affected by the solar radiation and therefore by the season. For this reason, the use of energy surplus for a long-term storage should be preferred and the generation scheduling implements this policy.

Figure 4.11(b) shows the commitment of the electrolyzer and fuel cell for the week under consideration whereas the corresponding power flows are shown in Figure 4.11(c). The electrolyzer is committed in the first 4 days when the highest surplus of energy occurs. Two main advantages are achieved: the electrolyzer can work close to its nominal power output with a high conversion efficiency while the requirement of a high battery current, with a consequent drop in the battery voltage efficiency, is avoided. No commitment of the hydrogen storage system occurs during the fourth day due to the decrease in the power production for the presence of clouds while the surplus of energy observed during the fifth day is used for the battery charging.

Finally, the electrolyzer is used again in the last test day. Unlike the large use of the hydrogen storage system during the day, the energy deficit at night is completely supplied by the batteries and consequently the use of the fuel cell is not required. At the end of the week the electrolyzer has worked for 18.25 h with 8 start-up while the batteries have worked for the remaining 149.75 h.
Figure 4.11(d) shows the charge status of the two storage systems during the period under examination, expressed in terms of SOC and H_2 storage level (HL). The battery SOC is always kept below the maximum threshold (90%) for all the duration of the test, thus avoiding overcharging problems or actions to reduce the power produced by the renewable generators.
The final level of stored hydrogen is equal to about 88%, which means an increase of 15% compared to the initial level. This increment compared with the few hours of use of the electrolyzer highlights the inadequacy of the current hydrogen storage capacity of the microgrid for a long-term storage. This fact is also confirmed by extending the analysis on an annual basis, as will be shown in the next paragraph.

In-between season case

A better match between energy production and demand occurs during autumn and spring. In these cases, the batteries are mainly used to compensate for the minor difference between energy production and energy demand, whilst the hydrogen storage system works only for few hours. An October week is used as case study and results are shown in Figure 4.12.

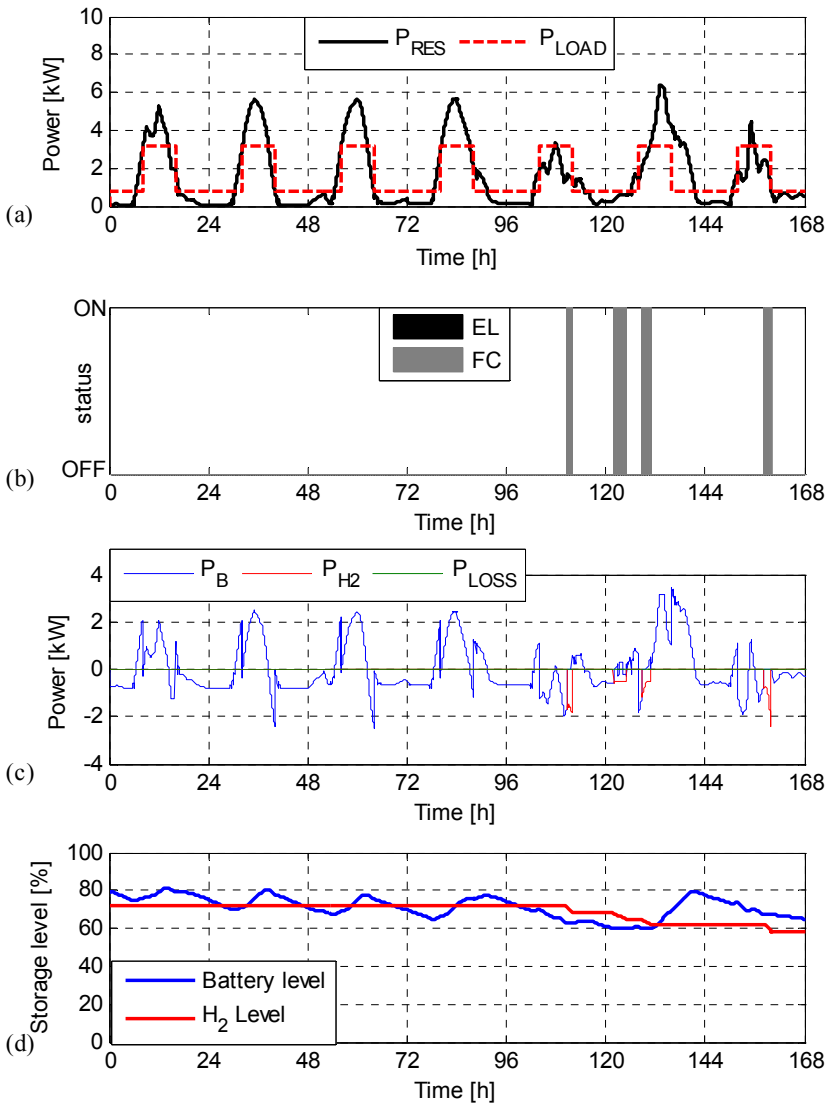

Figure 4.12 - (a)Power generation and load demand, (b)Generation scheduling of the hydrogen storage system, (c) Power flow and (d)time evolution of battery SOC and H_2 tank pressure for the in-between season case

The weekly energy production by the RES (267.5 kWh) diminishes in comparison with the summer week and the difference between energy production and energy demand becomes very low. Batteries are preferred by the proposed control system to balance energy production and consumption due to their lower utilization costs compared to the hydrogen

storage system. The fuel cell is committed only at the end of the fourth day after a low power production period due to clouds. In this situation, the battery SOC is close to its lower value and the fuel cell is forced to work close to its minimum power and far from its nominal conditions. Another fuel cell commitment is scheduled at the end of the last day where the daily energy production is lower than energy demand.

Unlike the summer day, no hydrogen storage occurs during the autumn week whereas the fuel cell is committed for 8.25 hours with 4 fuel cell start-up. A reduction in the amount of stored energy occurs during this week, as shown in Figure 4.12(d). In particular, the hydrogen storage level decreases by 14% in comparison with its initial level whereas the final battery SOC is 65%. Therefore, the initial storage conditions for the next week will be different than those of the week under consideration, and there is a high probability that the load requirements will not be satisfied.

Winter case

Because of low solar irradiation, electricity production by RES is usually very low during the winter. As expected, a large deficit occurs during the week under consideration when the daily energy produced by the PV and WT power generation plants could only partially cover the user energy demand (the weekly energy produced is 243.1 kWh). As shown in Figure 4.13(a), a constant energy deficit occurs during the first four days of the week. Batteries are unable to supply all this energy deficit and the minimum SOC is reached after just two days. The control system prefers the use of the fuel cell in the first and last hours of the day where the production of energy is almost zero and the power request is still high. In this case, the fuel cell works near its nominal point with high efficiency whereas a decrease in battery efficiency would occur.

Because of the low capacity of the energy storage system, the load shedding is unavoidable, despite the control system try to minimize it. No difference between primary and secondary loads is introduced and therefore the control system prefers not to satisfy the base load during the night. A raise in the energy production occurs in the fifth and sixth days, thanks to the wind turbine energy production.

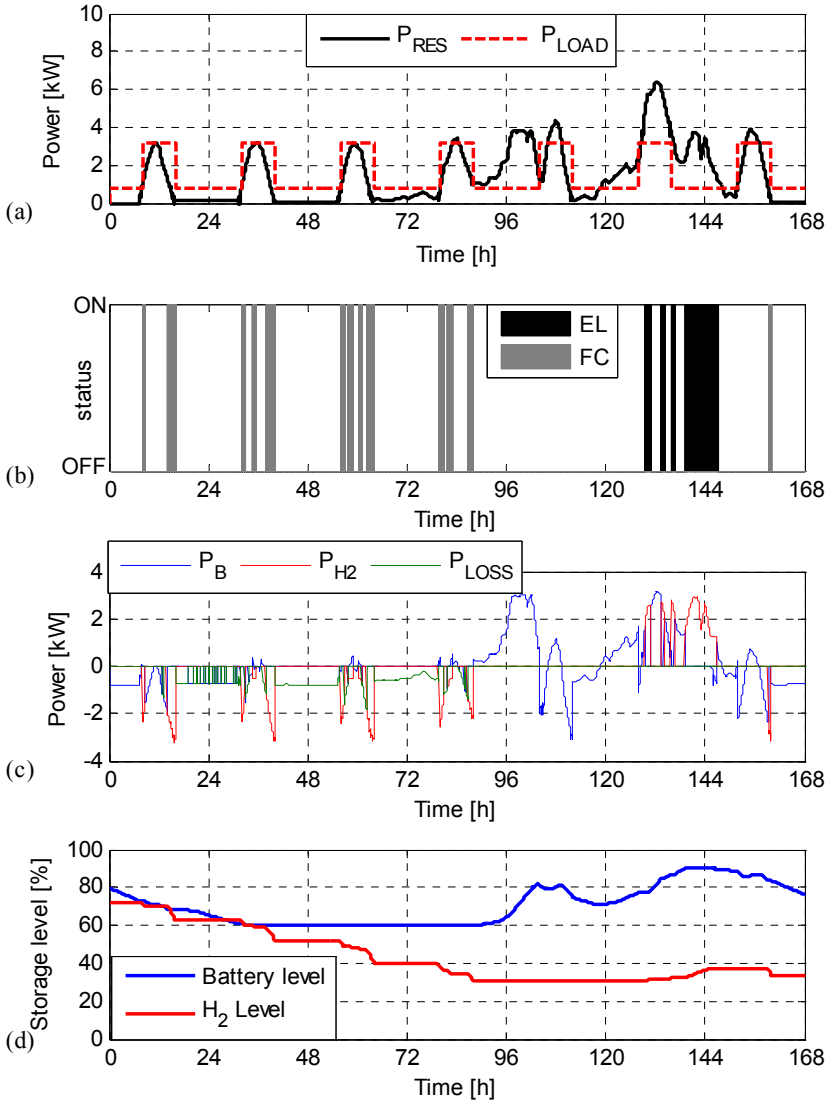

Figure 4.13 - (a)Power generation and load demand, (b)Generation scheduling of the hydrogen storage system, (c) Power flow and (d)time evolution of battery SOC and H_2 tank pressure for the winter case

The battery SOC raises up to its maximum value and the electrolyzer is committed by the control system to partially cover the hydrogen consumption of the previous days. At the end of the week, the electrolyzer and the fuel cell are committed for 10.5 h (4 start-ups) and 15.25 hours (13 start-ups) respectively, whereas 31.3 kWh of load request are not satisfied

(corresponding to about 11% of the weekly energy demand). Despite the final battery SOC is almost equal to its initial value (80%), the hydrogen level decreases by about 40% in comparison with its initial value and a greater amount of undelivered power will probably occur in the following week.

4.3.2. EMS comparative analysis

A standard procedure to evaluate and compare the EMS performance is not currently available. However, it is possible to introduce some indicators that highlight the benefits and defects of the various control systems and help in the assessment of the EMS performances.
The definition of some "key performance indicators" (KPI) [52] may be related to energetic aspects - average energy conversion efficiencies, capacity to meet the load request etc. – or economic ones, such as operating costs. However, these KPIs are strongly influenced by the period of time taken into account. Annual-based analysis definitely give more accurate information but they are often impossible to carry out. Weekly or daily assessments are easier to achieve, but they could give only partial indications that are often highly influenced by the considered week/day. Moreover, a high sensitivity of the KPI to initial states is observed in these cases. The definitions of KPIs used in this comparative analysis are outlined below:

a. ***Percentage of unmet demand (%UMD)****:* defined as the ratio between the energy demand not satisfied or imported from the grid and the whole energy demand.
b. ***Percentage of unused energy from renewables (%UNE)***: defined as the ratio between the energy losses or exported to the grid instead of being stored or used to satisfy the demand and the total RES electricity production.
c. ***Average hydrogen storage efficiency ($\bar{\eta}_{H_2}$):*** This indicator evaluates the average efficiency during the operation of the hydrogen storage system, relative to the lower heating value of hydrogen:

$$\eta_{H_2} = \sum_{t=1}^{\theta} \frac{n_{H2} LHV_{H2}}{P_E} \cdot \sum_{t=1}^{\theta} \frac{P_{FC}}{n_{H2} LHV_{H2}} = \bar{\eta}_{FC} \cdot \bar{\eta}_E \qquad (4.32)$$

d. ***Average batteries efficiency ($\bar{\eta}_B$):*** as the previous indicator, it evaluates the average efficiency during the batteries operation. Its definition is already presented in the previous paragraph (Eq. (4.14)):

$$\eta_B = \frac{E_{B,DIS}}{E_{B,CH}} = \frac{V_{B,DIS}}{V_{B,CH}} \cdot \frac{\int I_{B,DIS} dt}{\int I_{B,CH} dt} = \eta_{B,V} \cdot \eta_{B,C}$$

e. ***Energy path Efficiency (η_{path}):*** This indicator gives the overall electricity losses from the renewable energy sources to the final user. It is defined as follows:

$$\eta_{path} = \sum_{t=1}^{\theta} \frac{P_{DIR} + P_{BC}\eta_{BC} + P_E\eta_E}{P_{RES}} \cdot \frac{P_{LD} - P_{UN}}{P_{DIR} + \frac{P_{BD}}{\eta_{BD}} + \frac{P_{FC}}{\eta_{FC}}} \qquad (4.33)$$

f. ***Final hydrogen storage level*** (***HL_{FIN}***): It indicates the final level of the hydrogen storage tanks. For a given running time, it is an indirect measure of the conversion efficiency.

g. ***Final batteries state of charge (SOC_{FIN}):*** It indicates the final SOC of batteries. A value close to its minimum threshold should be considered a drawback because the system will face the next period without the battery contribution.

h. ***Fuel Cell and Electrolyzer running time (t_{FC},t_E)***: It indicates the overall operation time of the electrolyzer and of the fuel cell. It is directly connected to the operating costs of the hydrogen storage system.

i. ***Fuel Cell and electrolyzer number of start-stop events (δ_{FC}, δ_E)***: This indicator counts each time the electrolyzer or fuel cell is started and stopped. A high number of switching is recognized as a major cause of their degradation [53].

j. ***Operating costs***: they comprises the cost of equipment replacement and the O&M costs. They are partially already defined in the previous chapter, such as battery costs during the discharge phase (Eq. (3.16) and fuel cell costs (Eq. (3.18). Similarly, it can be defined the battery costs during the charge phase and electrolyzer costs:

$$C_{BC} = \frac{C_{B,IN}\, P_{BC}}{N_B U_B\, Q_B N_{CYCLES} \eta_{BC}} \quad (4.34)$$

$$C_E = C_{E,IN}/L_E + C_{O\&M,E} \quad (4.35)$$

To highlight the capabilities of the proposed EMS, in this section its operational schedules are compared with those of two different EMS: the "SOC-based" EMS introduced at the beginning of this Chapter. and a so-called "perfect" EMS. The latter is based on the optimal generation scheduling produced by a perfect forecast of wind speed, solar radiation and energy demand. In this study, the perfect EMS is calculated by using real data as input values and therefore it includes only one scenario. The perfect EMS obviously achieves the best results in terms of both minimization of utilization cost and maximization of overall system efficiency. However, in real applications, load and meteorological data cannot be exactly predicted and perfect EMS is used only as a reference and ideal EMS.

Figure 4.14, Figure 4.15 and Table 4.4 summarize and compare the main results in terms of energy flows, operating hours and utilization costs of the three aforementioned EMS.

The proposed EMS demonstrates several advantages in comparison to the SOC-based EMS, especially in the summer and winter weeks. Although the total energy exchanged with the hydrogen storage system is almost the same (Figure 4.14), a decrease in the operating hours of both electrolyzer and fuel cell occurs. Consequently, the hydrogen storage system operates closer to its nominal conditions and therefore closer to its maximum efficiency with a reduction in the operating cost (Figure 4.15) and an improvement of the energy conversion efficiency. Obviously, the greater the use of the hydrogen storage system is, the more visible the improvements led by the introduction of an optimal generation scheduling will be.

Nevertheless, Table 4.4 highlights the impossibility for the proposed EMS to reach the perfect EMS performance: for all 3 cases, a lower value of operating costs and a higher conversion efficiency would be obtained if the weather and load condition were perfectly forecasted. Results of the proposed EMS should improve and approach those obtained by the perfect EMS with a decrease in rolling time and a more frequent updating of

meteorological data. However, a reduction in the maximum allowable computational time may occur and the EMS could not find the optimal solution in time for every rolling time.
Furthermore, Table 4.4 shows that final values of battery SOC and hydrogen tank level are quite similar for the compared EMS. At the end of the summer week, the hydrogen tank pressure increases by more than 3 bar with respect to the initial value (10 bar). This obviously leads to a different initial situation for the following week when the storage tank may be completely filled. Vice versa, the hydrogen tank pressure reaches a lower level at the end of the winter week. This can lead to a significant increase in undelivered power for the following weeks. As will be discussed in the following paragraph, the low storage capacity of the studied microgrid does not allow to fully highlight the benefits led by the proposed control system in the long-term period.

The main disadvantage of the proposed EMS is the high computational time required to find the optimal solution. The use of linear approximations to avoid nonlinear equations has led to the use of efficient algorithms for linear problems and has given the certainty to find the global optimum. On the other hand, this choice increased the number of constraints and variables and the complexity of the problem. For this case study the problem was solved within 1 h on a 2.57 GHz Core i7 processor. The computation time decreases significantly to about 20 min for the perfect EMS and 5 min for the SOC-based EMS. In all cases, the optimum is found within the available decision time (1 h).

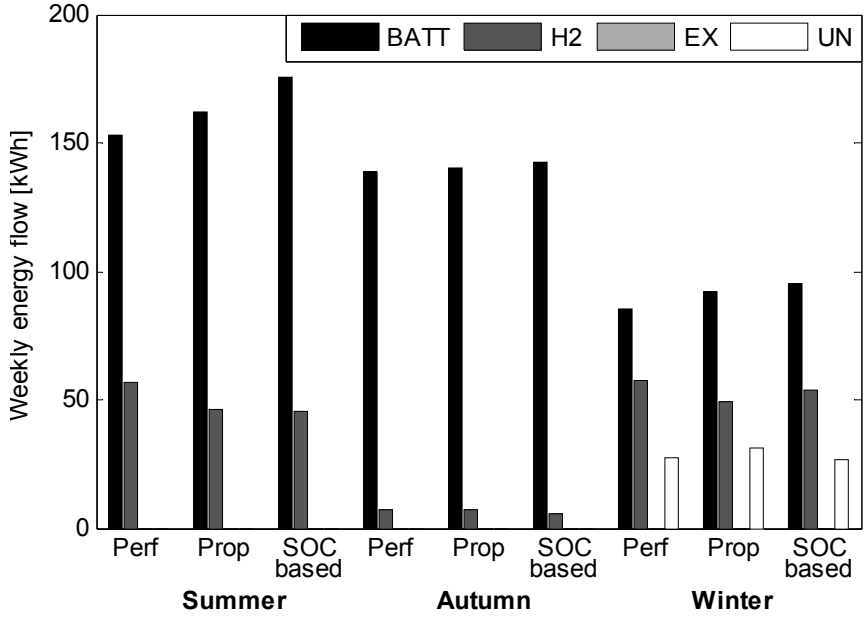

Figure 4.14 - Weekly energy flows in the two storage system devices

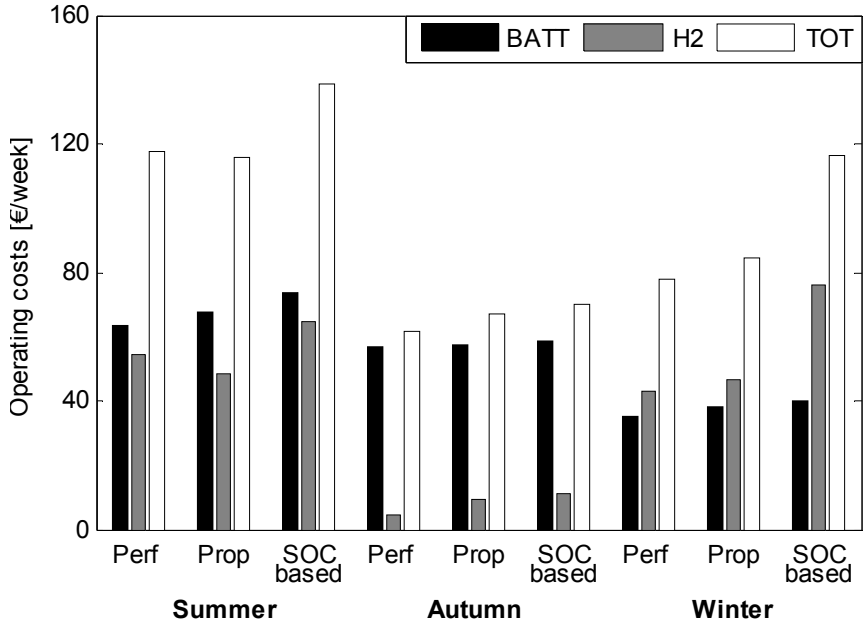

Figure 4.15 - Weekly operating costs of storage systems

Table 4.4 - Summary of results obtained from the EMS comparative analysis

	%UMD	$\overline{\eta}_{H_2}$ [%]	$\overline{\eta}_B$ [%]	η_{PATH} [%]	HL_{FIN} [%]	SOC_{FIN} [%]	t_E [h] (δ_E)	t_{FC} [h] (δ_{FC})	Operating cost [€/week]
Summer									
Perfect	-	51.4	76.5	85.6	92.3	76.7	17.14 (8)	-	113.8
Proposed	-	51.2	76.2	85.6	88.2	83.9	18.32 (8)	-	114.4
SOC-based	-	38.3	75.6	84.1	85.2	83.9	23.13 (9)	-	138.4
In between									
Perfect	-	41.2	77.5	89.8	60.1	65.1	-	4.05 (2)	61.4
Proposed	-	34.9	77.5	89.0	58.4	65.0	-	8.25 (4)	66.8
SOC-based	-	32.2	77.4	89.2	61.0	62.3	-	9.93 (3)	69.8
Winter									
Perfect	10.2	46.3	77.3	77.5	25.6	78.3	8.30 (3)	17.38 (13)	78.1
Proposed	11.6	40.4	77.3	76.1	33.9	76.5	10.48 (4)	15.22 (13)	84.8
SOC-based	10.0	35.8	76.8	72.6	20.7	72.1	12.92 (2)	35.35 (4)	116.1

4.4. Annual analysis

The benefits in terms of reducing in the operating costs and improving the system performance led by an optimal management of the unit commitment has been highlighted in the previous paragraph. However, the period under consideration - a week - although representative of the seasonal microgrid behavior does not allow to analyze the actual feasibility of a microgrid powered exclusively by renewable energy sources as well as to compare the benefits led by the proposed EMS over a year.
Therefore, to evaluate the annual behavior of the microgrid and to test the capabilities of the proposed EMS, a typical meteorological year was considered. Because of the shortage of weather forecast data, data of both solar and wind resources were obtained through the software "Meteonorm", for the location of Cagliari. Meteonorm is a meteorological database containing comprehensive climatological data for every location in the world. Based on the coupling of historical meteorological data and computational models, Meteonorm provides the 8760 hourly values of both global horizontal radiation and wind velocity. The annual average daily radiation for Cagliari is 4.82 kWh/m^2, but average daily radiation is strongly influenced by season. Figure 4.16(a) shows daily radiation as a function of month. Daily radiation in summer exceeds 6 kWh/m^2, 2-3 times above daily radiation during winter. An hourly annual average of about 5 m/s for wind velocity was calculated. Monthly variation (Figure 4.16(b)) is quite small, with a peak in July, leading to a WT energy production fairly constant throughout the year.

Since past forecasting data on a yearly basis were not available, a random perturbation of both solar radiation and wind speed was introduced to generate fictitious forecasting data. In particular, a normal distribution on the difference between real and forecasting data is supposed with a mean value and a standard deviation (σ) equal to 0 and 0.5 respectively. Therefore, the generic forecast condition (Forecast) as a function of the real value (Real) is given by:

$$\text{Forecast} = \text{Real} \cdot (1 + \sigma\xi) \tag{4.36}$$

where ξ is a pseudorandom number in the range [-1,1] drawn from the standard normal distribution.

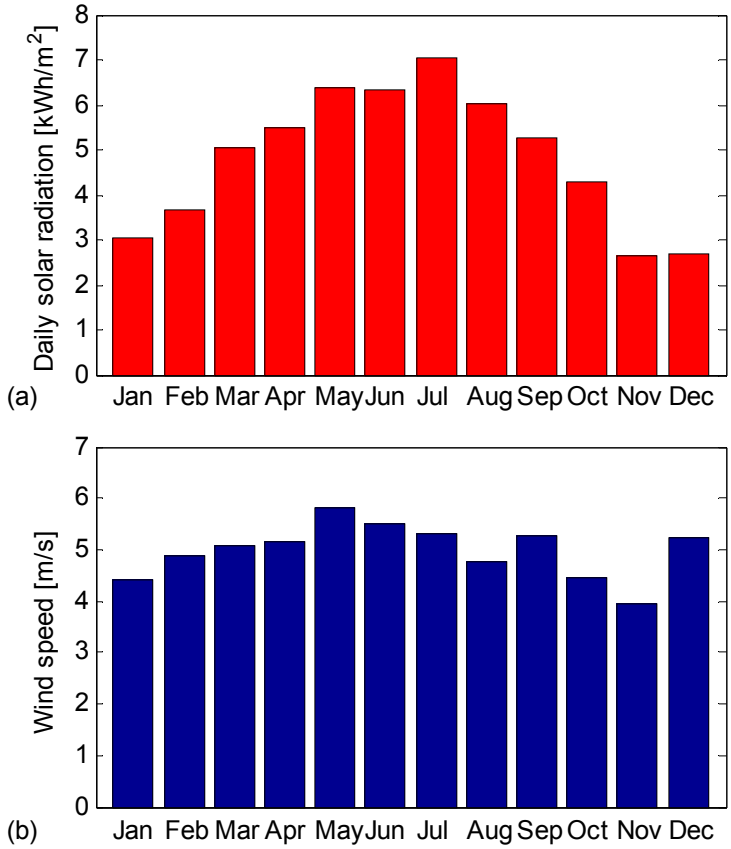

Figure 4.16 - (a) Daily solar radiation and (b) mean wind speed for Cagliari

The first branching time was set at 6 h and the time horizon at 4 days. The microgrid schedule was updated every hour to consider changes in weather and load conditions. Since the microgrid is powered only by non-programmable renewable sources, PV and WT are operated at their maximum power point and their power output depends only on solar radiation and wind speed. Overall, the annual energy produced by RES is about 17.78 MWh while users' annual energy consumption is 13.17 MWh. The power produced by the photovoltaic system and the wind turbine is partially used to directly supply the load and partially sent to the energy storage system (batteries and hydrogen storage section). Figure 4.17(a) shows the distribution of the hourly energy flows at the inlet and outlet of the two storage sections. Moreover, the left side of Figure 4.17(b) shows

the distribution of the annual energy produced by the PV and WT generators between direct load supplying, batteries, hydrogen storage section and excess energy production.

Although the annual energy produced exceeds the annual energy demand, the RES generators are unable to satisfy all the user's energy demand during winter months and a significant adoption of load shedding is unavoidable (about 5% of the annual load demand). Vice versa, a large excess of energy production occurs during spring and summer months (24% of the annual RES production) due to the low storage capacity of the microgrid.

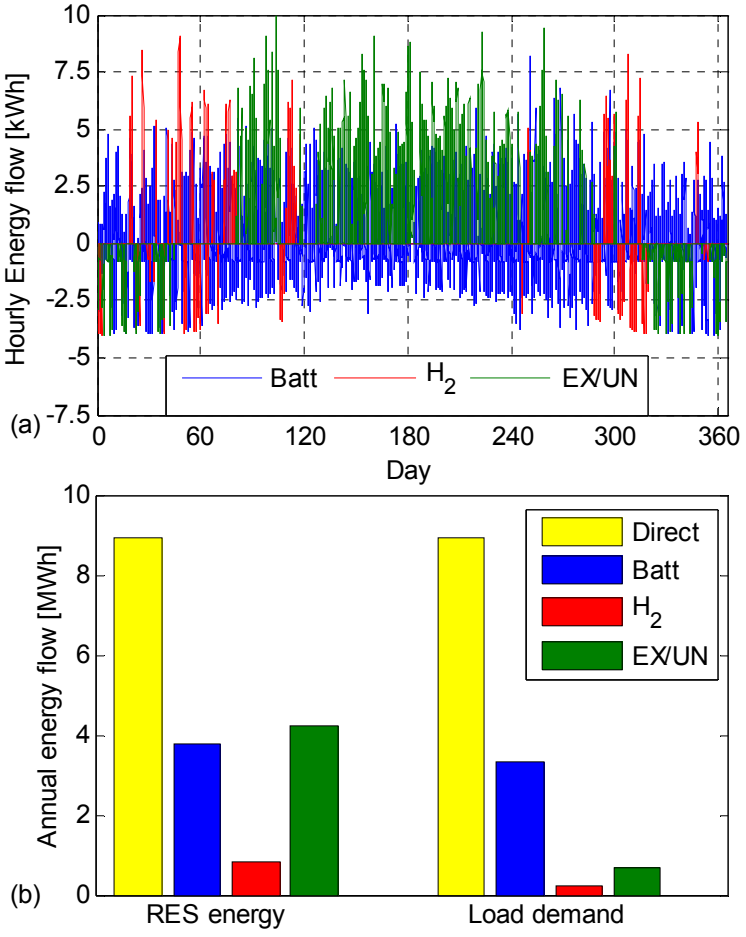

Figure 4.17 - Annual energy flows between the energy storage devices

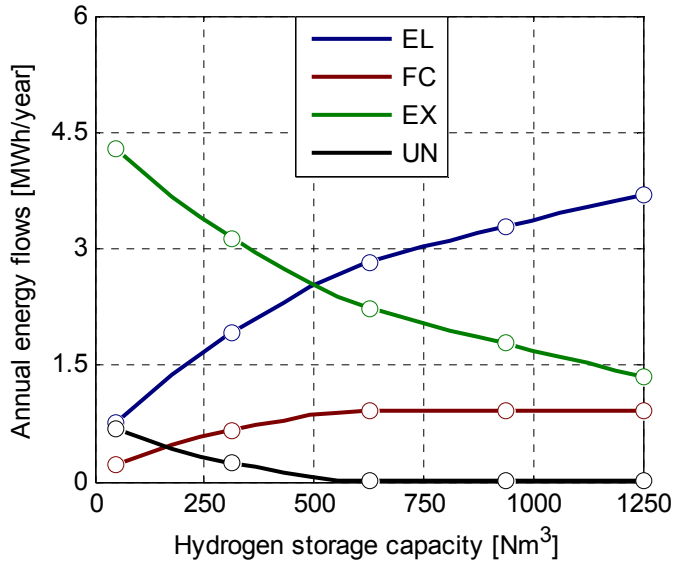

Figure 4.18 - Annual energy flow in the storage system on varying the storable hydrogen.

In other words, the storage capacity of the system is unsuitable for a long-term energy storage (in particular from summer to winter) and an improvement of this parameter would be required to completely fulfill the load demand. Especially the hydrogen storage capacity is really low and it allows to use the hydrogen storage system only for 300 hours per years (less than 4% of the annual operation time). For this reason, a parametric analysis is carried out by varying the amount of the hydrogen storage capacity and the results are summarized in Figure 4.18 and Figure 4.19. Starting from the current hydrogen storage capacity (55 Nm^3), Figure 4.18 shows that a much larger storage capacity (about 550 Nm^3, corresponding to 10 times the current capacity) would be required to completely cover with RES energy the overall annual consumption and to avoid load shedding. However, even with this increased storage capacity, a considerable amount of excess energy is still present (16% of the overall energy production).
A further increase in the hydrogen storage capacity is useless to meet the annual energy demand, but allows to produce an additional amount of hydrogen that can be used for other purposes (laboratory requirements). The increase in the hydrogen storage capacity can be achieved either by increasing the overall tank volume or by increasing the hydrogen storage pressure by means of a suitable compressor. It is worth mentioning that a

similar increase in storage capacity requires remarkable capital costs and the introduction of the hydrogen compressor decreases the overall conversion efficiency.
The annual operating costs are shown in Figure 4.19 as a function of hydrogen storage capacity. Obviously, an increase in the storage capacity increases the annual operating hours of the different devices and therefore their annual operating costs. Moreover, a sensitivity analysis was also carried out by considering 4 different values of the branching time. Figure 4.19 demonstrates that the operating costs are only slightly affected by the branching-time and only minor differences occur in the four cases studied.

4.4.1. Comparison with a SOC-based EMS:

To test the capabilities of the proposed EMS, it was compared with a SOC-based EMS.
Figure 4.20 summarizes the results of the comparative analysis between the SOC-based and the proposed EMS. For the actual hydrogen storage capacity (55 Nm^3) there are no substantial differences between the two management models compared.
By increasing the hydrogen storage capacity both EMSs produce a gradual decrease in energy losses and an increase in annual operating costs. However, for storage capacities higher than that adopted by the microgrid here considered, the proposed EMS leads to a 5-10% decrease in both operating costs and energy losses. In particular, for a hydrogen storage capacity 10 times higher than the current one, the decrease in the operating costs is about 10% and the energy losses decrease by about 6%.

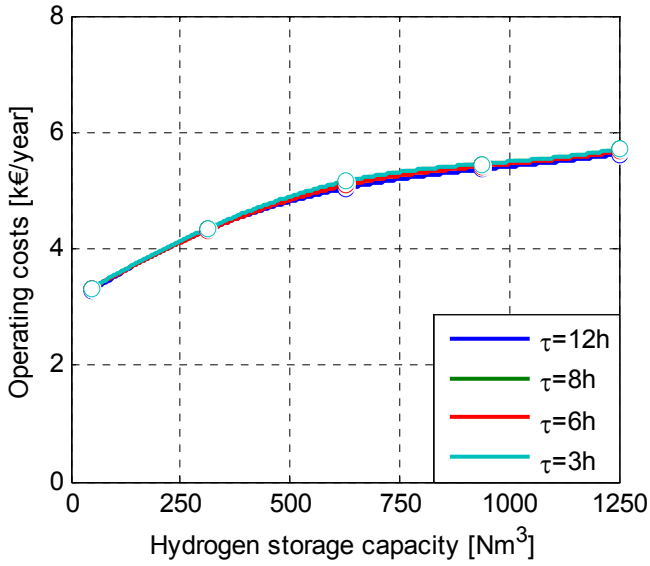

Figure 4.19 - Operating costs in function of the hydrogen storage capacity and first branching time

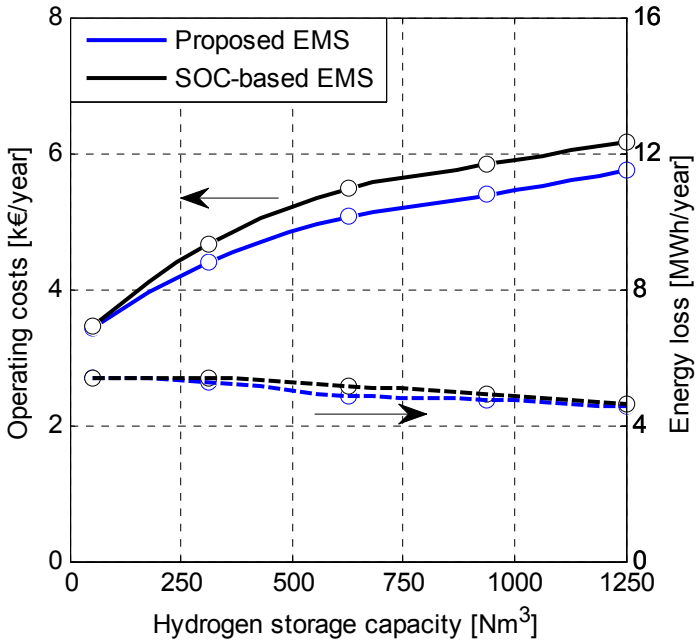

Figure 4.20 - Performance comparison of proposed and SOC-based EMS in function of the hydrogen storage capacity

Chapter 5

Optimal generation scheduling for the microgrid at the Seville University

The work presented in the previous chapter has demonstrated the feasibility of applying the optimal generation scheduling to the microgrid of the H_2FER Lab. However, two criticisms may arise from the analysis just presented. The first is dictated by the lack of experimental results: no matter how much refined the modeling and simulation can be, it cannot be disregarded by the experimental results to validate the proposed thesis. The second involves the adaptability and generality of the proposed control system: despite the development of the proposed EMS is directly linked to the study of plants with RES generators and hydrogen storage systems, it could be, however, flexible and adaptable both to similar installations with different capacities and to plants with other system architectures.

To overcome these two issues, the proposed EMS was implemented and tested in a microgrid located at the University of Seville (Spain). The latter has been the subject of several works in the literature ([54] [55] [56] [57]). In particular, a model predictive controller was already implemented and tested. In this case, the time horizon was set to some seconds that is more suitable for a real-time control with respect to a generation scheduling control. Therefore, the two strategies are not in conflict with each other but rather coupled to generate a synergic action: it is possible to exploit the

potential and peculiarities of both control strategies, with the aim to achieve an improvement in the performance of the plant.

In this chapter, after a briefly description of the experimental set-up and the control strategy adopted, the results obtained in a summer day case and in a cloudy day case are reported and discussed. Moreover, a comparative analysis is also carried out to investigate the advantages and disadvantages led by the implementation of the proposed control system.

5.1. Microgrid description

As shown in Figure 5.1, the microgrid under study is very similar to the $LABH_2FER$ microgrid despite a lower energy storage capacity. The microgrid simulates the behavior of a domestic system powered by a photovoltaic array. In case of excess power production, the electricity is used to produce and store hydrogen through an electrolyzer. A fuel cell generates electricity by using the stored hydrogen when required. A battery bank is also incorporated in the main power distribution line in order to maintain a fixed voltage on the line, thus simplifying the converter design.

Unlike the $LABH_2FER$ microgrid described in the previous chapter, all the units are coupled on a DC bus. The main advantage is the avoidance of inverter losses and a more easily control system even if the configuration is less flexible and problems could occur in future grid extensions. Furthermore, the system is designed to work in a grid-connected mode: if the PV production and the storage system is unable to completely satisfy the load demand, the gap is fulfilled by the external grid. The selling of energy is also possible when a full charge of the energy storage systems occurs.

The experimental set-up is shown in Figure 5.1 and the main characteristics of the different devices are listed in Table 5.1. The photovoltaic array is emulated by a programmable electronic power source, which permits the simulation of a PV array under different weather conditions. Analogously, another programmable electronic load simulates the domestic power demand. Therefore, the configuration of the microgrid allows to simulate different power inputs and outputs. The hydrogen system includes a 1 kW PEM electrolyzer, a metal hydride storage tank and a PEM fuel cell.

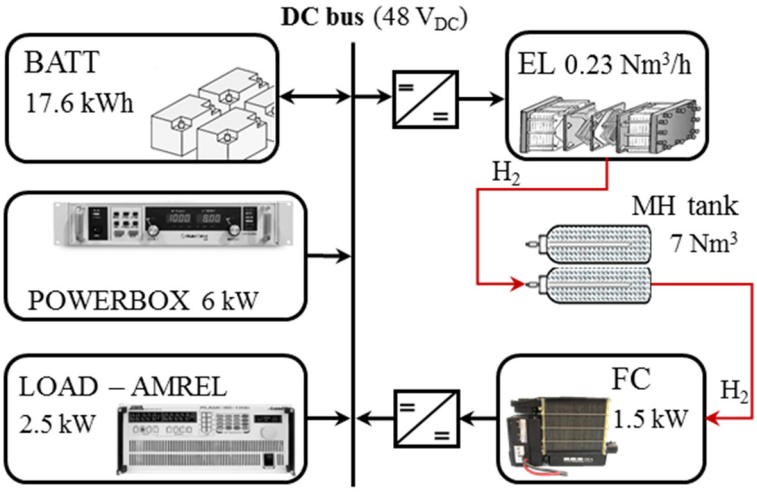

Figure 5.1 - Configuration of the Seville University microgrid.

Hydrogen purification systems are not required since the electrolyzer produces high purity hydrogen. The hydrogen is stored in a $LaNi_5$ metal hydrides alloy storage tank with a 7 Nm^3 storage capacity. Since heat is required to release the hydrogen storage content, a cooling/heating system is incorporated into the test bench. Finally, a 1.5 kW PEM fuel cell completes the hydrogen installation.

Table 5.1 - Main components and characteristics of the Seville University microgrid.

Electronic power source		**Electrolyzer**	
Panel peak power	0.225 kW	H_2 Net Production Rate:	0.23 Nm^3/h@ 5 barg
Channel	2	Nominal power	900 W
Manufacturer	POWERBOX	Manufacturer	HAMILTON-STD
Electronic load		**Fuel Cell**	
Rated power	2.5 kW	Nominal power	1.5 kW
Channel	2	H_2 rated consumption	20 Nl/min
Manufacturer	AMREL	Manufacturer	MES-DEA
Batteries		**Hydrogen Tank**	
Nominal voltage	12 V	Alloy	$LaNi_5$
Rated Capacity (C_{120})	367 Ah	Storage capacity	7 Nm^3
Manufacturer	EXIDE	Manufacturer	LABTECH

The purchase and sale of energy is carried out by the power source and programmable load devices respectively, which are able to simulate this actions thanks to the presence of an independent output channel.

All the electronic devices are connected to a 48 V_{DC} bus supported by a 24-monoblock battery bank of advanced lead acid batteries with a capacity $C_{120,bt}$ = 367 Ah. For the sake of simplicity, the performance of the DC/DC converter, which connects the photovoltaic array to the main 48-V_{DC} bus, is emulated by the programmable power source and the DC/DC and DC/AC converters, which connect the domestic loads and the external grids to the bus, are simulated by the programmable power load.

Regarding the microgrid Supervisory Control and Data Acquisition (SCADA) system, an M-340 programmable logic control (PLC) is installed as the main plant control platform. The communication system includes two OPC (OLE for process control) servers. One server is connected to the PLC and the other one is connected to the electrolyzer on-board PLC (Allen-Bradley). The servers are able to read and write the PLC variables and serve the relevant standard by a client application, in this case a SCADA system. In addition, the SCADA acts as a variable exchanger between the two PLCs.
The controller is provided with data acquisition cards in order to communicate with the programmable load and power source, the plant devices and sensors. The communication between the DC/DC converters and the PLC is performed employing the Canbus communication protocol. The control system monitors the pressure limits in order to guarantee a safety operation. Safety interlocks depend on the pressure limits and any out of normal range operation parameter is reported by the monitoring system. An emergency protocol was implemented in the system. Thus, the control system automatically interlocks the electronic power source in case of major alarms. Immediately, the microgrid is disconnected from the load and an inert gas (nitrogen) purges the pipe lines.

5.1.1. MPC controller

The development of a MPC controller for the power management of the microgrid under consideration was already developed and presented to the scientific community [54], therefore it is not the objective of this thesis.

However, for a better understanding of the results obtained during the experimental activities, a brief description of the MPC controller is introduced hereafter.

The MPC controller designed at the Seville University is based on a Generalized Predictive Control formulation [58]. The supervisor control target is to determine the optimal operating power references for the electrolyzer (P_{EL}), the fuel cell (P_{FC}) and the power purchased or sold to the grid (P_{GRID}). The MPC controller guarantees that only the optimal values are applied to the system. The controller is also designed to set P_{NET} to zero. In this way, the $\{P_{GEN}\text{-}P_L\}$ adds a perturbation on P_{NET} that the controller must balance using the rest of control variables (P_{EL}, P_{FC}, P_{GRID}) in order to track the reference outputs. Furthermore, the following objectives have been explicitly taken into account in the MPC development:

1. Protect the battery bank from deep discharging and overcharging;
2. Limit the power rate of the fuel cell and the electrolyzer in order to protect such expensive equipment from intensive use;
3. Track the SOC and HL references in forecasted conditions;
4. In case an expected event occur, use the battery bank as first way of energy storage and the hydrogen path for long-term energy mismatch.

These objectives are implemented in the MPC through the formulation of a deterministic optimization model with a proper objective function and several constraints. In this way, the MPC computes for each time step the control action by solving the finite-horizon open loop optimal control problem.

In order to achieve all of the previous goals, a multi-objective function is used and the solver tries to minimize it:

$$\begin{aligned} f = \min \sum_{k=0}^{N} & \alpha_1 P_{FC_k}^2 + \alpha_2 P_{EL_k}^2 + \alpha_3 P_{GRID_k}^2 + \alpha_4 P_{NET_k}^2 \\ & + \beta_1 \Delta P_{FC_k}^2 + \beta_2 \Delta P_{EL_k}^2 + \beta_3 \Delta P_{GRID_k}^2 + \beta_4 \Delta P_{NET_k}^2 \\ & + \gamma_1 (SOC_k - SOC_{REF}) + \gamma_2 (HL_k - HL_{REF}) \end{aligned} \tag{5.1}$$

Where N is the time horizon and α, β and γ are the weights for each variable. Three different group of objective function can be recognized in Eq. (5.1)

power variables (P_i), power rate variables (ΔP_i) and storage level variable (SOC and HL).

The four α_i weight penalize the use of the manipulated power variables. Usually the highest weight value is assign to the P_{NET} variable in order to drive the system reach the power balance of the system ($P_{NET} = 0$). The choice of weighting factors allows some flexibility and they can be selected by a trial and error approach. Fuel cell and electrolyzer weighting factors are the same because these devices are based on the same PEM technology. The grid has been more penalized intending to force towards a minor use of it.
The following four β terms penalize the increments on manipulated variables in order to limit the power slew rate. Typically, the electrolyzer power rate is the most bounded because experience advices to prevent frequent set point changes due to the removable source volatility.
Finally, the ability to track SOC and HL reference provided by another controller is introduced in the objective function of the MPC controller by the weight values γ_i. Despite the possibility to follow SOC and HL references, the MPC controller has not previously integrated with an algorithm for the generation of these reference values and the weights values γ_i were usually set equal to zero.

The constraints introduced in the optimal control problem include the unit generation limits, as follow:

$$P_{EL,MIN} \leq P_{EL_k} \leq P_{EL,MAX} \tag{5.2}$$

$$P_{FC,MIN} \leq P_{FC_k} \leq P_{FC,MAX} \tag{5.3}$$

$$P_{GRID,MIN} \leq P_{GRID_k} \leq P_{GRID,MAX} \tag{5.4}$$

The fuel cell and the electrolyzer are both based on PEM technologies and therefore the ramp constraints regarding the power slew rate can be formulated as:

$$\Delta P_{EL,MIN} \leq \Delta P_{EL_k} \leq \Delta P_{EL,MAX} \tag{5.5}$$

$$\Delta P_{FC,MIN} \leq \Delta P_{FC_k} \leq \Delta P_{FC,MAX} \tag{5.6}$$

Lastly, limit in the storage level should be introduced:

$$SOC_{MIN} \leq SOC_k \leq SOC_{MAX} \tag{5.7}$$

$$HL_{MIN} \leq HL_k \leq HL_{MAX} \quad (5.8)$$

To finalize the controller setup, the parameters of sample time, time horizon and control horizon (correspondent of the first branching time for the scenarios tree approach) must be chosen. For this controller, the values have been set to 1 s, 10 s and 2 s respectively. It has been found that shorter sampling time do not give any advantage to the computational time. In the same way, increasing the control horizon above the selected value does not improved the system response.

The performance achieved with the implementation of this control system with the weight of the reference tracking equal to zero, following called MPC-only control, will be compared with those achieved by the MPC controller integrated with the generation scheduling algorithm presented in the Chapter 3.

5.2. Control system design

The novel energy management strategy adopted for the microgrid is designed as a two level control:

- the long-term energy management, which includes production and load forecast, maintenance intervals and disconnection of controllable loads, is entrusted to the proposed generation scheduling
- the short-term energy management, which considers real-time power dispatching among internal sources and loads, is deal with the MPC controller proposed by [54].

The exchange of information and commands between these control modes can be set according to different options.

A possible option is to adopt a hierarchical control structure: the generation scheduling decides which energy source (battery or FC/ electrolyzer) has to absorb/generate the net power, working as a master controller. The slave control is carried out by the MPC controller, in which the power flow of the different sources is determined according to the master control decisions.

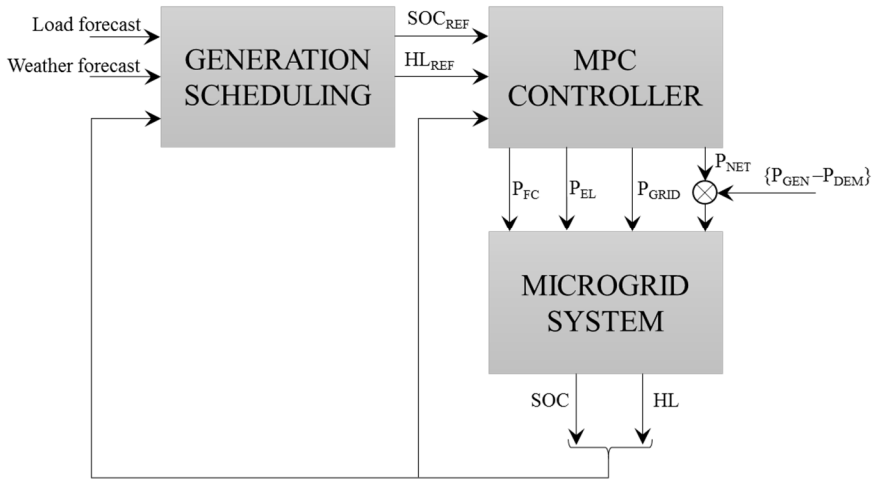

Figure 5.2 - Control system design adopted by the Seville microgrid.

However, the use of the generation scheduling, where the computation time is not negligible, as master control could lead to stability problems in the management of a system with high uncertainty and volatility, such as the microgrid under consideration.

For this reason, a more flexible structure is introduced in the energy management strategy. In particular, the MPC controller works as a master controller while the generation scheduling acts as advisor. In other words, thanks to the MPC controller ability of reference tracking, the generation scheduling sends to the MPC controller the SOC and HL reference values for the next hour, depending on weather and load forecast and the current condition of the energy storage systems. The MPC controller recognizes this information and try to reach this target. However, if some unexpected events occur that make impossible or inopportune the reference tracking, the MPC controller notices it and manages by itself the power flows of the system. A simplified scheme of the exchange of information between the different control levels and the microgrid system is shown in Figure 5.2.

5.2.1. MPC controller set up

As shown by Eq. (5.1), the two γ weighting factors may strongly condition the system behavior and represent the link between generation scheduling and MPC controller. For this reason, unlike the MPC-only control system (were the γ weights are set to 0), high values are imposed for the γ

weighting factors. Because of the generation scheduling mainly involves the hydrogen storage commitment in comparison with batteries, the weight for the HL tracking is higher than the SOC tracking. In other words, the control system tries to keep the difference between the actual HL values and the HL reference value as low as possible while the weight of the SOC tracking is more marginal. Thus, the influence of the generation scheduling for the battery management is low, while variation of the HL reference often lead to an actual commit of the hydrogen storage system.

The weight values for each term of Eq. (5.1) are reported in Table 5.2. The values of the generator and storage level limits are shown in Table 5.3. Unlike the values introduced in Table 5.1, two changes are imposed in the controller that take into account the wear of some devices, in particular batteries and fuel cell. The first is the actual battery capacity, which is lower than the nominal one due to the series of cycles of charge and discharge of the battery. From laboratory tests, the residual capacity is about 150 Ah with respect to the value of 367 Ah declared by the manufacturer. The second wear phenomenon is related to the maximum power output of the fuel cell. Because of the degradation of the membrane and other wear phenomena, this value is less than half of the rated power of the fuel cell. Both phenomena will affect the storage capacity and the flexibility of the overall system: the batteries will reach the maximum or the minimum SOC more quickly with a lower storage capacity whereas the fuel cell will be unable to satisfy high load power demands and the purchasing of power from grid will be often necessary.

Table 5.2 - Weight values imposed in the MPC multi-objective function for the GS+MPC control system

Power variables weights		Power rate weights		Storage level weights	
α_1	0.005	β_1	1	γ_1	10
α_2	0.005	β_2	1.5	γ_2	60
α_3	0.008	β_3	0.0001		
α_4	100	β_4	0.0001		

Table 5.3 - Limited and initial values imposed in the control system

Battery	
Minimum State-of-charge (SOC_{MIN})	40%
Maximum State-of-charge (SOC_{MAX})	75%
Initial State-of-charge (SOC_{IN})	52%
Maximum charging/discharging power ($P_{B,MAX}$)	2640 W
H2-Storage	
Minimum H_2 tank level (HL_{MIN})	10 %
Maximum H_2 tank level (HL_{MAX})	90 %
Initial H_2 tank level (HL_{IN})	85 %
Minimum electrolyzer power ($P_{E,MIN}$)	100 W
Maximum electrolyzer power ($P_{E,MAX}$)	900 W
Minimum fuel cell power ($P_{FC,MIN}$)	100 W
Maximum fuel cell power ($P_{FC,MAX}$)	500 W

5.2.2. Generation scheduling set up

The generation scheduling is implemented in a different computer and a network communication is set up for the exchange of information with the MPC controller. In order to provide SOC and HL reference values, instead of the on/off status of devices, a reoptimization process is needed, as explained in the paragraph 3.3.6. Starting from the current microgrid conditions, the load request and the power production forecast, the proposed control system firstly solves the stochastic optimization problem for the determination of the optimal unit commitment. This choice is imposed as a constraint in the reoptimization problem to find the SOC and HL reference values. The trend of the reference values is a piecewise linear function, which is updated each hour with a rolling time approach.

The objective function of the problem is the sum of the utilization costs defined in the paragraph 3.3. The investment and O&M costs, required for the evaluation of the operating costs, are reported in Table 5.4, in accordance with the actual costs incurred by the laboratory.

As regards the generation of the scenarios tree, according to the previous case study, 3 and 5 different scenarios for solar radiation and wind speed are respectively generated by the control system starting from the foreseen conditions, while 5 scenarios of possible load curves are generated from the expected demand. The 75 scenarios are analyzed and reduced to 15 scenarios to allow a real-time control.

Table 5.4 - Costs and estimated lifetime for storage devices

	Batteries:	**Electrolyzer:**	**Fuel Cell:**
Investment cost	125 €/battery	12000 €	7000 €
Estimated lifetime	1500 cycles (DOD = 35%)	30000 h	20000 h
O&M cost	-	0.1 €/h	0.1 €/h

Limit values for generator power output and storage levels are introduced in accordance with Table 3.3.

5.3. Results and discussion

With the aim to evaluate the performance of the control system under consideration on the microgrid, two different representative tests were conducted over 24 hours of experimental duration. The first test is based on a typical summer day, with high values of solar radiation and sunshine duration. The power produced by the photovoltaic array is mainly concentrated during the middle of the day. A domestic power demand profile is used as a load curve with two peak periods (midday and late afternoon) and a base load during the night.

This power produced by the PV generator is used in part directly by the load and in part sent to the two storage systems. Figure 5.3 shows the evolution of produced power during the day. At the end of the summer day, the total energy produced is 13.6 kWh, whereas the total energy required by the load is 14.3 kWh.

The profile evolution of the power produced and demanded is shown by Figure 5.3(a). This data are introduced in the programmable electronic power source and the programmable electronic load to proper simulate the real behavior of the photovoltaic array and the domestic load demand. The experimental results in terms of power flows are shown by Figure 5.3(b-c). In particular, Figure 5.3(b) shows the power flows during the periods of excess power production, while Figure 5.3(c) shows how the microgrid deals with a deficit of power production.

The yellow line, common for both of figures, indicates the power directly used by the load without any storage conversion.

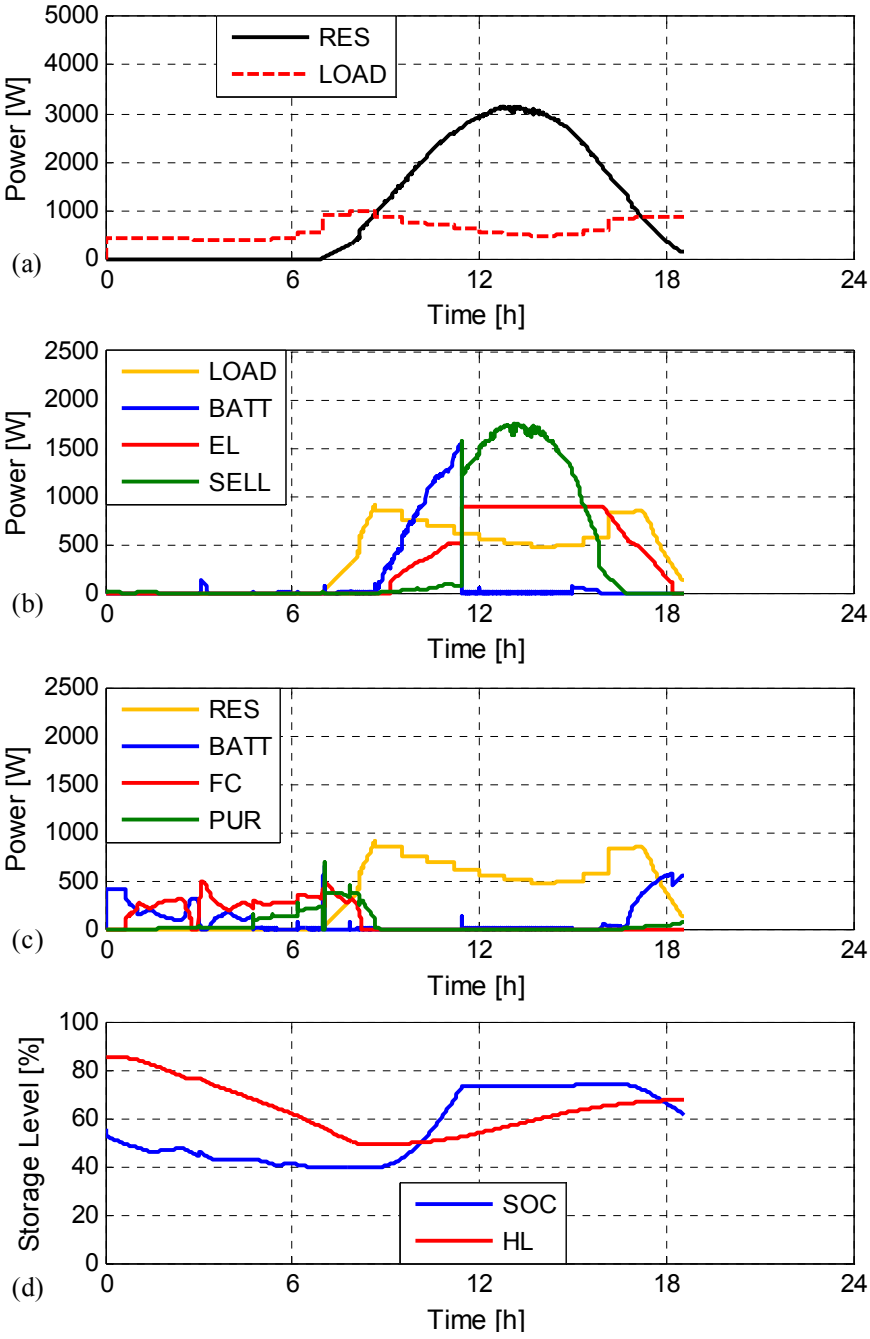

Figure 5.3 - Power flows and storage levels for the summer day case

A power deficit occurs during the first hour of the day. At the beginning, the batteries are used to cover the deficit but the control system realizes the impossibility to completely satisfy the demand only with batteries and the fuel cell is switched on after 30 minutes. The fuel cell is used all night long until the RES production exceed the load (around at 8:30) with only a short stop in the middle of the night. Despite the large use of hydrogen storage, the minimum SOC is anyway reached at 4:30. From this point, the control system starts to purchase power from the upstream grid to cover the demand not satisfied by the fuel cell. The energy purchase could be probably avoided by increasing the maximum fuel cell power, as the minimum hydrogen level reached at the end of the night (about 50%) is far from its lowest value.

During the day, 9 hours of excess power production occur. The control system prefer to charge the batteries in the first part of the morning until the maximum SOC is reached. The charging phase duration is about 3 hours. Despite the batteries are not fully charged, the commitment of the electrolyzer occurs at 9:30. In fact, as for the fuel cell, the control system notices the large excess of energy that probably will occur in the next hours and decides to restrict the charge current of batteries (that means an higher battery efficiency). At the same time the control system, partially smooth the power rate of the electrolyzer. A large excess of power is produced in the middle of the day. Due to the fact that the batteries are fully charged and the maximum electrolyzer power is reached, a large amount of excess energy is sold to the upstream grid.

Despite the large use of the electrolyzer, the final hydrogen level does not reach its initial value, while batteries are use to cover the deficit of energy during the evening.
In order to identify the role of the generation scheduling in the control system of the microgrid, Figure 5.4 shows a comparison between the reference values provided by the generation scheduling and the actual evolution of the storage levels. In the first part of the test, the difference between reference values and real level is negligible, especially for the HL, and the MPC control system takes strongly into consideration the reference tracking. A bigger mismatch between reference and real level occurs during the power surplus period. The control system prefers to fully charge the batteries, despite the reference suggests to use the electrolyzer.

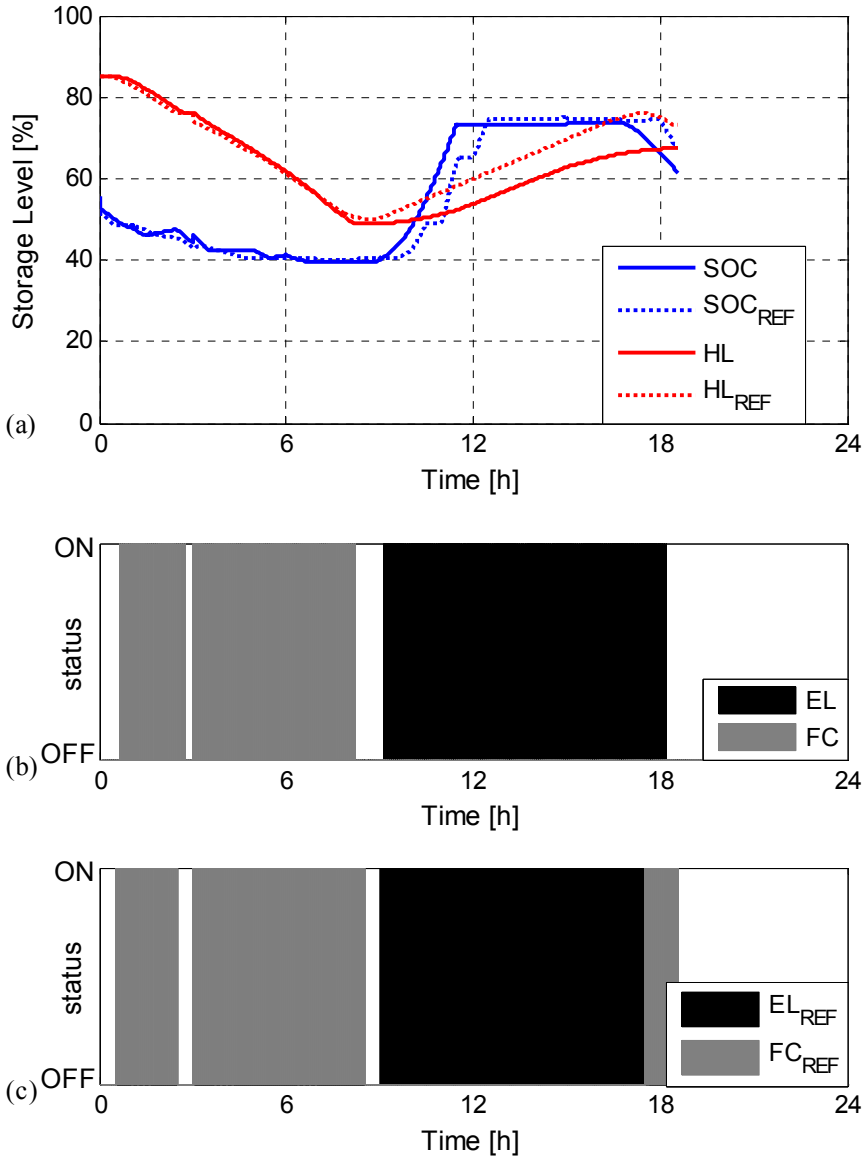

Figure 5.4 - Comparison between reference and real value for the summer case

In fact, the first two weighting factors in Eq. (5.1) prefer the use of batteries instead of electrolyzer and the difference between actual HL and reference HL is unable to counteract the others weights.

In general, a delay in the decision of the control system occurs with respect to the generation scheduling. This is due to two main reasons: the electrolyzer presents the highest power rate weight (β), that means a very slow dynamic response while the power weight (α) of the electrolyzer is much higher than that if the batteries. With reference to Eq. (5.1), these two terms contrast the tracking, and a greater difference between the reference level and the actual value is obtained so that the weight of this term becomes predominant over the other two. This fact is confirmed by the comparison between Figure 5.4 (b) and (c): the first shows the actual use of the hydrogen storage system while the second shows the unit commitment found as a solution of the stochastic optimization problem.
On the average, a delay of about 8-10 min occurs in the start/stop of the hydrogen storage devices. Moreover, a difference in the power rate also arise in the comparative analysis, especially for the electrolyzer, with greater running time with respect to the commitment given by the generation scheduling. For instance, the electrolyzer is used for 9.10 h instead of 8.50 h scheduled.

The second test is conducted for a typical cloudy day of autumn. This test is much more difficult for the control system. In fact, the control system has to face firstly a clear sky situation but, suddenly, the sky becomes cloudy around noon resulting in a significant decrease of the energy produced by the photovoltaic system.
The power production profile together with the load profile is shown in Figure 5.5 together with the power flows during the excess or deficit energy periods and the storage level. As the previous case study, the control system starts to satisfy the demand using the batteries but after 30 minutes the fuel cell is switched on despite the SOC is far from its minimum value. The load request is satisfied by the fuel cell for almost 5 hours and the batteries are used only for balancing the power inside the microgrid. After that, the batteries are committed to cover the deficit of power.
However, the batteries reach their minimum SOC after 1.5 h and the fuel cell is again used.
Due to the constraints in the power rate and the power limits, the fuel cell is unable to satisfy by itself the load request and the purchase of power from the grid is unavoidable.

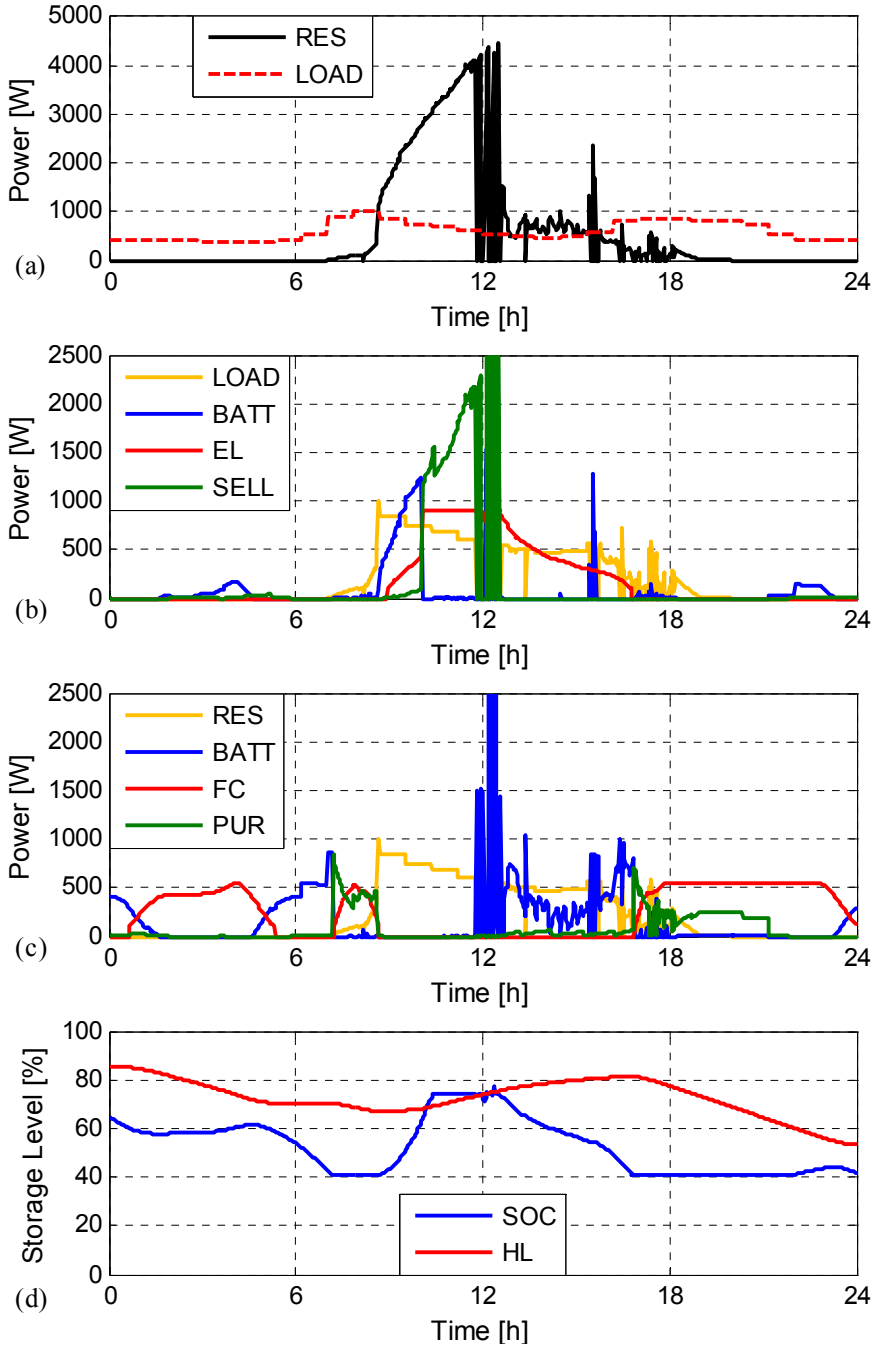

Figure 5.5 - Power flows and storage levels for the cloudy day case

Like the previous case, the batteries charging is a priority for the control system in the morning, although the commitment of the electrolyzer starts already at about 8 o'clock. High fluctuation in the production power occurs around noon. The hydrogen storage system is unable to follow it due to power rate constraints and therefore the batteries are used to balance the power in the microgrid. In this situation, the MPC rarely follows the reference provided by the generation scheduling. In fact, the weight of the other two terms, especially the power rate weight, considerably increases at the expense of the ability of tracking the reference values. A general decrease in the power production is observed in the afternoon when the production match the demand. However, the electrolyzer power is slowly reduced by the MPC due to the little power rate imposed despite the low excess of power. Therefore, the batteries are again used to balance the power and a decreasing of the SOC occurs. Such behavior is disadvantageous from the point of view of energy efficiency as the energy losses increase due to the double energy conversion (source - batteries - hydrogen - load). Furthermore, the batteries reach the minimum SOC again in the evening and the fuel cell has to cover by itself the demand of energy in the last hours of the day.

In order to better understand the results of the unit commitment provided by the generation scheduling and how much these indication are taken into account by the MPC controller during the real behavior, a comparison between real values and reference values is shown in Figure 5.6. Unlike the summer case, a general reduction in the ability of the MPC to track the references is observed. As the previous case, the control system needs a delay to increase the weight of the reference tracking into the objective function and to follow the scheduling of the upstream control.

Furthermore, an increase in the running time of the hydrogen storage system is again observed: the electrolyzer is used for 7.80 h although the generation scheduling commits it for 5.25 h while the fuel cell is used for 13.20 h against a scheduling of 10.25 h.

The persistence of the electrolyzer use in the afternoon, despite the generation scheduling does not commit it, demonstrates the disadvantage in the use of MPC as master control instead of a hierarchical control. However, several improvements could be introduced, especially in the weight values.

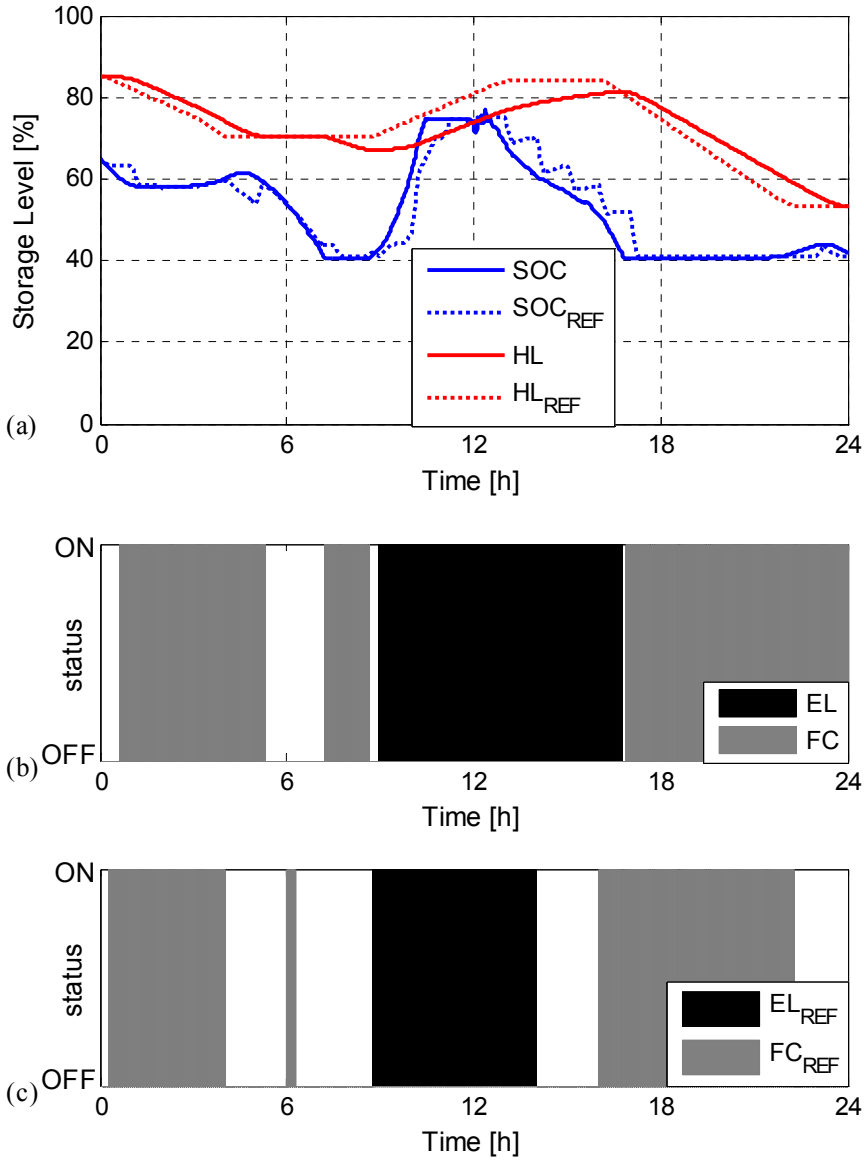

Figure 5.6 - Comparison between reference and real value for the cloudy case

5.3.1. Comparative analysis

As carried out in the previous chapter for the microgrid at H_2FER Laboratory, a comparative analysis is carried out to study the benefit and

the drawbacks of the proposed control system. In this chapter, the performances of the proposed control system (GS+MPC) applied to the Seville microgrid are compared with the expected performance of the MPC controller without the contribution of the generation scheduling algorithm (MPC-only). In the latter case, the control is totally committed by the MPC since the γ weights of the reference tracking are put to zero. Unfortunately, the experimental results obtained with the implementation of the MPC-only control system are at this moment unavailable and the following analysis was carried out based on simulation results for both the control systems.

The comparative analysis was carried out through the evaluation of the key performance factor (KPI) defined in Chapter 4 and summarized in Table 5.5. A minor use of the upstream grid is observed with the determination of both the %UMD and the %UNE with the use of the proposed control system. In particular, a lower amount of unmet load occurs for both the case studies thanks to a higher use of the fuel cell (especially for the summer day case). Furthermore, a higher commit of the electrolyzers is also observed for the GS+MPC control system due to the greater capacity to manage the surplus of energy without the use of the upstream grid. Such benefits are mainly due to the ability of the novel control system to forecast the commitment of the fuel cell and electrolyzer and properly switch on and off these devices. Vice versa, the MPC-only control system often is faced with high energy demands with the inability to use battery ($SOC = SOC_{MIN}$) and with the constraint of the maximum fuel cell power rate. The only way to conserve the energy balance is to purchase power from the grid or to shed the load. Similarly, during the energy surplus periods, the MPC-only control system commits the electrolyzer just when the batteries are almost fully charged. However, the electrolyzer has some limitations in the power rate, even more of the fuel cell, and the controller is forced to sell energy to the grid or to decrease the energy production to close the energy balance of the microgrid.

Regarding the conversion efficiency, there are no large differences between the two control systems. Despite the higher use of the hydrogen storage system (which present a lower efficiency than batteries), the energy path efficiency (η_{PATH}) of GS+MPC control system is slightly higher for both the two cases. Despite the analysis of a single day is not significant for evaluating the actual improvement in the system performance, positive signals are anyway detected.

The main drawback of the GS+MPC control system is given by the increase of the operating costs due to the increase of the fuel cell and electrolyzer running times. This fact is especially noted in the summer case where the operating hours of the hydrogen storage system are 4 h higher than those obtained for the MPC-only control system. However, it is worth to note that the final value of the battery SOC is equal to the minimum value with the use of the MPC-only control system. This fact means that the system will be forced to use the fuel cell throughout the following night with the inevitable increase in operating costs for the following day. Vice versa, the final SOC is higher than the threshold value for the GS + MPC case, especially for the summer case, which means that the system can still use the batteries for satisfy the energy demand during the night.

Figure 5.7 confirms the increased use of the storage systems with respect to the exchange of energy with the grid by using the GS + MPC control system. This fact is evident in the summer case, where all the energy flows are higher than those for the cloudy day case.

Table 5.5 - Summary of KPI obtained from comparative analysis between GS+MPC control system and MPC-only control system

	Summer day case		***Cloudy day case***	
	GS+MPC	**MPC-only**	**GS+MPC**	**MPC-only**
%UMD	5.6	8.2	12.9	13.5
%UNE	30.7	33.3	27.0	35.3
$\overline{\eta}_{H_2}$ **[%]**	38.5	38.8	41.3	41.3
$\overline{\eta}_{B}$ **[%]**	85.5	85.5	85.5	85.5
η_{PATH} **[%]**	60.5	60.2	60.6	60.0
HL_{FIN} **[%]**	31.7	53.2	53.3	53.8
SOC_{FIN} **[%]**	69.2	40	41.8	40
t_E **[h]** (δ_E)	8.7 (1)	7.6 (1)	7.8 (1)	7.1 (1)
t_{FC} **[h]** (δ_{FC})	14.5 (2)	11.5 (2)	13.2 (3)	13.2 (2)
Operating Cost [€/day]	14.0	12.9	14.9	14.3

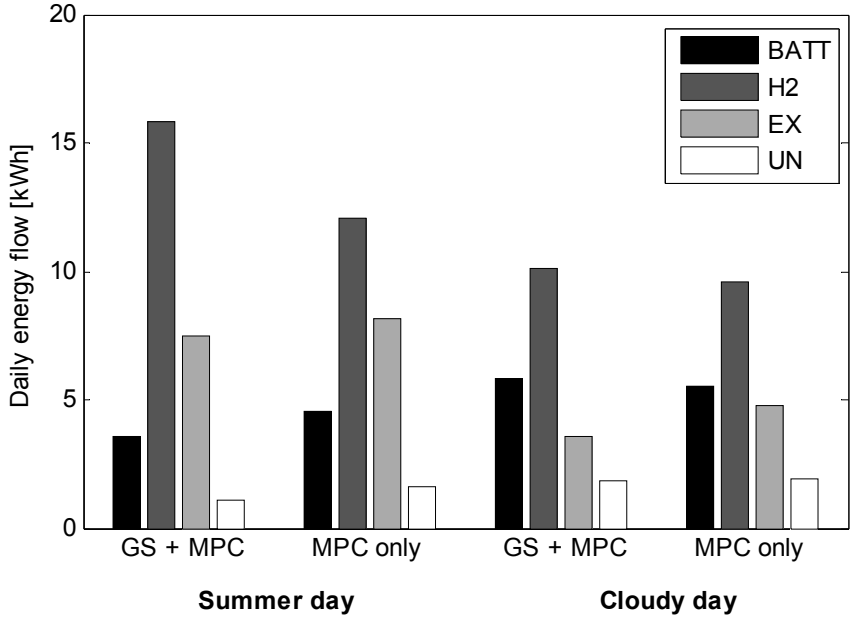

Figure 5.7 - Comparison of the daily energy flows between the GS+MPC control system and the MPC-only control system

In particular, 56% of the overall daily energy exchanged by the two energy storage systems and the grid is exchanged by the hydrogen storage system for the GS + MPC case, and only 42% for the MPC-only case. Little differences are obtained in the cloudy day case. However, a rise in the use of the energy storage systems with respect to the grid is also observed. For instance, the total energy exchanged with the grid is equal to 25% of the overall daily energy flow with the GS+MPC control system while it increases to the 30% with the use of the MPC-only control system.

The comparison between the time variation of the storage levels as well as the electrolyzer and fuel cell status are shown in Figure 5.8 and Figure 5.9. Depending on the implemented control system, significant differences in the change of storage levels are noted for the summer case. In particular, the hydrogen level for the GS + MPC case is always lower than the MPC-only one.

On the contrary, there is a significantly decrease in the period in which the batteries are completely discharged becoming just 1.6 h respect with 10.25 h for the MPC-only case. This is a very important factor, especially for stand-alone configurations: the preservation of the remaining battery SOC

helps in the power management especially during very quickly power changes that the fuel cell is not able to satisfy.

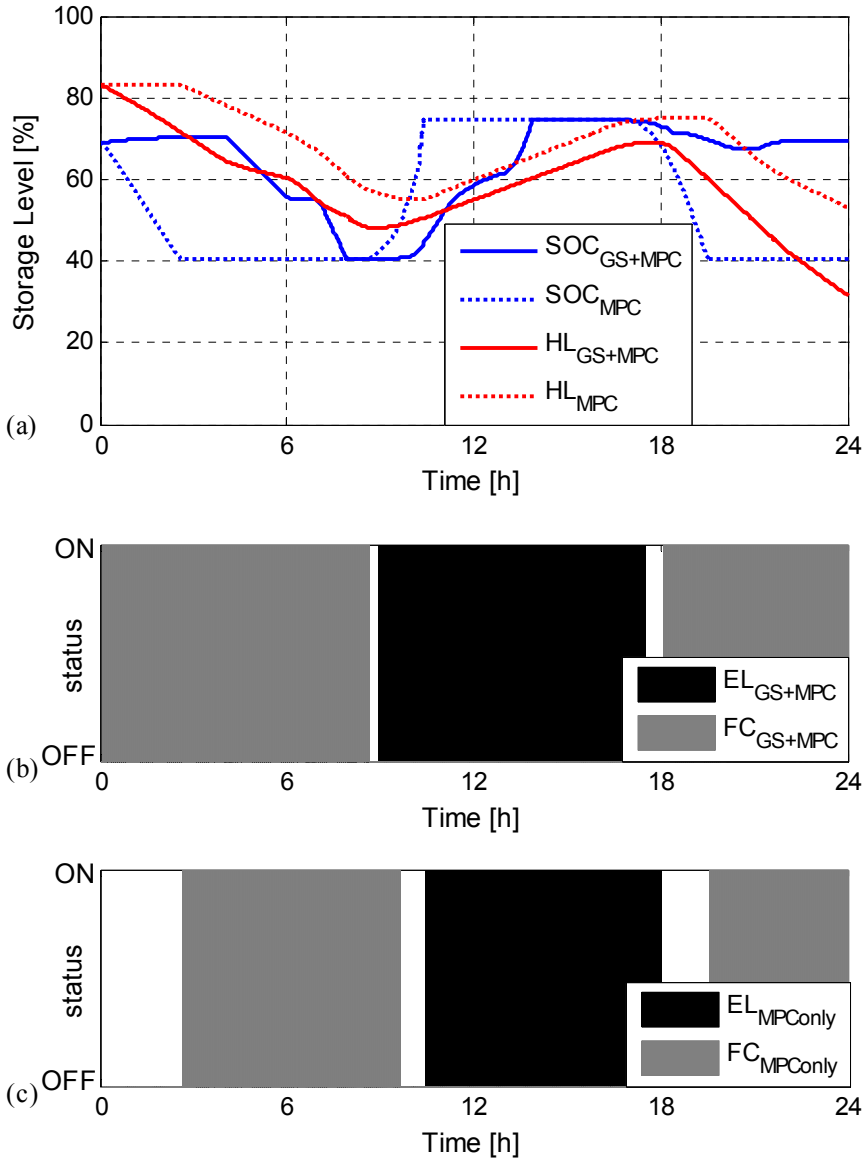

Figure 5.8 - Storage levels and on/off status of electrolyzer and fuel cell for the GS+MPC and MPC-only control systems for the summer day case

Finally, a considerable difference is observed in the final storage levels, which will strongly influence the microgrid management in the following day. From the Figure 5.8(b) and (c), a time advance in the commitment of the hydrogen storage system is observed, in addition to an higher running time.

For the cloudy day case, Figure 5.9(a) shows a similar trends in the storage levels especially in the second part of the day. In the first part of the day, the GS helps the control system to minimize the hours where the battery is completely discharge. In fact, the period in which the SOC is the minimum value is 1.4 h unlike the MPC-only case where the SOC_{MIN} is kept for 8 hours. The large fluctuations occurring from midday led the GS to have less influence in the control strategy of the microgrid while the MPC controller assumes greater autonomy in management decisions. This is due to the increase of the P_{NET} weight (α_4) in order to preserve the energy balance of the microgrid in this hard situation and the power slew rate weighting factors that limit the shut down of the electrolyzer. As the previous case, an advance in the commitment of the hydrogen storage system occurs for the GS+MPC control. Three different fuel cell start-up are observed: this should be a drawback as the number of start/stop largely influenced the degradation of the fuel cell and its lifetime.

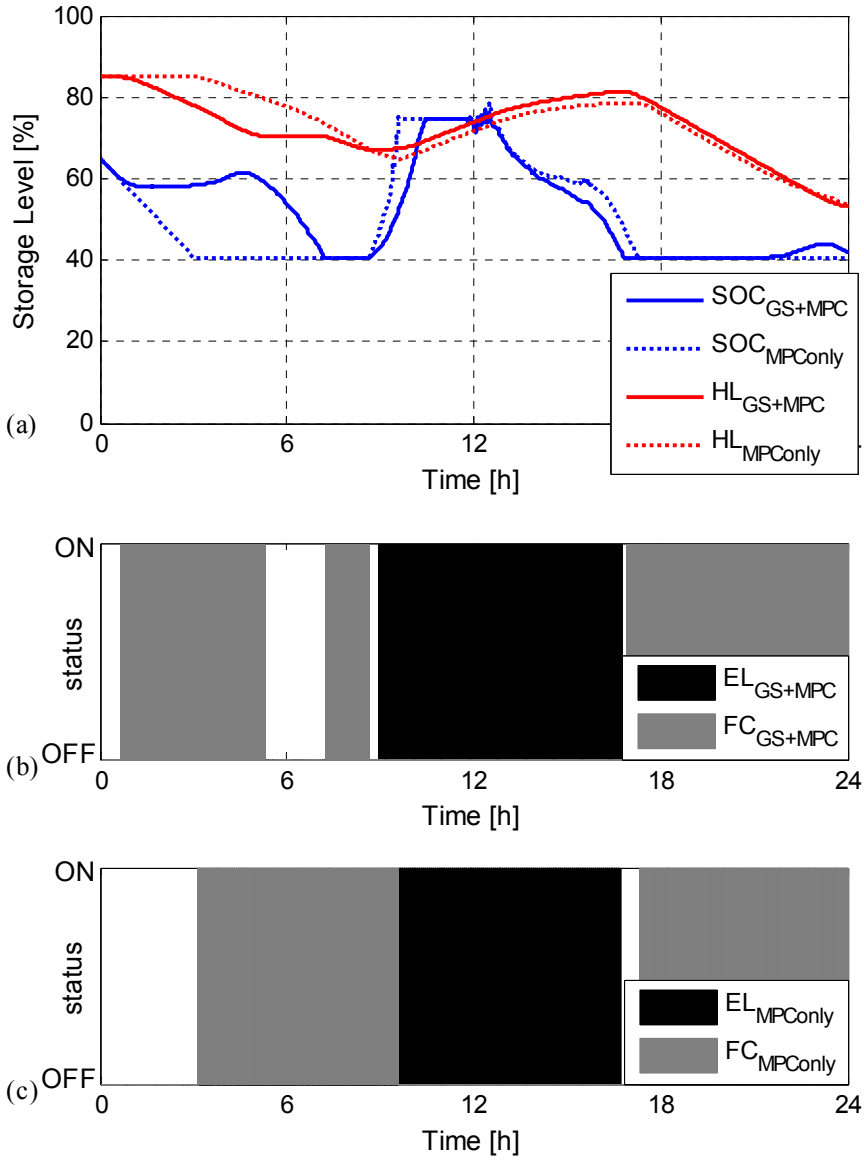

Figure 5.9 - Storage levels and on/off status of electrolyzer and fuel cell for the GS+MPC and MPC-only control systems for the cloudy day case

Chapter 6

Conclusions and future research

The availability of more accurate and efficient energy management strategies is one of the main factors for the development of effective integrated systems based on distributed generation. In this framework, a novel generation scheduling algorithm for the optimal management of microgrids based on different energy storage systems and generators is presented in this thesis. Starting from the forecasts of weather conditions and load requirements, the proposed algorithm calculates the optimal generation scheduling that minimize the operating costs of the microgrid. Unlike the algorithms presented in literature, the optimal alternative between short-term and long-term energy storage and their integration with others Diesel generators is an integral part of the optimization process.
A statistical approach based on the generation of a scenario tree has been introduced to account for forecasting uncertainties. This approach has demonstrated an intrinsic ability to make decisions about the optimal management of devices for the upcoming period, taking into consideration the probable evolutions in weather conditions and load demand for the following days as well as their possible errors. More robust solutions has been therefore achieved, which is a fundamental result for an effective long-term energy management of energy systems with high volatility such as microgrids with high penetration of RES.

The novel energy management strategy was firstly applied to the stand-alone microgrid of the H_2FER laboratory of Sardegna Ricerche powered by

RES and integrated with an energy storage section based on a battery bank and a hydrogen storage system. To compare the results obtained with the standard EMS widely applied in the literature and based on the use of state variable control, a comparative analysis was introduced. In particular, the comparative analysis was carried out with reference to three different climatic situations (a summer week, an in-between season week and a winter week). The results show an improvement in system performance compared to the EMS based only on the use of the SOC as a control variable. Furthermore, performance deviated only slightly from that obtained with a perfect EMS, where input data are perfectly forecasted. The proposed EMS allows a reduction in operating costs of the energy storage section, especially during the summer and winter weeks.
The analysis was subsequently extended to a year to study the annual performance of the microgrid. The annual analysis showed that the current hydrogen storage capacity of the studied microgrid cannot meet annual energy requirements, especially during winter months, and produces a significant amount of excess energy during summer months. Owing to its low energy storage capacity, the annual performance of the overall microgrid is only slightly affected by the energy management strategy adopted. On the contrary, the adoption of a more complex EMS is able to yield significant benefits in the case of hydrogen storage systems designed for long-term energy storage (from summer to winter). With higher hydrogen storage capacities, the results of a comparative analysis between the proposed EMS and a simpler SOC-based EMS highlights the benefits of including weather forecast and operating cost in the EMS. In fact, for higher storage capacities the proposed EMS provides a decrease of almost 5-10% in annual operating costs and energy losses. In particular, for a hydrogen storage capacity 10 times higher than the current one, the decrease in annual operating costs is about 10% and energy losses decrease by about 6%.

Finally, the generation scheduling was implemented as control system of the microgrid of the Seville University. The proposed algorithm is interfaced with another algorithm already implemented based on model predictive control to manage the storage system not only for optimal short-term energy control but also for optimal long-term energy management.

The new configuration was tested on two different cases: a summer case, with a high and stable power production and a cloudy day with a quick variation in the power supply. The comparative analysis with a MPC-only control demonstrates different advantages brought by the proposed control. In particular, a lower use of the upstream grid is achieved with a better integration between the two storage systems. However, some disadvantages are present, such as the increase in fuel cell and electrolyzer running time with the subsequent increase in operating costs.

6.1. Future research

The proposed algorithm was mainly used as control system for microgrids integrated with PV systems, wind turbine, hydrogen storage systems and batteries. However, it can be applied to other system configurations based on the use of different renewable energy sources and different energy storage systems. The proposed generation scheduling can be applied not only for the management of energy storage systems but also for thermal energy storage systems (TESs), which are characterized by a slow dynamic behaviors.

Further improvements in the generation scheduling can be introduced, as the possibility of equipping the control system with self-regulation of the weights according to the analysis of historical data of the user behavior and energy generation systems.

The coupling with smart control systems, such as model predictive control, showed interesting results. However, it can be improved especially on the possibility of optimization of the weights depending on the instability of the microgrid.

Bibliography

[1] N. Padhy, "Unit commitment-a bibliographical survey.," *IEEE Transactions on Power Systems,* vol. 19, no. 2, pp. 1196-1205, 2004.

[2] H. Farhangi, "The path of the smart grid," *Power and Energy Magazine, IEEE,* vol. 8, no. 1, pp. 18 - 29 , 2010.

[3] T. Ackermann, G. Andersson and L. Soder, "Distributed generation: a definition," *Electric Power Systems Research,* vol. 57, pp. 195 - 204, 2001.

[4] W. El-Khattam and M. Salama, "Distributed generation technologies, definitions and benefits," *Electric Power Systems Research,* vol. 71, pp. 119 - 128, 2004.

[5] Z. Melhem, Electricity Transmission, Distribution and Storage Systems, Woodhead Publishing, 2013.

[6] S. Chowdhury, S. Chowdhury and P. Crossley, Microgrids and Active Distribution Networks, Institution of Engineering and Technology, 2009.

[7] N. Jenkins, J. Ekanayake and G. Strbac, Distributed Generation, Institution of Engineering and Technology, 2010.

[8] "Measuring progress towards energy for all," in *World Energy Outlook*, International Energy Agency, 2012, pp. 529-547.

[9] J. K. Kaldellis, Stand-Alone and Hybrid Wind Energy Systems - Technology, Energy Storage and Applications, Woodhead Publishing, 2010.

[10] J. Twidell and T. Weir, Renewable Energy Resources, UK: Spon Press, 2000.

[11] M. Baran and N. Mahajan, "Distribution for industrial system: opportunities and challanges," *IEEE Transactions on Industry Applications,* vol. 39, no. 6, pp. 1596-1601, 2003.

[12] F. Katiraei, M. Iravani and L. P.W., "Micro-grid autonomous operation during and subsequent to islanding process," *IEEE Transactions on Power Delivery,* vol. 20, no. 1, p. 248–57, 2005.

[13] J. Justo, F. Mwasilu, L. J. and J. Jung, "AC-microgrids versus DC-microgrids with distributed energy resources: a review," *Renewable and Sustainable Energy Reviews,* vol. 24, pp. 387-405, 2013.

[14] H. R.A, Energy Storage, Spriger, 2010.

[15] J. Barton and I. D.G., "Energy Storage and Its Use With Intermittent Renewable Energy," *IEEE TRANSACTIONS ON ENERGY CONVERSION,* vol. 19, no. 2, pp. 441- 448, 2004.

[16] G. R.B, Hydrogen Fuel: Production, Transport and Storage, New York: CRC Press, 2009.

[17] N. Amjady, "Short-term bus load forecasting of power systems by a new hybrid method," *IEEE Transaction Power System,* vol. 22, no. 1, pp. 334-341, 2007.

[18] N. Amjady, F. Keynia and H. Zareipour, "Short-Term Load Forecast of Microgrids by a New Bilevel Prediction Strategy," *IEEE Transaction on Smart Grid,* vol. 1, no. 3, pp. 286-294, 2010.

[19] P. Ruiz, C. Philbrick, E. Zak, K. Cheung and P. Sauer, "Uncertainty management in the unit commitment problem," *IEEE Transaction on Power System,* no. 24, pp. 642-651, 2009.

[20] P. A. Ruiz, C. R. Philbrick, E. Zak, K. W. Cheung and P. W. Sauer, "Applying stochastic programming to the unit commitment problem," in *10th International Conference on Probabilistic Methods Applied to Power Systems*, 2008.

[21] S. Pallottino, G. Sechi and P. Zuddas, "A DSS for water resources management under uncertainty by scenario analysis," *Environmental Modelling & Software,* no. 20, pp. 1031-1042, 2005.

[22] A. Y. Saber and G. K. Venayagamoorthy, "Resource Scheduling Under Uncertainty in a Smart Grid With Renewables and Plug-in Vehicle,," *IEEE Systems Journal,* vol. 6, no. 1, pp. 103-109, 2012.

[23] M. Wang and H. B. Gooi, "Spinning Reserve Estimation in Microgrids," *IEEE Transactions on Power Systems,* vol. 26, no. 3, pp. 1164-1174, 2011.

[24] A. M. Zein Alabedin, E. F. El-Saadany and M. M. A. Salama, "Generation Scheduling in Microgrids under Uncertainties in Power Generation," in *IEEE Electrical Power and Energy Conference* , 2012.

[25] R. Doherty and M. O'Malley, "A New Approach to Quantify Reserve Demand in Systems With Significant Installed Wind Capacity," *IEEE TRANSACTIONS ON POWER SYSTEMS,* vol. 20, no. 2, pp. 587-595, 2005.

[26] R. Dufo-López, J. Bernal-Agustín and J. Contreras, "Optimization of control strategies for stand-alone renewable energy systems with hydrogen storage.," *Renewable Energy ,* no. 32, pp. 1102-1126, 2007.

[27] M. El-Sharkh, A. Rahman and M. Alam, "Short term scheduling of multiple grid-parallel PEM fuel cells for microgrid applications," *International journal of hydrogen energy ,* no. 35, pp. 11099-11106, 2010.

[28] N. Zendehde, A. Karimpour and O. M., "Optimal Unit Commitment Using Equivalent Linear Minimum Up and Down Time Constraints," in *2nd IEEE International Conference on Power and Energy*, Malaysia, 2008.

[29] G. Gahleitner, "Hydrogen from renewable electricity. An international review of power-to-gas pilot plants for stationary applications," *International Journal of Hydrogen Energy,* vol. 38, no. 5, pp. 2039-2061, 2013.

[30] M. Little and M. I. D. Thomson, “Electrical integration of renewable energy into stand-alone power supplies incomporating hydrogen storage,” *International Journal of Hydrogen Energy,* vol. 32, no. 10, pp. 1582-1588, 2007.

[31] Ø. Ulleberg, “The importance of control strategies in PV–hydrogen systems,” *Solar Energy ,* vol. 76, pp. 323-329, 2004.

[32] D. Ipsakis, S. Voutetakis, P. Seferlis, F. Stergiopoulos and C. Elmasides, “Power management strategies for a stand-alone power system using renewable energy sources and hydrogen storage,” *International Journal of Hydrogen Energy ,* vol. 34, pp. 7081-7095, 2009.

[33] C.-R. A.U, J. Cruz, R. Espinosa-Lumbreras, J. Ledesma-García, S. Durón-Torres and L. Arriaga, “Design and set up of a hybrid power system (PV-WT-URFC) for a stand-alone application in Mexico,” *International Journal of Hydrogen Energy,* vol. 38, pp. 12623-12633, 2013.

[34] J. Torreglosa, P. García, L. Fernández and F. Jurado, “Hierarchical energy management system for stand-alone hybrid system based on generation costs and cascade control,” *Energy Conversion and Management,* vol. 77, pp. 514-526, 2014.

[35] M. Castañeda, A. Cano, F. Jurado, H. Sánchez and L. Fernández, “Sizing optimization, dynamic modeling and energy management strategies of a stand-alone PV/hydrogen/battery-based hybrid system,” *International Journal of Hydrogen Energy,* vol. 38, pp. 3830-3845, 2013.

[36] M. Masoum, H. Dehbonei and E. Fuchs, “Theoretical and Experimental Analyses of Photovoltaic Systems with Voltage- and Current-Based Maximum Power-Point Tracking,,” *IEEE Transaction on Energy Conversion,* no. 17, pp. 514-522, 2002.

[37] Y. Sukamongkol, S. Chungpaibulpatana and W. Ongsakul, “A simulation model for predicting the performance of a solar

photovoltaic system with alternating current loads," *Renewable Energy,* no. 27, pp. 237-258, 2002.

[38] A. Rabl, Active solar collectors and their applications, Oxford University Press.

[39] M. Khan and I. M.T., "Analysis of a small wind-hydrogen stand-alone hybrid energy system," *Applied Energy,* vol. 86, pp. 2429-2442, 2009.

[40] O. Tremblay, L. Dessaint and A. Dekkiche, "A generic battery model for the dynamic simulation of hybrid electric vehicles," *Proc. Vehicle Power and Propulsion IEEE Conference,* pp. 284-289, 2007.

[41] O. Al-Naseem, R. W. Erickson and P. Carlin, "Prediction of switching loss variations by averaged switch modeling," in *Applied Power Electronics Conference and Exposition*, 2000.

[42] Ø. Ulleberg, Stand-alone power system for the future:optimal design, operational and control of solar-hydrogen energy systems, Norway: Ph.D. thesis, Norwegian University of Science and Technology, 1998.

[43] K. Harrison, Design, Integration and Control of Proton Exchange Membrane Electrolyzer for Wind Based Renewable Energy Application, USA: Ph.D. thesis, University of North Dakota,, 2006.

[44] N. Dale, M. Mann and H. Salehfa, "Semiempirical model based on thermodynamic principles for determining 6 kW proton exchange membrane electrolyzer stack characteristics," *Journal of Power Sources,* no. 185, pp. 1348-1353, 2008.

[45] L. Zhou and Y. Zhou, "Determination of compressibility factor and fugacity coefficient of hydrogen in studies of adsorptive storage," *International Journal of Hydrogen Energy,* no. 26, pp. 597-601, 2001.

[46] M. Khan and M. Iqbal, "Modeling and Analysis of Electrochemical, Thermal, and Reactant Flow Dynamics for a PEM Fuel Cell System," *Fuel Cells,* no. 4, pp. 463-475, 2005.

[47] A. d. Real, A. Arce and C. Bordons, "Development and experimental validation of a PEM fuel cell dynamic model," *Journal of Power Sources,* no. 173, pp. 310-324, 2007.

[48] M. I. M. Khan, "Modeling and Analysis of electrochemical, thermal and reactant flow dynamics for a PEM fuel cell system," *Fuel Cells,* vol. 5, no. 4, pp. 463-475, 2005.

[49] I. A. F. w. service. [Online]. Available: http://www.meteoam.it/.

[50] I. S. R. A. Italian National Agency for New Technologies Energy and Sustainable Economic Development (ENEA). [Online]. Available: http://www.solaritaly.enea.it/Previsioni/Previsioni-dettagliEn-casaccia.php.

[51] G. Cau, D. Cocco, P. M. and T. V., "Assessment of a hybrid stand-alone power system with hydrogen production and storage," in *3rd International Conference on Microgeneration and Related Technologies*, Naples, 2013.

[52] L. Valverde, F. Pino, F. Rosa and J. J. Guerra, "Simulation and Experimental evaluation of Operating Modes in a hydrogen-based microgrid," in *EHEC 2014- European Hydrogen Energy Conference.*, Seville, Spain, 2014.

[53] M. B. Stevens, Hybrid fuel cell vehicle powertrain development, Ph.D. dissertation., University of Waterloo, 2008.

[54] L. Valverde, C. Bordons and F. Rosa, "Power management using model predictive control in a hydrogen-based microgrid," in *38th Annual Conference on IEEE Industrial Electronics Society, IECON 2012*, Montreal, QC; Canada, 2012.

[55] L. Valverde, F. Rosa and C. Bordons, "Design, planning and management of a hydrogen-based microgrid," *IEEE Transactions on Industrial Informatics,* vol. 9, no. 3, pp. 1398-1404, 2013.

[56] L. Valverde, F. Rosa, A. Del Real, A. Arce and C. Bordons, "Modeling, simulation and experimental set-up of a renewable

hydrogen-based domestic microgrid," *International Journal of Hydrogen Energy,* vol. 38, no. 27, pp. 11672-11684, 2013.

[57] J. Salazar, L. Valverde and F. Tadeo, "Predictive control of a renewable energy microgrid with operational cost optimization," in *39th Annual Conference of the IEEE Industrial Electronics Society, IECON 2013*, Vienna; Austria, 2013.

[58] E. Camacho and C. Bordons, Model Predictive Control, London: Springer-Verlag, 2004.

[59] H. Ibrahim, A. Ilinca and J. Perron, "Energy storage systems—characteristics and comparisons.," *Renewable and Sustainable Energy Reviews,* Vols. 1221 - 1250, no. 12, 2008.

[60] E. Zakrisson, The Effect of Start/Stop strategy on PEM fuel cell degradation Charasteristics, Gothenburg, Sweden: Master of Science, 2011.

[61] P. García, J. Torreglosa, L. Fernández and F. Jurado, "Optimal energy management system for stand-alone wind turbine/photovoltaic/hydrogen/battery hybrid system with supervisory control based on fuzzy logic," *International Journal of Hydrogen Energy,* vol. 38, pp. 14146-14158, 2013.